SOME ASPECTS OF LASER-PLASMA INTERACTION FOR ELECTRON ACCELERATION

THESIS

Submitted to

DELHI TECHNOLOGICAL UNIVERSITY

For the Award of the Degree of

DOCTOR OF PHILOSOPHY

By

MONIKA YADAV

(2K16/PhD/AP/03)

Under the supervision of

Prof. Suresh C. Sharma
Professor
Department of Applied Physics
Delhi Technological University

Dr. Devki Nandan Gupta
Associate Professor
Department of Physics & Astrophysics
University of Delhi

Department of Applied Physics
Delhi Technological University
Shahbad Daulatpur, Main Bawana Road,
Delhi-110042, India

MARCH 2021

DEDICATED

TO

MY FAMILY

Delhi Technological University

(Govt. of National Capital Territory of Delhi)
Shahbad Daulatpur, Bawana Road, Delhi-110042

CERTIFICATE

This is to certify that the thesis entitled ***"Some aspects of Laser Plasma Interaction for Electron Acceleration"*** submitted by **Ms. Monika Yadav (2K16/PhD/AP/03)** to Delhi Technological University (DTU), Delhi, India for the degree of Doctor of Philosophy, is a bonafide record of the research work carried out by her under my supervision and guidance. The work embodied in this thesis has been carried out in the Plasma Lab, Department of Applied Physics, Delhi Technological University (DTU), Delhi, India and Plasma Lab, Department of Physics and Astrophysics, University of Delhi, Delhi, India. The work of this thesis is original and has not been submitted in parts or fully to any other Institute or University for the award of any other degree or diploma.

Prof. Suresh C. Sharma
Supervisor
Delhi Technological University
Delhi-110042, India

Dr. Devki Nandan Gupta
Co-Supervisor
University of Delhi
Delhi-110007, India

Delhi Technological University

(Govt. of National Capital Territory of Delhi)
Shahbad Daulatpur, Bawana Road, Delhi-110042

CANDIDATE'S DECLARATION

I, herby certify that the thesis titled ***"Some aspects of Laser Plasma Interaction for Electron Acceleration"*** submitted in the fulfilment of the requirements for the award of the degree of Doctor of Philosophy is an authentic record of my research work carried out under the supervision of **Prof. Suresh C. Sharma** and **Dr. Devki Nandan Gupta**. Any material borrowed or referred to is duly acknowledged.

Monika Yadav
(2K16/PhD/AP/03)
Delhi Technological University
Delhi-110042, India

ACKNOWLEDGEMENTS

First and above all, I thank the Almighty for giving me the strength and patience to work through all these years.

I express my sincere thanks to my esteemed research supervisor, ***Prof. Suresh C. Sharma****, for his supervision, valuable guidance, and genuine advice from the early stage of research. His dedication, timely advice, scientific intuition and motivation have exceptionally inspired me. I owe him special thanks for always helping me out in all the official works and enabling me to accomplish my Ph.D. thesis on time. Despite all his other tasks, he still finds time to discuss about research and our well-being too.*

Special thanks to my research co-supervisor, ***Dr. Devki Nandan Gupta****, for integrating me in his group and providing a nice scientific environment. I am grateful for the insightful discussion, valuable advice and trust he showed during the research work. He is a person with foresight, benevolence, enthusiasm, patience, and endurance. He never turns me to wait for any research related discussion and work. Throughout my Ph.D. duration, he provided sound advice, a good company and a lot of good ideas for research related work. I feel very fortunate having had the opportunity to complete this challenging journey under his guidance.*

My sincere thanks also goes to Hon'ble Vice Chancellor, DTU, ***Prof. Yogesh Singh*** *and officials of DTU for their precious support and providing ample research facilities to conduct this research. I would also like to thank Head of the Department,* ***Prof. Rinku Sharma*** *for developing a research friendly environment in the department. Moreover, I would also thank all other faculty and staff members of Department of Applied Physics, DTU for their help and cooperation throughout my research period.*

I express my heart-felt gratitude to all my colleagues and friends ***Umang, Jyoti, Anshu, Harender, Rajesh, Mansha, Neha, Jyotsna and Ravi***

for their constant motivation and support during the course of my Ph.D. The fun we had in the last few years kept me sane during my ups and downs. Their personal and professional helps, moral support and encouragement have always made me feel at ease. The time I spend with them will remain as a golden memorable time in my life. I would also like to thank my labmates and friends, ***Saurabh****,* ***Arohi, Mukesh, Ravi, Anand, Gaurav,*** *and my seniors* ***Mamta, Maninder, Krishna Gopal,*** *and* ***Pinki.*** *Saurabh and Arohi are the most selfless and beautiful souls I have met till now. Their scientific inputs, fruitful discussions, selfless help, motivation, and all the fun we had, kept me going in this difficult yet beautiful journey. Arohi's willingness to lend an ear to all my personal and professional problems, helped me a lot. I owe them a special thanks for their immense help in simulations. I am also indebted to my lovely friend* ***Ruchi*** *for being there for me at every step. I wouldn't have started this journey without her encouragement.*

I would like to pay high regards to my father ***Mr. Chitra Pal Yadav,*** *my mother* ***Mrs. Raj Bala,*** *my elder brother* ***Dr. Pravesh,*** *and sister-in-law* ***Dr. Madhu*** *for their love, constant care, and support throughout my life. Their faith, trust and confidence in me always pushed me towards my goal. I owe a special thanks to my family-in-law, specially my mother-in-law* ***Mrs. Shanti*** *and father-in-law* ***Mr. Ishwar Singh Yadav****. Without her love, patience and support, I would not have been able to come so far. The encouragement and blessings from my sister-in-law* ***Mrs. Nitisha****, chai on table by my brother-in-law* ***Dr. Vikas*** *motivated me to accomplish this thesis work. My family's cooperation, understanding, patience and encouragement were the sustaining factors in this tough journey. Last but not the least, I would like to thank my husband* ***Mr. Vipin*** *for always being there for me. The love from my beautiful daughter* ***Vedanshi Rao****, born during my Ph.D., kept me motivated throughout.*

I acknowledge University Grant Commission (UGC), Government of India, for financial assistance to carry out my research work.

Monika Yadav

ABSTRACT

This thesis focuses on investigation of laser-plasma interaction relevant to electron acceleration to high energies. This work explores various ideas for producing an energetic and good quality electron beam from laser wakefield acceleration (LWFA) in plasmas. In LWFA, a high-intensity laser pulse excites a plasma wave, which propagates behind the laser pulse with the equal speed of the laser group velocity. For efficient accelerations, electrons should be injected into the wakefield. Thus, the wakefield evolution and electron injection both are quite important aspects in LWFA. In order to draw the maximum output from the wakefield structure, which is called wakefield bubble in case of high-intensity laser, the basic understanding behind the factors controlling electron injection into wake structure must be very clear. This thesis work focus toward controlling the electron beam quality by understanding the factors affecting bubble wake evolution. The dependence of beam energy and the beam quality on the shape of the bubble is the main motivation behind this investigation. Particle-in-cell (PIC) simulations are conducted to study the bubble dynamics for optimum electron accelerations. A good quality electron bunch with pC to nC charge are obtained with current laser-plasma parameters. During LWFA, generation of wakefield results in variation of refractive index that may distort the laser pulse shape. Thus, the laser pulse shape may be a significant factor to control the electron beam parameters in LWFA. Various shapes such as q-Gaussian laser pulse and flattened-Gaussian laser pulse have been taken into account to observe the laser pulse effect on electron beam parameters in LWFA. The implications of laser pulse shape was shown to control and optimize the bunch charge as well as the bunch energy. Our insights into the acceleration process might be quite supportive in the future optimization of electron beam stability and quality. The electron bunch generated by LWFA could be used to obtain femtosecond x-rays and subsequent applications in medical sciences.

CONTENTS

LIST OF FIGURES

Fig. No. **Page No.**

Chapter: 1

Chapter: 2

Chapter: 3

Chapter: 5

LIST OF TABLES

1

INTRODUCTION

1.1 Background

Particle acceleration has been a fascinating area of research due to the curiosity of human to explore the universe and understand the laws of nature. As the particle acceleration physics has been acting as the major milestone in the nuclear and high-energy physics research, it can restructure our knowledge about universe. In addition, particle acceleration has enormous range of applications in medical diagnostic, X-ray radiotherapy, proton therapy for cancer treatment, radiation processing, food preservation, plasma heating, radioactive waste incineration, synchrotron light sources, condensed matter physics, cosmology and astrophysics and so on [1-5].

The physics behind particle acceleration basically deals with the interaction of the charged particles with static and dynamic electromagnetic fields. The advancement in particle physics demands high energy particle beams. As the requirement for beam energy grew, the size of the conventional accelerators also kept increasing, which increases the cost accordingly. The progression to the circular accelerators reduced the size as well as cost, but it had limitations regarding synchrotron radiation losses. The radio frequency (RF) cavities also have limitations on accelerating field. The accelerating field is restricted by an upper limit of 100 MV/m. Beyond this accelerating field, the material breakdown occurs on the walls of the accelerating structure which restricts the accelerator operation [6]. Although, the quality of the beam obtained using conventional accelerators is commendable, but the size of the accelerators, building cost and inability to withstand high accelerating gradients are the major challenges. The development of high-power laser facilities has

made it possible to achieve very high accelerating gradients. But the problem with using laser field as accelerator is that the field direction is perpendicular to the propagation direction. Also, the particle to be accelerated needs to co-propagate with the wave with the phase velocity of the laser, i.e. the speed of light (c). To accelerate the charge particles to high energies, achieving such a condition is a major challenge. The sustainable answer to overcome these limitations of conventional accelerators is to introduce the plasma medium [7-10]. Firstly, as plasma is already in ionized state, it can sustain large field gradients. Secondly, these accelerators can have fields in the direction of propagation. Therefore, it can meet the challenge for electron energy gain. Also, the electric field yielded in plasma can be of the order of $\sim 100\ GV/m$. This accelerating field can accelerate the plasma electrons to GeV energies in a very short distances, on the order of a few millimetres. Laser-plasma based accelerators have potential to generate good quality electron bunch with femtosecond duration, several nanocoulomb or even picocoulomb charge, very low emittance of the order of 0.1 mm.mrad and energy spread of the order of 1%. Such high quality electron beams are highly beneficial for innumerable applications ranging from high energy physics to medical and industrial applications.

1.2 Laser-plasma interaction

In the early stages of laser-plasma acceleration research, low-intensity lasers were mainly employed. The electron beams obtained by these low-intensity laser have very low energy. The main reason behind this problem was the low laser intensity. The chirped pulse amplification (CPA) technique [11] make it possible to realize extremely intense and short laser pulses. The recent rapid progress [12] in femtosecond laser pulse amplification technology is responsible for the milestones achieved in the areas relying on lasers. The development of such a laser system has enabled the utilization of the laser wakefield acceleration. This section describes the basics of laser-plasma interaction including the concepts of laser and plasmas. And then, the propagation of laser in plasma relevant to acceleration is outlined.

1.2.1 Basics of laser

The fields of the laser pulse in space and time can be written as:

$$\boldsymbol{E}(z,t) = \boldsymbol{E_0}\hat{x}\, Sin(\omega t - kz + \phi) \tag{1.1}$$

$$\boldsymbol{B}(z,t) = \frac{\boldsymbol{k} \times \boldsymbol{E}}{\omega} \tag{1.2}$$

where ω is the electromagnetic wave frequency, k is the wave number ($k = \omega/c$), c is the speed of light, and ϕ represents the absolute phase. The propagation of the electromagnetic wave can be explained using Maxwell's equations

$$\nabla . \boldsymbol{E} = \frac{\rho}{\varepsilon_0}, \tag{1.3}$$

$$\nabla \times \boldsymbol{E} = -\frac{\partial \boldsymbol{B}}{\partial t}, \tag{1.4}$$

$$\nabla . \boldsymbol{B} = 0, \tag{1.5}$$

$$\nabla \times \boldsymbol{B} = \mu_0 \boldsymbol{J} + \frac{1}{c^2}\frac{\partial \boldsymbol{E}}{\partial t}, \tag{1.6}$$

where ρ and J are the charge and current density, respectively. ε_0 and μ_0 are the electric permittivity and magnetic permeability in vacuum, respectively. Using Lorentz gauge, the electric and magnetic field can be expressed in terms of scalar (ϕ) and vector potential ($\boldsymbol{A}$) as:

$$\boldsymbol{E} = -\frac{\partial \boldsymbol{A}}{\partial t} - \nabla\phi, \tag{1.7}$$

$$\boldsymbol{B} = \nabla \times \boldsymbol{A}. \tag{1.8}$$

The energy per unit area per unit time transported by the electromagnetic wave can be described by Poynting vector, $\boldsymbol{S} = \frac{1}{\mu_0}(\boldsymbol{E} \times \boldsymbol{B})$. The intensity (average power per unit area) of the laser is given by time averaging the Poynting vector over a cycle:

Monika Yadav, Department of Applied Physics, Delhi Technological University, Delhi, India

$$I = \langle S \rangle = \frac{1}{2} c \varepsilon_0 E_0^2 \tag{1.9}$$

1.2.1.1 Gaussian laser pulse

The fundamental transverse (TEM_{00}) mode that develops in the optical resonator has the Gaussian profile in the direction transverse to the direction of propagation. This kind of intensity profile maintain its Gaussian profile during propagation. Therefore, it has been extensively used for investigating laser based studies. The laser pulses are mostly approximated by the Gaussian profile as

$$\boldsymbol{E}(\boldsymbol{r}, \boldsymbol{z}, \boldsymbol{t}) = \frac{E_0}{2} \hat{x} f(t,z) \frac{w_0}{w(z)} exp\left(-\frac{r^2}{w^2(z)} - i\frac{k_0 r^2}{2R(z)} - i(\omega t - kz + i\varphi(z) \right), \tag{1.10}$$

where $f(t,z) = exp\left(-2ln2\left(\frac{t-z/c}{\tau^2}\right)^2\right)$. Here, w_0 is the laser waist at the focal plane. It is the minimum beam radius at $z = 0$. $w(z)$ is the beam waist at a distance z from the focal plane ($z = 0$). It can easily be calculated using formula, $w(z) = c(1 + (z/Z_R)^2)^{1/2}$. Z_R is the Rayleigh length, which is the distance at which the width of the beam becomes $\sqrt{2}$ times the width at the focus (where $w = w_0$). It is given by $\pi w_0^2/\lambda$. The depth of focus (b) is $2Z_R$. $R(z)$ is the radius of curvature of the wavefronts at position z from the focus. It evolves with z as $z(1 + (z/Z_R)^2)^{1/2}$. τ is the pulse duration of the pulse, k and ω are the wave number and frequency of laser beam with wavelength λ. $\varphi(z)$ is the Gouy phase, which is the phase advancement by beam given by $tan^{-1}(z/Z_R)$. The schematic of Gaussian laser beam illustrating beam parameters is shown in Fig.1. For Gaussian pulse, peak intensity in terms of energy (at focus) is given by:

$$I_{peak} = \frac{2E}{\pi w_0^2 \tau}, \tag{1.11}$$

where πw_0^2 is the area of the beam at focus and E is the energy of the pulse. For example, a pulse of energy 1 Joule, spot size of 20 μm, pulse duration (τ) 30 fs,

Monika Yadav, Department of Applied Physics, Delhi Technological University, Delhi, India

has the peak intensity of 5×10^{18} W/cm^2. In calculations, inspite of using the laser intensity, we use normalized vector potential (a_0) as it is convenient to define a dimensionless parameter. It is often called as laser strength parameter.

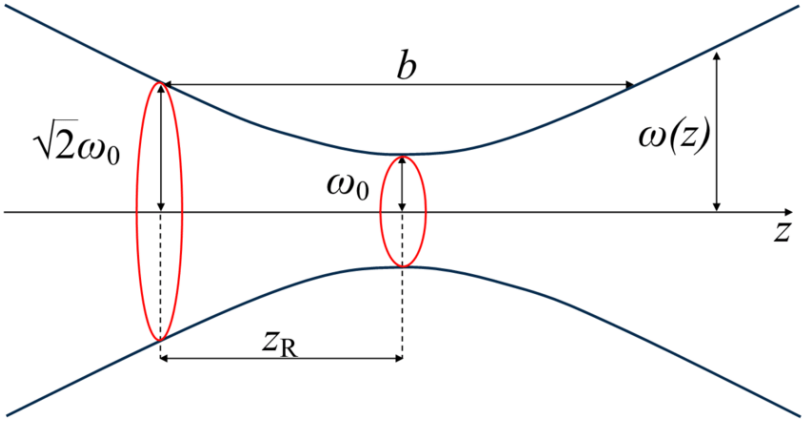

Fig. 1.1. Schematic of Gaussian beam indicating beam waist (w_0), beam width ($w(z)$) at distance (z), Rayleigh length (Z_R), and depth of focus (b).

1.2.1.2 Laser strength parameter

At lower laser intensities, plasma behaves in a linear manner on interaction with laser. As the laser intensity is sufficiently increased, the plasma starts to show non-linear/ relativistic behaviour. The laser strength parameter sets the scale for this transition from low-to-high intensity regime. It can be defined as the normalized quiver momentum of electron in laser field,

$$a_0 = \frac{p_0}{m'c} = \frac{v_e}{c}, \tag{1.12}$$

where p_0 and m' are the quiver momentum and rest mass of electron, respectively. v_e is the electron quiver velocity and c is the speed of light. For low intensity laser, electrons in the plasma oscillate linearly with the quiver velocity (v_e). As the laser intensity increases, the laser-plasma interaction becomes nonlinear. Then the electron quiver velocity, defined as $v_e = \frac{eB_0}{m'\omega}$, exceeds the speed of light, which is known as the relativistic regime. So,

Monika Yadav, Department of Applied Physics, Delhi Technological University, Delhi, India

depending on the value of a_0 $(a_0 \ll 1)$ or $(a_0 \geq 1)$, the relativistic and non-relativistic regimes can be classified.

The variation of a_0 makes a considerable difference in the physics of laser-plasma interactions. To estimate the order of the magnitude of this parameter, a relation between laser strength parameter and peak electric field can be set up. Laser electric field is related to the potential vector as: $\boldsymbol{E} = -\partial \boldsymbol{A}/\partial t$, as in vacuum $\phi = 0$. Normalized vector potential is given by $a_0 = eA/m'c$. In terms of E_0, the laser strength parameter can be written as

$$a_0 = \frac{eE_0}{m'\omega c} \tag{1.13}$$

This gives $E_0 \simeq 3.21 a_0/\lambda$ with electric field in TV/m and wavelength in μm (for the linearly polarized Gaussian laser profile). Also, this parameter can be related to the peak intensity as

$$a_0 \simeq \sqrt{7.3 \times 10^{-19} [\lambda(\mu m)]^2 I_0 (W/cm^2)}\,, \tag{1.14}$$

where I_0 is the laser peak intensity. For typical laser intensity $\geq 10^{18} W/cm^2$ and laser wavelength $\lambda = 1\mu m$, the laser strength parameter $a_0 \geq 1$. The relation between laser strength parameter and laser peak power (GW) can be written as:

$$P(GW) = \frac{\pi w_0^2 I_0}{2} \simeq 21.5 \left[\frac{a_0 w_0}{\lambda}\right]^2 \tag{1.15}$$

1.2.2 Plasma

There are four known naturally occurring states of matter in the universe- *solid, liquid, gas* and *plasma*. This classification is done depending on the thermal energy of the atoms/molecules and the interparticle binding energy. The binding energy between the constituent particles is stronger in solids, comparatively weaker in liquids, and almost negligible in gases. When solids are heated, the thermal energy of the particles overcome the potential energy, interparticle bonds break, and phase transition to liquid occurs. When liquids are heated to a certain temperature, a gaseous state is obtained. And when a gas is

Monika Yadav, Department of Applied Physics, Delhi Technological University, Delhi, India

heated to a very high temperature (10,000˚K or above), atoms in the gas collide with each other knocking off the electrons out of the atoms. The resulting state consisting of electrons and ions is known as ionized gas or plasma.

At a particular temperature, the degree of ionization in a gas can be determined using Saha's Equation:

$$\frac{n_{ion}}{n_n} \approx 2.4 \times 10^{21} \frac{T^{3/2}}{n_{ion}} \exp(U_{ion}/K_b T)\,, \qquad (1.16)$$

where n_{ion} and n_n are the density of the ionized gas and the density of neutral atoms, respectively. T is the temperature of the gas in ˚K , U_{ion} is the ionization energy of the gaseous atoms, and K_B is the Boltzmann's constant. At very high temperature, the n_{ion} exceeds the n_n and the gas becomes fully ionized. This is the reason for the natural occurrence of plasma in the astronomical bodies (with millions of degrees temperature). Almost 99% of the visible universe is made up of plasma.

Definition: Plasma can be defined as the collection of ions, electrons and neutral particles that interact via strong long range Coulombic force.

One can not define any ionized gas as a plasma. There are certain conditions that need to be fulfilled by the ionized gas to be called as plasma: quasineutrality and collective behaviour [13]. 'Quasineutrality' in plasma means the number density of ions is approximately equal to the number density of electrons for the plasma of length much greater than the Debye length ($l \gg \lambda_d$). Debye length is the characteristic distance over which the potential due to a charge inside plasma can be shielded out. In general, the Debye length can be related to the electron density (n_e) and temperature (T) using the expression given by

$$\lambda_d = \left(\frac{\varepsilon_0 K_B T}{n_e e^2}\right)^{1/2}. \qquad (1.17)$$

As the plasma consists of charged particles, their motions give rise to electric and magnetic fields. So, the particles far away also get affected by the

Monika Yadav, Department of Applied Physics, Delhi Technological University, Delhi, India

long range electromagnetic forces. In general, the collective behaviour means that the motion of the charge particles does not only depend on the local conditions but also on the plasma far away. It also requires that the number of particles in Debye's sphere (N_D) must be much greater than 1, $N_D \gg 1$. This is because the concept of Debye shielding has some meaning only if there are enough particles in the charge cloud.

A plasma may be defined using two scales: length scale (λ_d) and time scale (${\omega_p}^{-1}$). The Debye length concept has already been discussed. However, the understanding of time scale requires knowledge about plasma oscillations. When the electrons are displaced from their mean position in plasma with the ions in background, a space-charge separation is created. An electric field comes in to the picture to store the neutrality of the plasma. It pulls the electrons back. Due to inertia, electrons overshoot their mean positions and start oscillating about it (see Fig. 1.2). The frequency of oscillation is termed as the *plasma frequency*. Ions in the background are considered immobile as they are much heavier, hence they do not get time to respond to the high frequency electric field. Mathematically, plasma frequency (*rad/sec*) can be defined as

$$\omega_p = \sqrt{\frac{ne^2}{\varepsilon_0 m'}}, \tag{1.18}$$

where n, m', and e are the number density, mass and charge of the plasma electron and ε_0 is the permittivity in vacuum. Any plasma must have $\omega_p \tau > 1$, where τ is the mean time between collisions of particles in plasma. It means plasma frequency must be greater than the collision frequency otherwise the motion won't be controlled by the Coulomb forces.

Monika Yadav, *Department of Applied Physics, Delhi Technological University, Delhi, India*

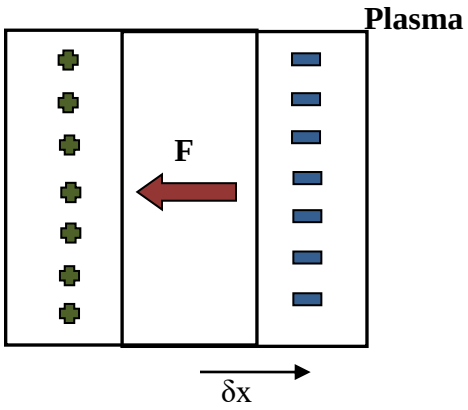

Fig. 1.2. Schematic of a slab of plasma where electrons (-) are displaced by δx from the ions (+). A restoring force (**F**) pulls the electrons back and plasma oscillations set up about the equilibrium position.

1.2.3 Laser propagation in plasmas

As the electromagnetic waves are transverse, wave equation can be derived for transverse waves using Maxwell's Eqs. (1.3)-(1.6). Taking curl of Eq. (1.4) and then using Eq. (1.6), we get the

$$\nabla^2 \boldsymbol{E} - \nabla(\nabla . \boldsymbol{E}) + \frac{\omega^2}{c^2}\varepsilon \boldsymbol{E} = 0. \tag{1.19}$$

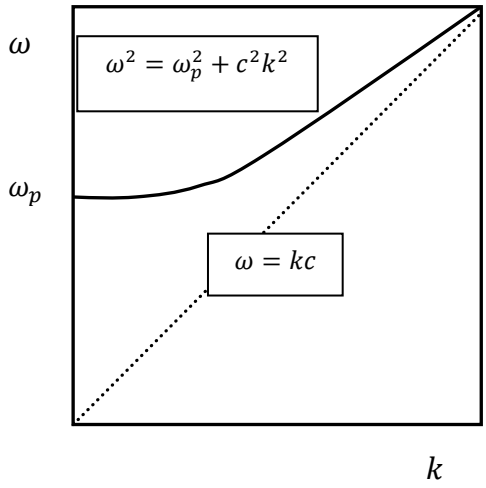

Fig. 1.3. Illustration of dispersion relation of electromagnetic wave propagating in vacuum (dotted line) and plasma (solid line).

Monika Yadav, Department of Applied Physics, Delhi Technological University, Delhi, India

Here, ε is the dielectric constant of plasma given by $1 - \omega_p^2/\omega^2$, where ω is the laser frequency and ω_p is the electron plasma frequency. The dispersion relation for electromagnetic wave in plasma (see Fig. 1.3) is given as

$$\omega^2 = \omega_p^2 + c^2k^2 \tag{1.20}$$

It relates the electromagnetic wave frequency (ω) with the wave number (k) and plasma parameters through ω_p [14,15]. The group and the phase velocity of the wave in plasma can be derived from the dispersion relation using mathematical formulas, $v_p = \omega/k$ and $v_g = d\omega/dk$. The phase velocity and group velocity are given by:

$$\left.\begin{aligned} v_p &= c/\sqrt{1 - \omega_p^2/\omega^2}\,, \\ v_g &= c\sqrt{1 - \omega_p^2/\omega^2}. \end{aligned}\right\} \tag{1.21}$$

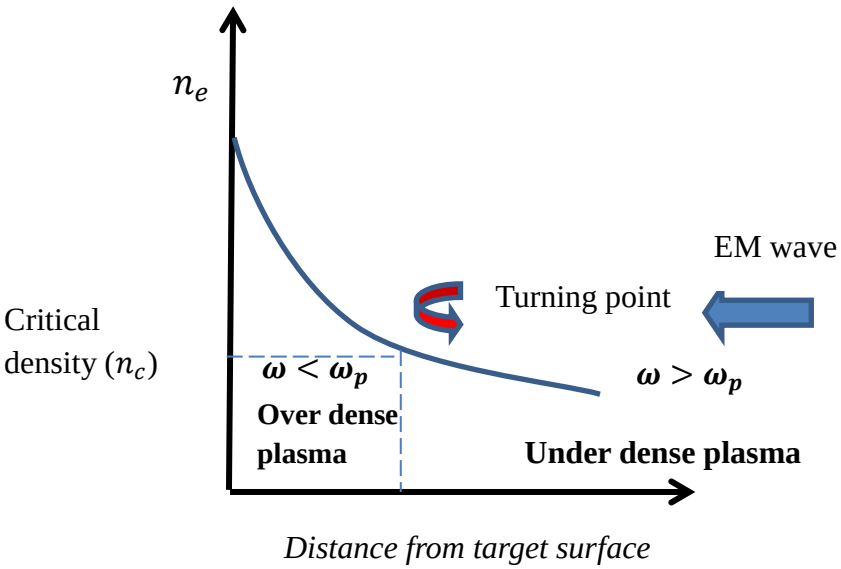

Fig. 1.4. Schematic showing propagation of electromagnetic wave in plasma illustrating underdense and overdense plasma region.

When $\omega < \omega_p$, the wave vector (k) becomes imaginary and hence, the electromagnetic wave cannot propagate through the plasma. This kind of plasma is called the *'overdense plasma'*. And when $\omega > \omega_p$, k is real and plasma acts as a transparent medium to the electromagnetic wave. Plasma, in this case, is called the *'underdense plasma'*. The condition when $\omega = \omega_p$ is called the cut-off condition, where wave is reflected back. It occurs at critical density (n_c), which gives the turning point (transition from penetration to reflection). Usually, the critical plasma density is defined as

$$n_c(cm^{-3}) = m\varepsilon_0\omega^2/e^2 \approx 1.1 \times 10^{21}/\lambda(\mu m)^2 \qquad (1.22)$$

Typically, the laser of wavelength 1 μm reflects back at the plasma density of $1.1 \times 10^{21} cm^{-3}$. The schematic of propagation of electromagnetic wave in plasma illustrating underdense and overdense plasma is shown in Fig. 1.4. All the work discussed in this thesis has been carried out for underdense plasma.

1.2.4 Laser field and electron motion

When the laser intensity is high enough to knock the electrons off the atoms through tunnelling or multiphoton ionization, the gas becomes ionized. The laser intensity greater than 10^{18} *W/cm*^{2} corresponds to the electric field of amplitude greater than 10^{12} *V/m*. Such high field of laser is not able to accelerate the electrons as the laser field is transverse. Hence the single electron just oscillate in this field and can't be accelerated directly. In the laser field, the motion of an electron is given by Lorentz equation, given by

$$m\gamma \frac{d\boldsymbol{v}}{dt} = -e\left(\boldsymbol{E} + \frac{\boldsymbol{v}}{c} \times \boldsymbol{B}\right), \qquad (1.23)$$

where e and m are the electron charge and mass, respectively. γ is the relativistic factor, given by, $\gamma = (1 - (v/c)^2)^{-1/2}$. For the non-relativistic case, $v/c \ll 1$, the 2nd term on the right hand side of Eq. (1.23) can be neglected. The solution of Eq. (1.23) suggests that the rest electron, starts oscillating in the transverse direction without energy gain.[16, 17] For relativistic case, $v \to c$, the

Monika Yadav, Department of Applied Physics, Delhi Technological University, Delhi, India

second term has to be taken in to account. Eq. (1.23) can be solved in the frame co-moving with the laser pulse. The electrons are pushed forward by $\boldsymbol{v} \times \boldsymbol{B}$ force.

The electron motion in transverse direction is dominated by longitudinal drift motion. Hence, in relativistic case, the aim to traverse the electron in the propagation direction of laser is achieved. But still, electrons do not gain energy from the laser due to plane wave assumption [18]. The non-uniform intensity profile of the laser pulse can allow the electron to retain the overall energy gain. Thus, the Gaussian shaped laser may be appropriate for this purpose. The inhomogenous laser field exerts the Lorentz force (also known as the ponderomotive force). In case of plasma, the $\boldsymbol{v} \times \boldsymbol{B}$ force associated with the inhomogenous laser field is termed as the ponderomotive force. This ponderomotive force is basically responsible to excite electrostatic field to accelerate the plasma electrons to high energies.

1.2.4.1 Ponderomotive force

In case of homogenous plane electromagnetic wave, the electron oscillates and also experiences a forward drift in the laser propagation direction. The electron comes to rest as soon as the laser passes away. Hence, the net energy gain remains zero. For wakefield excitation, we use ultrashort and tightly focussed laser pulse in order to achieve high intensity. Due to tight focusing, a strong spatial intensity gradient is created. In such an inhomogeneous oscillatory electromagnetic wave, electron experiences a non-linear force called *ponderomotive force* [16]. This causes an additional gradient force which accelerates the oscillating electron towards the lower intensity. We can say, the centre of oscillation drifts from high intensity region to the low intensity region.

In general, the ponderomotive force is written as

$$\boldsymbol{F}_p = -\frac{1}{4}\frac{e^2}{m\omega^2}\nabla \boldsymbol{E}_0^2 \,. \tag{1.24}$$

The ponderomotive force is a negative intensity gradient force ($\propto -\nabla I$). It means that the charge will be drifted from a high intensity region to a low

Monika Yadav, Department of Applied Physics, Delhi Technological University, Delhi, India

intensity region. It is also evident from the formula that it is a charge independent force. Electrons as well as ions will be pushed towards the lower intensity region of the laser. But, as the ponderomotive force has an inverse dependence on mass of the charge, ions can be considered as an immobile background due to their heavy mass. This ponderomotive force acts as the main driving force for the wakefield excitation in plasmas.

1.3 Plasma based electron acceleration

Laser-plasma based acceleration is capable to generate electron bunch in very short distance. There are several mechanisms to accelerate the electrons by laser-plasma interactions. This includes the wakefield acceleration and self-modulated laser wakefield acceleration. The availability of high-power laser makes it possible to achieve the electron energy gain in GeV range from laser-plasma acceleration. The quality of electron bunch has been one of the crucial issues in these accelerators. The laser and plasma parameters mainly determine the bunch quality. The high quality electron bunch may enable a variety of applications of laser-plasma acceleration. Various methods for generating energetic electron bunches are briefly discussed as follows:

1.3.1 Plasma beat-wave acceleration (PBWA)

When two long-pulse lasers ($\omega_1$and ω_2) with the frequency difference equal to the plasma frequency (ω_p) are propagated in an underdense plasma, a ponderomotive force due to the laser pulses is experienced by the plasma electrons. The frequency difference matches the natural oscillation frequency of plasma electrons i.e., $\Delta\omega = \omega_1 - \omega_2 = \omega_p$ and a large amplitude plasma wave can be driven resonantly [19-22]. This satisfies the energy and momentum conservation relations such as $\omega_1 - \omega_2 = \omega_p$ and $k_1 - k_2 = k_p$, where $k_1$and k_2 are the wave numbers of the two lasers and k_p is the wave number of the plasma wave. The excited plasma wave moves with the phase velocity ($v_p =$

$\Delta\omega/\Delta k$) equal to the group velocity of the laser pulses. The electrons moving with the velocities comparable to the phase velocity of plasma wave may get trapped in the plasma wave and are accelerated to higher energies. This acceleration scheme was further studied by various researchers to accelerate electrons efficiently [23-25]. The major advantage of this scheme is to accelerate the electron using low-intensity laser pulsers.

1.3.2 Self modulated laser wakefield acceleration (SM-LWFA)

This scheme of laser wakefield acceleration involves resonant self modulation of laser pulse. A single long laser pulse is employed in this acceleration mechanism and the pulse gets modulated at plasma frequency due to simultaneously occurring forward Raman scattering. The two requirements for SM-LWFA operation are: the pulse length much longer than the plasma wavelength ($c\tau > \lambda_p$), and power of the laser pulse greater than the critical power that is needed for optical guiding ($P > P_c$). Various researchers employed this acceleration scheme and observed electron energies in MeV [26-29]. Krall *et al.* (1993) [30] explained several advantages of this scheme over laser wakefield acceleration. A larger wakefield is excited in this configuration as it operates at high plasma densities. High laser power means higher values of laser strength parameter and hence, larger accelerating field. The interaction length reaches to several Rayleigh lengths due to relativistic self-focusing.

1.3.3 Laser wakefield acceleration (LWFA)

Out of the various schemes possible for plasma based electron acceleration, this thesis work is focused to laser wakefield acceleration mechanism. In this acceleration scheme, a single, short and highly intense laser pulse is employed to excite the wakefield in plasma [31,32]. This concept was firstly introduced by Tajima and Dawson in 1979. The CPA technology in laser system made this scheme to operate efficiently. When an highly intense laser

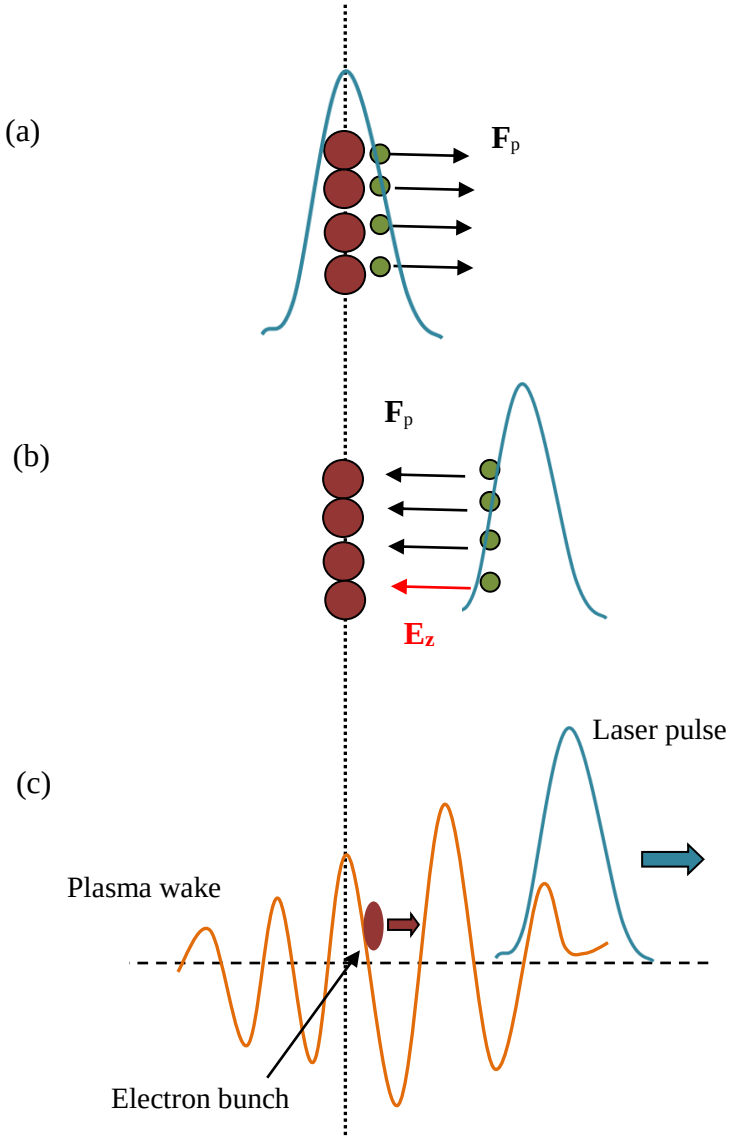

Fig. 1.5. Mechanism of plasma wave generation (a) Interaction of laser pulse with plasma consisting of electrons (represented by green circles) and ions (represented by red circles) (b) Electrons pushed forward due to ponderomotive force ($\mathbf{F}_p$) , creating a charge separation. Electrons are pulled backward due to the space-charge field ($\mathbf{E}_z$). (c) Plasma wave (laser wakefield) is excited, which accelerate the electrons.

pulse with the pulse length comparable to the plasma wavelength is introduced in an underdense plasma, the electrons are pushed radially outward due to the ponderomotive force exerted by the focussed laser pulse. This nonlinear force can be understood as the radiation pressure of the laser pulse, which is a

negative intensity gradient force. Hence, it pushes the plasma electrons from high-intensity region towards low- intensity region. As the ions are heavier in mass, they don't get time to respond to the ponderomotive force exerted by the laser pulse. Hence ions are considered fixed in the background. The displacement of plasma electrons creates a space-charge field in the plasma. The electrons are thus pulled back to their original positions. The electrons due to their inertia overshoot the original position and plasma oscillations set up. As the laser moves forward in plasma with the group velocity (v_g), a plasma wave trails behind the laser pulse with the phase velocity equal to the group velocity of driving pulse. The mechanism of plasma wave excitation is shown in Fig. 1.5. The most efficient wake is excited when the resonance condition is satisfied i.e., when the laser pulse length is comparable to the plasma wavelength ($L = c\tau \approx \lambda_p$). This scheme can be better understood using the analogy with the motorboat sailing in the water bodies. It leaves a water wake behind it as it displaces the water during sailing, which is similar to the plasma wave driven by the laser pulse in a plasma.

1.4 Electron acceleration in blow-out regime

A very intense and tightly focussed laser beam propagates in plasma, giving rise to complete cavitation of electrons, which is called 'bubble structure' or 'blow-out regime'. When an ultrashort laser pulse with $c\tau \lesssim w_0 \simeq 2\sqrt{a_0}c/\omega_p$ [33] (where a_0 is the laser strength parameter, w_0 is the laser spot size, and $c\tau$ is the pulse length) interacts with the plasma, a complete expulsion of electrons takes place [34]. An ion channel structure is created behind laser pulse which is almost devoid of electrons. Ions are immobile due to their heavy mass. Hence, a strong space-charge force is exerted by the cavitated region on the blown-out electrons. This causes the electrons to be pulled towards the axis, thus, creating a bubble wake. The schematic of bubble evolution is shown in Fig. 1.6. This structure has an enhanced focusing property. Hence, electrons when injected (either self-injected or externally injected) in the accelerating and

focusing region, can be accelerated to achieve high energies. A snapshot of wakefield bubble is shown in Fig. 1.7.

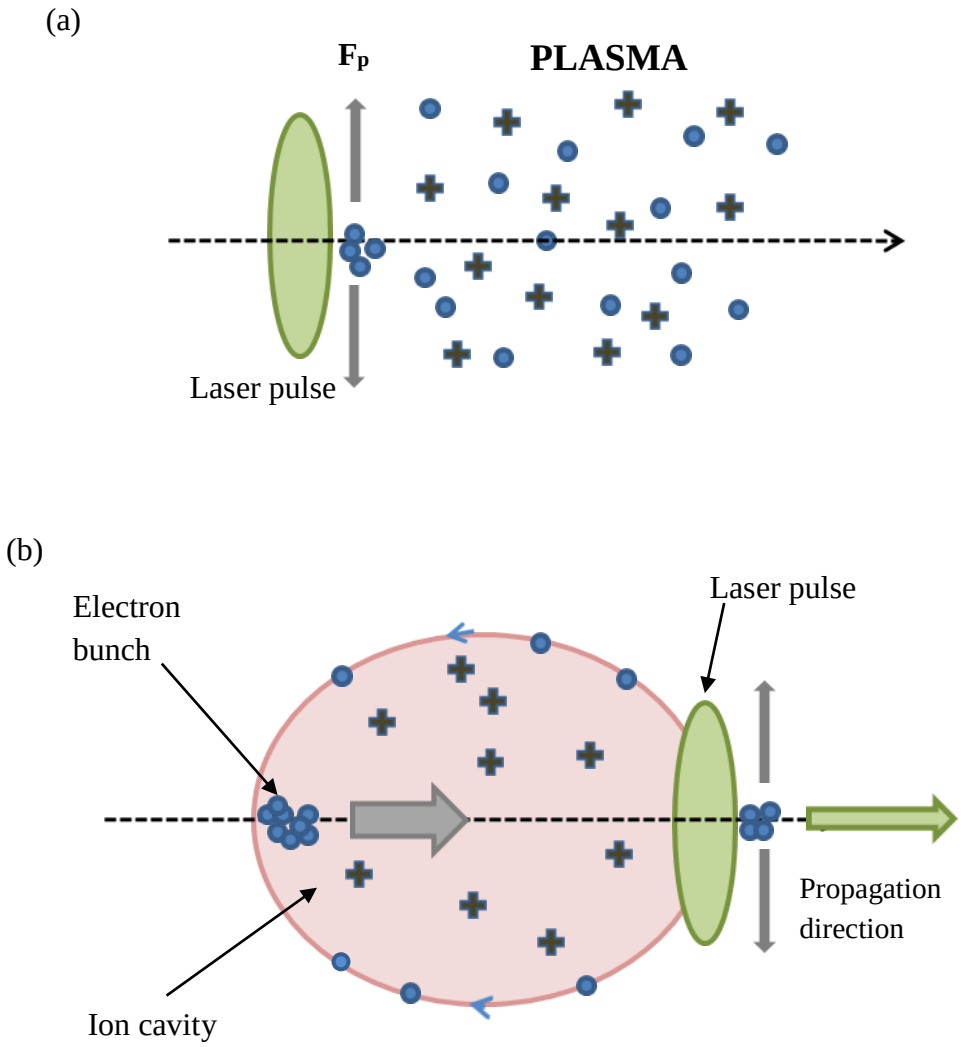

Fig. 1.6. (a) Laser pulse propagating in plasma, consisting of electrons (represented by blue circles) and ions (represented by plus sign), exerts ponderomotive force (F_p) on electrons. (b) Schematic diagram of the bubble or blow-out regime illustrating ion cavity formation and electron acceleration in the bubble.

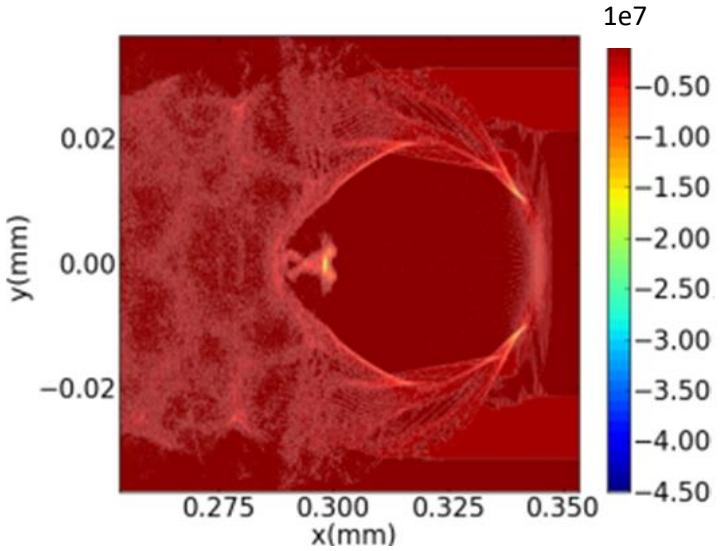

Fig. 1.7. A snapshot of electron density showing the bubble or blow-out regime.

1.5 Electron trapping and injection mechanisms in LWFA

The maximum electric field supported by the plasma gives the wave breaking field. When the oscillation amplitude of plasma electrons reaches the plasma wavelength and then crosses it, the wave breaks. It is analogous to the wave breaking in oceans. The amplitude of the sea wave keeps on increasing such that it causes the wave to break. In linear regime, the maximum amplitude of the plasma wave can be calculated using Poisson's equation, $\nabla . E = 4\pi e(n_0 - n_e)$. Considering all electrons in plasma are oscillating with frequency ω_p. Now, evaluating the maximum electric field using Poisson's equation gives the cold and non-relativistic limit of wave breaking [35],

$$E_{max.} = E_0 = \frac{mc\omega_p}{e}. \tag{1.25}$$

In non-linear regime, the value of maximum electric field can exceed this wave breaking limit. In 1D non-linear case, employing cold fluid equations, the maximum field can be given by [36,37]:

$$E_{max.} = \sqrt{2}\left(\gamma_{pw} - 1\right)^{1/2} E_0 \tag{1.26}$$

Monika Yadav, Department of Applied Physics, Delhi Technological University, Delhi, India

When the electrons at the peak of the density structure oscillates faster than the plasma wave itself, the weak breaking occurs. If these electrons fall in to the right phase of the plasma wave, they get trapped and accelerated to high energies.

In 3-dimension (3D), non-linear plasma wave has a larger plasma wavelength on-axis than off-axis. This curves the wave front of the plasma wave and it seems horse-shoe shaped. This curvature may lead to the transverse wave breaking. For highly relativistic laser pulse, a bubble shaped structure which is devoid of electrons, is created in 3D. At the bubble's back, the electron density is too high, whereas, inside bubble, there is almost complete cavitation. Hence, the electrons at the back of the bubble acquire a longitudinal momentum in forward direction due to large Coulomb force. It may lead to trapping of the electrons in the cavitated region and be called self-injected. It has already been reported in various works that electrons from the background plasma can be self-injected at the back of the bubble and get accelerated by the longitudinal space-charge field of the bubble. This self-injection phenomena is highly desirable as it is experimentally simple and feasible. There are few disadvantages also of this injection scheme. The major drawback is the lack of control over the injection process. Electrons might continue to be self-injected leading to a large energy spread. Also, continuous injection, sometimes, alters the electric fields inside the bubble and may distort the wake structure. This degrades the beam quality which is not desired in many applications. Meanwhile, several techniques have been developed to induce the electron injection externally in order to achieve an external control on the stability of the electron bunch. Some of the injection schemes are: colliding pulse injection [38-40] ionization induced injection [41,42], density transitions [43,44], 2 colour injection [45-47] etc. But it is highly desirable to get the electrons self-injected in the bubble. Various experiments still rely on self-injection scheme realizing the experimental challenges related to small spatial and temporal scales of laser wakefield acceleration.

1.6 Beam loading in laser wakefield

In laser wakefield accelerators, there is a possibility of achieving up to several picocoulomb (pC) or nanocoulomb (nC) of charge in the accelerated electron bunch. Such a large bunch drives a field of itself. The field of accelerated electron bunch superimposes with the accelerating field of the wake. The effective accelerating field is modified and thus the wake structure also gets modified. The charges at different longitudinal position sees different accelerating field and therefore, experience a spread in the energy. Hence, the modification in wake structure affects the beam dynamics and bunch parameters. The energy of the accelerated electrons is decreased and the bunch quality is degraded due to the increase in energy spread. The maximum charge that can be injected, such that the wakefield within the bunch due to the current profile remains flat, was evaluated by Katsouleas *et al.* [48]. The flattening of the wakefield plot due to beam loading effect can be seen in Fig. 1.8. The maximum number of electrons that can be accelerated are estimated, considering the constraints on emittance and energy spread. Finally, the beam loading efficiency is also evaluated which depends on the overlapping of the self-fields of the injected bunch and the field of the wake. The bunch shaping concept has been used to maintain a constant field within bunch and thus, reduces the energy spread. The loading in non-linear regime is addressed by Tzoufras *et al.* [49]. If the bunch charge is efficiently controlled, the bunch can be driven to large distance without inducing energy spread.

Monika Yadav, *Department of Applied Physics, Delhi Technological University, Delhi, India*

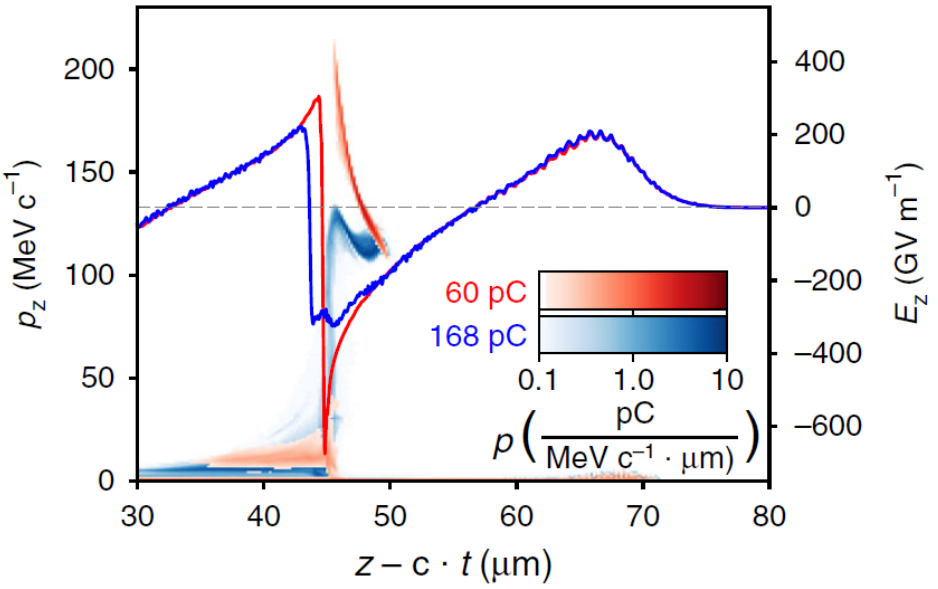

Fig. 1.8. Beam loading effect on electron phase space (p_z) and accelerating field (E_z) for different values of electron load in the wake, i.e. 60 pC in red and 168 pC in blue [50].

In non-linear bubble regime, the charge that must be injected in the bubble wake for the optimal loaded condition [50] is given by:

$$q(nC) \approx 1.504 \frac{1}{\omega} \sqrt{\frac{2 \times 10^{22} e^2}{17 m \varepsilon}} \sqrt{P(GW)}, \qquad (1.27)$$

where q is the loaded charge in nC, ω is the laser frequency, and P is the laser power in *GW*. This optimal loading condition represents a balance between the wakefield and the self-field of the injected charge. It leads to the situation where the resultant field remains constant along the length of the electron bunch. Hence, all the electrons present in the bunch experience same accelerating field, therefore, minimizing the energy spread.

Monika Yadav, *Department of Applied Physics, Delhi Technological University, Delhi, India*

1.7 Limitations of LWFA

There are various phenomena occurring during laser-plasma interaction those limit the electron acceleration, and thus the electron energy gain. The electron energy gain depends on the combined effects of all the possible limitations. Few of the possible limitations are discussed below.

1.7.1 Pulse energy depletion

When the laser pulse drives the electron plasma wake in the plasma, it looses its energy to the wake. When the intense laser pulse interacts with plasma, it pushes the electrons outwards. Hence, the refractive index of plasma is modified due to relativistic mass correction and density variation. This leads to decrease in laser frequency due to photon deceleration. As the number of photons is an invariant quantity, it leads to the attenuation of the laser energy. Therefore, when the laser gives energy to the electrons as kinetic energy, it itself depletes. Length beyond which the laser energy gets depleted is called laser pulse depletion length. It can be calculated using the fact that the energy of the laser pulse is equal to the energy that is left in the wake i.e.

$$E_z^2 L_d = E_l^2 L. \tag{1.28}$$

Here, E_z is the electric field gradient in wake, L_d is the depletion length, E_l is the laser electric field and L is the pulse length. The depletion length of the laser is given by [51]:

$$L_d \approx \left(\frac{\lambda_p}{\lambda}\right)^2 \lambda_p \frac{2}{a_0^2} \ , \qquad for\ a_0^2 \ll 1 \tag{1.29}$$

$$L_d \approx \left(\frac{\lambda_p}{\lambda}\right)^2 \lambda_p \frac{\sqrt{2}}{\pi a_0} \ , \qquad for\ a_0^2 \gg 1 \tag{1.30}$$

For example, in the non-relativistic regime, if a laser pulse with wavelength $\lambda = 0.8\,\mu m$ propagates in a plasma of density $n_0 = 10^{18}/cm^3$

Monika Yadav, Department of Applied Physics, Delhi Technological University, Delhi, India

$(\lambda_p = 33\ \mu m)$, the pulse depletes on propagating a distance of approximately 1.2 m.

1.7.2 Electron dephasing

As the laser pulse depletes in plasma, its leading part etches back with a velocity called etching velocity, $v_{etch} \approx c(\omega_p^2/\omega^2)$. Hence, the plasma wave excited by the pulse front also etches back with the same velocity. The modified phase velocity of the plasma wave can be expressed as $v_p' \approx v_g - v_{etch}$, where v_p' is the new phase velocity of the plasma wave and v_g is the group velocity of the laser pulse in underdense plasma. However, the electrons accelerated by the plasma wave tend to increase their energy during acceleration process. The velocity of the electrons approaches the speed of light. The electrons keep on accelerating and gaining energy until they outrun the accelerating phase of the plasma wave and reach to the dephasing (decelerating) phase (Fig. 1.9). This restricts the energy gained by the electrons to a certain value and the electrons are said to be 'dephased'. The length after travelling which the electrons slips the phase by half of the plasma period is termed as dephasing length. In simple words, it is the distance after travelling which the electrons outrun the accelerating phase of the plasma wave [52]. It can be calculated using,

$$\left(\frac{c - v_p}{c}\right) L_{dh} \approx \frac{\lambda_p}{2}. \tag{1.31}$$

The dephasing length can be evaluated by putting phase velocity of plasma wave as

$$L_{dp} \approx \lambda_p \left(\frac{\omega}{\omega_p}\right)^2. \tag{1.32}$$

However, in order to achieve a high quality electron bunch with low energy spread, the accelerated electrons have to slightly cross the dephasing length. It leads to phase space rotation and thus, minimize the energy spread of the electron beam.

Monika Yadav, Department of Applied Physics, Delhi Technological University, Delhi, India

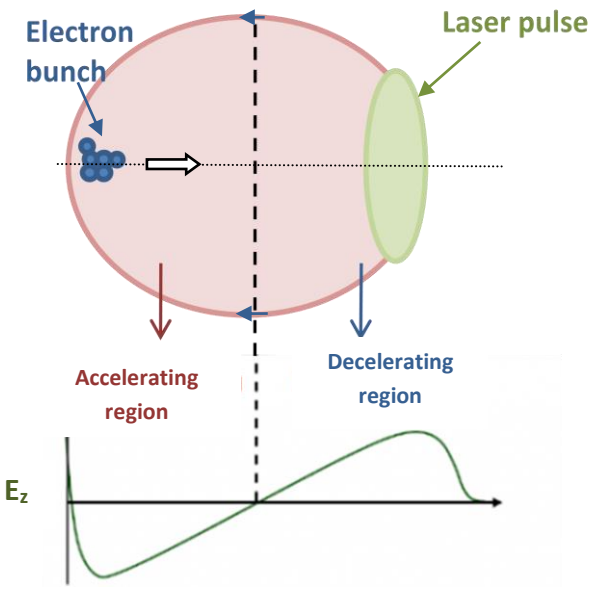

Fig. 1.9. Schematic diagram showing accelerating and deaccelerating phase of the plasma wave in bubble regime.

1.7.3 Pulse diffraction

An intense and focussed laser beam is required to drive a stronger wakefield in plasma. But the focussed beam faces laser diffraction. The propagation length is limited to a few Rayleigh lengths in the absence of any optical guiding. To increase the interaction length, the beam needs to remain focused. It can be done via relativistic self-focusing or density variation due to ponderomotive nonlinearity. Although self-focusing is the simplest way to be employed using plasma density channel is also a very efficient way to keep laser guided to a larger distance. The basic idea of plasma channel is to generate a structure that can compensate for the diffraction. It has a density minimum on axis and nearly parabolic radial density variation up to the edges [53,54], $\Delta n_{pc} \sim \Delta n(r^2/r_0^2)$, where Δn is the difference between the density on-axis $(r = 0)$ and at $r = r_0$, r_0 is the radius of the density channel. This means $\partial\eta/\partial r < 0$ and hence, possibility of guiding of the laser beam. A Gaussian beam is focussed for a matched spot size of the beam, $r_b = r_0$, provided $\Delta n = \Delta n_c = 1/\pi r_e r_0^2$, where Δn_c is the critical channel depth and r_e is the classical electron radius.

Monika Yadav, Department of Applied Physics, Delhi Technological University, Delhi, India

1.8 Particle-in-cell (PIC) simulation

The conventional experimental and theoretical approaches were unable to provide profound insight into the large scale complex physical systems. As the degree of freedom of such systems is large enough to make theoretical technique almost unrealistic. Therefore, computer simulations came up as a powerful tool for understanding the behaviour of intricate physical phenomena.

In particle model, the motion of charged particles is followed in their self-consistent electric and magnetic fields. But this model was also limited by the incompetence of the computers to track more than a few million particles for a considerable time duration. To eliminate this limitation, a new approach, particle-in-cell (PIC), was devised. The foundation of the PIC method was laid by Dawson [55] in 1962. The PIC was formalized later by Birdsall and Langdon [56] and Dawson [57]. PIC simulations are able to provide information about charge particle distributions in the phase-space, energy spectrum, trajectories of particles, distribution of charge densities, which are helpful in explaining the physics of laser-plasma interactions [58]. In this method, the system of plasma is divided into cells with the help of grids. The particles are considered in the continuum space, while fields are considered on grid points. Instead of considering individual particles, a group of particles called macroparticle or superparticles are considered as shown in Fig. 1.10. These macroparticles shift their positions in the space called 'cell'.

Typically, each macroparticle consists of 10^6-10^7 particles. It can be conceptualized as a small part of phase-space. This makes the computational manageable. This concept is termed as ‘finite size particle approach’. It reduces the computational load by minimizing the particle interactions [59], meanwhile resembling the behaviour of the real system [60]. This is because the force remains coulombic at larger distances and becomes zero when particles overlap. This helps in retaining the collective behaviour, meanwhile reducing the collision rate. Therefore, we achieve the real condition we are interested in.

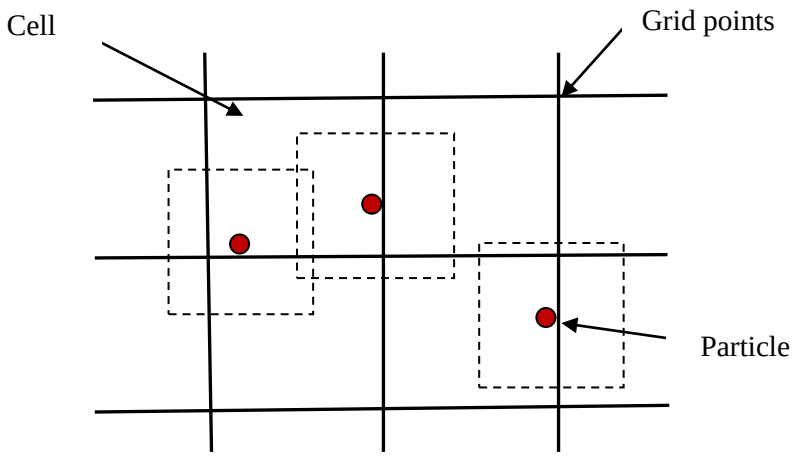

Fig. 1.10. Schematic of the grid with finite size particles in PIC method.

The algorithm of basic PIC code involves following typical steps (single PIC cycle shown in Fig. 1.11). In PIC algorithm, first the particle position and velocity information is loaded to a spatial grid simulation domain. The field information is also loaded. The particles are pushed due to the Lorentz force. Then, the charge and current densities are calculated on the grid points using initial positions and fields from nearest particles. Using Maxwell's equations, fields can be calculated using charge and current densities. The advanced fields are then interpolated to the particle positions, which exerts a Lorentz force on particles pushing them to their new positions and velocities. This cycle repeats at a specific time step Δt. PIC simulations in 3-Dimensions can be computationally challenging.

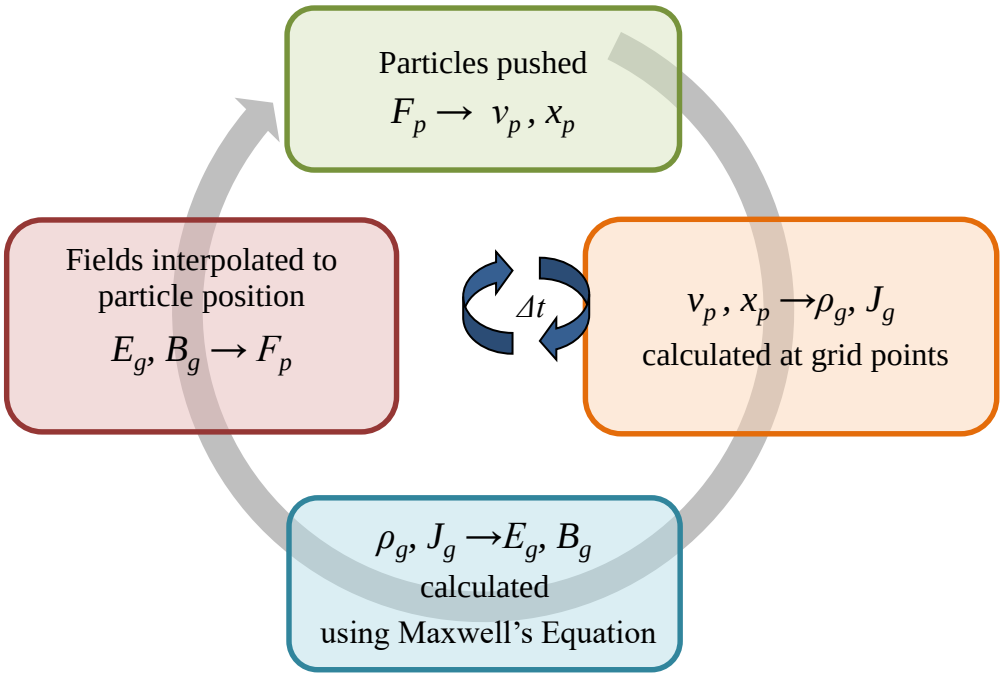

Fig. 1.11. Single computational cycle in particle-in-cell (PIC) method.

1.9 Potential applications of LWFA

Owing to the LWFA experimental verifications, we are able to realize a broad range of applications that employ unparallel characteristics of LWFA outcome. These applications range from ultrafast (fs) radiolysis, compact X-ray, γ-ray and THz sources, cancer therapy, free electron laser source, compact radioactivation machines such as PET sources, compact bunch decelerators, and plasma lens of charged particle beams, etc. Few of the applications are discussed below:

LWFA based electron beams have certain unique features which make them preferable for applications in radiobiology and radiotherapy. Such electron beam has an ultrashort pulse duration with a high instantaneous dose rate and compact size. With LWFA scheme, it is feasible to produce high energy electron beams (above 50 MeV). It has emerged as a pioneering idea for cancer radiotherapy in superficial targets [61]. These beams have a more favourable

dose distribution than advanced photon techniques. Low divergence of the LWFA produced electron beams may be beneficial in cancer therapy. Also, LWFA electron bunches are extremely short (order of a few femtoseconds) [62], which enables to perform radiolysis experiments at a much shorter time scale.

The electron bunch generated in the LWFA scheme is very small compared to the plasma wavelength in the longitudinal direction. In transverse direction, the size is much less than the laser transverse spot size. Hence, the bunch dimension is much smaller as compared to the conventional accelerators. As the charge of the electron bunch produced in LWFA scheme is comparable to the charge produced in the conventional accelerators. Therefore, the current of the electron beam is much larger as compared to the conventional case. This makes LWFA scheme highly desirable as a source of electromagnetic radiations. It is able to produce brilliant electromagnetic radiations such as betatron radiations, x-rays, terahertz (THz) radiations, gamma rays (γ-rays) etc. When an electron bunch oscillates in the wakefield, it radiates betatron radiations. The coherent and high energy electron bunches produced via LWFA acts as a suitable electron source for X-FELs. Such electron beams also have a potential application in high energy physics as they help in enhancing the understanding of matter and the origin of universe. The γ-ray pulses can be produced via LWFA betatron radiation or Compton backscattering. To obtain a compact γ-ray sources with low divergence, short pulse duration, high energy, and high peak brilliance is still a challenge. Nowadays, many advanced applications and scientific research rely on γ-rays with ultrahigh brilliance and photon energies much greater 1 MeV [63]. Such applications include exploring elementary particles, probing nuclear structures and photonuclear physics, which require γ-ray sources in the MeV to GeV range.

2.0 Organization of the thesis

This thesis is motivated to understand the laser pulse propagation in plasmas and its implications on electron acceleration by high-intensity laser. The thesis consists of six chapters dealing with physical phenomena occurring during laser-plasma interactions. Our work is mainly concentrated on theoretical and numerical simulations for electron acceleration.

- **Chapter 1:** A slight background and rationale of particle acceleration in plasma is presented in the first chapter. For better understanding of laser-plasma interaction, basic knowledge of laser and plasma is imparted in the initial part of this section. Various nonlinear phenomena occurring when laser propagates in plasma are briefly discussed. The plasma based electron acceleration mechanism is explained. We briefly discuss various plasma based acceleration schemes. Laser wakefield acceleration is specifically elaborated as the thesis work is based on this particular acceleration scheme.

- **Chapter 2:** Bubble regime of LWFA is the most fascinating and promising regime for electron acceleration. In this chapter, the dynamics of bubble, created during LWFA scheme, is investigated. The main motivation behind this work is the dependence of electron beam energy and quality on the bubble structure and its evolution. 2D particle in cell simulations are carried out to study the bubble structure. The change of bubble dimensions can be estimated by various determining factors such as the laser pulse focusing, the beam loading, the residual electrons, and the bubble velocity. It has also been confirmed that the shape of the bubble cannot be predicted using fixed shape models as spherical or elliptical. Hence, the bubble evolution strongly affects the self-injection of plasma electrons in wakefield. Various scaling laws for electron beam energy estimations are predicted in this study.

- **Chapter 3:** In this chapter, the electron beam charge and beam quality of the electron bunch generated from laser wakefield acceleration (LWFA) by a flattened Gaussian laser pulse is investigated. The change in the pulse profile in laser wakefield acceleration scheme affects the diffraction pattern, resulting the variation in laser intensity distribution during propagation in plasmas. It was observed that the flattened Gaussian laser pulse is capable to generate stronger wakefield which triggers the electron injection. Consequently, choosing a flattened Gaussian laser beam with n=6 (where n is the order of the flattened Gaussian) yields high quality electron bunch retaining relatively higher beam charge. The charge of electron bunch is about 5 times than the charge obtained by the Gaussian laser pulse. The numerical study has also been carried out to verify and validate the wakefield results generated by PIC simulations.

- **Chapter 4:** This chapter deals with the wakefield (plasma wave) excitation by a q-Gaussian laser beam and its consequence for electron acceleration. We theoretically study the propagation dynamics of a q-Gaussian laser beam in a plasma by considering the relativistic and ponderomotive nonlinearities. The q-Gaussian laser beam exhibits unique characteristics while interacting with the plasma. The q-Gaussian laser beam redistributes the plasma density in a different way, which affects the laser self-focusing. A comparative study of the self-focusing for Gaussian and q-Gaussian laser beams is reported. The results obtained from numerical analysis reveal a stronger self-focusing of the q-Gaussian laser beam in plasmas, which is desirable to excite a large amplitude plasma wave for electron acceleration by extending the interaction length. We then extended this study to investigate the electron plasma wave excitation by the q-Gaussian laser beam. The electron plasma wave is driven more efficiently by the q-Gaussian laser beam. Our results show that the electron plasma wave field intensity enhances more than twofold for the q-Gaussian laser beam in comparison with the case of a Gaussian laser beam. The electron plasma wave excited by a q-Gaussian beam can accelerate the plasma electrons to higher energies.

- **Chapter 5:** In this chapter, it has been explored that the electron plasma wave can be utilized to accelerate electrons to even higher energies in the presence of wiggler magnetic field. An additional resonance is provided to the electrons trapped in the plasma wave by the wiggler field, which contributes to the larger energy gain of electrons while accelerating. Numerical study using single particle code is carried out to validate the enhanced electron energy gain predictions due to resonance. The dependence of energy gain on plasma wave amplitude, initial electron energy, wiggler magnetic field strength is investigated. Using the theoretical model, the involvement and importance of inverse free-electron laser mechanism in electron acceleration by the plasma wave was analyzed. A scaling law for electron energy optimization was proposed for future electron accelerator development.

- **Chapter 6:** In this last chapter, a summary of outcome of this thesis work is presented. A brief on the future prospectus of this work is given.

References

[1] F. Albert, and Alec G. R. Thomas, *Plasma Phys. and Control. Fusion* **58**, 103001 (2016).

[2] M. Fuchs, R. Weingartner, A. Popp, Z. Major, S. Becker, J. Osterhoff, S. Cortrie, B. Zeitler, R. Hörlein, G. D. Tsakiris, U. Schramm, T. P. Rowlands-Rees, S. M. Hooker, D. Habs, F.Krausz, S. Karsch, and F. Grüner, *Nature Phys.* **5**, 826–829 (2009).

[3] A. E. Hussein, N. Senabulya, Y. Ma, M. J. V. Streeter, B. Kettle, S. J. D. Dann, F. Albert N. Bourgeois, S. Cipiccia, J. M. Cole, O. Finlay, E. Gerstmayr, I. Gallardo González, A. Higginbotham, D. A. Jaroszynski, K. Falk, K. Krushelnick, N. Lemos, N. C. Lopes, C. Lumsdon, O. Lundh, S.

P. D. Mangles, Z. Najmudin, P. P. Rajeev, C. M. Schlepütz, M. Shahzad, M. Smid, R. Spesyvtsev, D. R. Symes, G. Vieux, L. Willingale, J. C. Wood, A. J. Shahani & A. G. R. Thomas, *Scientific Reports* **9**, 3249 (2019).

[4] E. Pickwell and V. P. Wallace, *J. Phys. D: Appl. Phys.* **39**, R301(2006).

[5] P. Reimers , J. Goebbels, H.-P. Weise and K. Wilding, *Nucl. Instrum. Methods Phys. Res.* **221**, 201–206 (1984).

[6] A. W. Chao and M. Tigner, *Handbook of Accelerator Physics and Engineering*, World Scientific Pub. Co. (1998).

[7] C. Joshi and T. Katsouleas, *Phys. Today* **56**, 47 (2003).

[8] V. Malka, J. Faure, Y. A. Gaudue, E. Lefebvre, A. Rousse, and K. Ta Phuoc, *Nature Phys.* **4**, 447 (2008).

[9] W. Leemans and E. Esarey, *Phys. Today* **62**, 44 (2009).

[10] S. M. Hooker, *Nature Photonics* **7**, 775 (2013).

[11] D. Strickland, and G. Mourou, *Opt. Commun*. **56**, 219 (1985).

[12] C. N. Danson, C. Haefner, J. Bromage, T. Butcher, J. C. F. Chanteloup, E. A. Chowdhury, A. Galvanauskas, L. A. Gizzi, J. Hein, D. I. Hillier, N. W. Hopps, *High Power Laser Sci. Eng.* **7**, e54 (2019).

[13] J. A. Bittencourt, "*Fundamentals of Plasma Physics*," Springer-Verlag, New York (2004).

[14] F. F. Chen, *Introduction to plasma physics and controlled fusion*, Plenum Press, New York, USA (1984).

[15] N. A. Krall and A. W. Trivelpiece, *Principles of Plasma Physics*, McGraw-Hill, New York, USA (1973).

[16] P. Gibbon, *Short Pulse Laser Interactions with Matter* (Imperial College Press, London (2005).

[17] D. Umstadter, *J. Physics D: App. Phys.* **36**, 8 (2003).

[18] B. Cros, "Laser-driven plasma wakefield: Propagation effects." arXiv preprint arXiv:1705.10566 (2017).

[19] T. Tajima and D. Dawson, *Phys. Rev. Lett.* **43**, 267 (1979).

[20] Y. Kitagawa, T. Matsumoto, T. Minamihata, K. Sawai, K. Matsuo, K. Mima, K. Nishihara, H. Azechi, K. A. Tanaka, H. Takabe, and S. Nakai, *Phys. Rev. Lett*. **68**, 48 (1992).

[21] C. E. Clayton, K. A. Marsh, A. Dyson, M. Everett, A. Lal, W. P. Leemans, R. Williams, and C. Joshi, *Phys. Rev. Lett.* **70**, 37 (1993).

[22] M. Everett, A. Lal, D. Gordon, C. E. Clayton, K. A. Marsh, and C. Joshi, *Nature(London)* **368**, 527 (1994).

[23] C. Joshi, W. B. Mori, T. Katsouleas, J. M. Dawson, J. M. Kindel, and D. W. Forslund, *Nature (London)* **311**, 525 (1984) .

[24] C. M Tang, P. Sprangle, and R. N. Sudan, *Phys. Fluids* **28**, 1974 (1985) .

[25] W. Horton and T. Tajima, *Phys. Rev. A* **34**, 4110 (1986).

[26] C. Joshi, T. Tajima, J. M. Dawson, H. A. Baldis, and N. A. Ebrahim, *Phys. Rev. Lett*. **47**, 1285 (1981).

[27] K. Nakajima, et al., *Phys. Rev. Lett.* **74**, 4428 (1995).

[28] C. I. Moore, A. Ting, K. Krushelnick, E. Esarey, R. F. Hubbard, B. Hafizi, H. R. Burris, C. Manka, and P. Sprangle, *Phys. Rev. Lett.* **79**, 3909 (1997).

[29] W. P. Leemans, D. Rodgers, P. E. Catravas, C. G. R. Geddes, G. Fubiani, E. Esarey, B. A. Shadwick, R. Donahue, and A. Smith, *Phys. Plasmas* **8**, 2510 (2001).

[30] J. Krall, A. Ting, E. Esarey, and P. Sprangle, *Phys. Rev. E* **48**, 2157 (1993).

[31] L. M. Gorbunov, and V. I. Kirsanov, *Sov. Phys. JETP* **66**, 290 (1987).

[32] P. Sprangle, E. Esarey, A. Ting, and G. Joyce, *Appl. Phys. Lett.* **53**, 2146 (1988).

[33] P. Mora, and T. M. Antonsen, Jr., *Phys. Rev. E* **53**, R2068 (1996).

[34] A. Pukhov, and J. Meyer-ter-Vehn, *Appl. Phys. B: Lasers Opt.* **74**, 355 (2002).

[35] J. M. Dawson, *Phys. Rev.* **113**, 383 (1959).

[36] A. I. Akhiezer, and R. V. Polovin, *Sov. Phys. JETP* **3**, 696 (1956).

[37] E. Esarey and M. Pilloff, *Phys. Plasmas* **2**, 1432 (1995).

[38] C. B. Schroeder, P. B. Lee, J. S. Wurtele, E. Esarey, and W. P. Leemans, Phys. Rev. E **59**, 6037 (1999).

[39] E. Esarey, R. F. Hubbard, W. P. Leemans, A. Ting, and P. Sprangle, *Phys. Rev. Lett.* **79**, 2682 (1997).

[40] J. Faure, C. Rechatin, A. Norlin, A. Lifschitz, Y. Glinec, and V. Malka, *Nature* **444**, 7120 (2006).

[41] C. McGuffey, A. G. R. Thomas, W. Schumaker, T. Matsuoka, V. Chvykov, F. J. Dollar, G. Kalintchenko *et al*. *Phys. Rev. Lett*. **104**, 025004 (2010).

[42] C. E. Clayton, J. E. Ralph, F. Albert, R. A. Fonseca, S. H. Glenzer, C. Joshi, W. Lu, K. A. Marsh, S. F. Martins, W. B. Mori, A. Pak, F. S. Tsung, B. B. Pollock, J. S. Ross, L. O. Silva, and D. H. Froula, *Phys. Rev. Lett.* **105**, 105003 (2010).

[43] S. Bulanov, N. Naumova, F. Pegoraro, and J. Sakai, *Phys. Rev. E* **58**, R5257 (1998).

[44] H. Suk, N. Barov, J. B. Rosenzweig, and E. Esarey, *Phys. Rev. Lett.* **86**, 1011 (2001).

[45] X. Zhang, V. Khudik, A. Bernstein, M Downer, and G. Shvets, *AIP Conf. Proc*. **1812**, 040011 (2017).

[46] V. B. Pathak H. T. Kim, J. Vieira, L. O. Silva, and C. H. Nam, *Scientific Reports* **8**, 11772 (2018).

[47] Li, Song, Guangyu Li, Quratul Ain, Min Sup Hur, Antonio C. Ting, Victor V. Kulagin, Christos Kamperidis, and Nasr AM Hafz, *Sci. Adv.* **5**, eaav7940 (2019).

[48] T. Katsouleas, S. Wilks, P. Chen, J.M. Dawson, and J.J. Su, *Part. Accel.* **22**, 81 (1987).

[49] M. Tzoufras, W. Lu, F. S. Tsung, C. Huang, W. B. Mori, T. Katsouleas, J. Vieira, R. A. Fonseca, and L. O. Silva, *Phys. Rev. Lett.* **101**, 145002 (2008).

[50] J. P. Couperus, R. Pausch, A. Köhler, O. Zarini, J. M. Krämer, M. Garten, A. Huebl R. Gebhardt , U. Helbig, S. Bock, K. Zeil, A. Debus, M. Bussmann ,U. Schramm and A. Irman, *Nature commun*. **8**, 487 (2017).

[51] B. A. Shadwick, C. B. Schroeder, and E. Esarey, *Phys. Plasmas* **16**, 056704 (2009).

[52] E. Esarey, B. A. Shadwick, C. B. Schroeder, and W. P. Leemans, in *Proceedings of the Advanced Accelerator Concepts Workshop*, edited by V. Yakimenko AIP, New York, **737**, 578–584 (2004).

[53] X. L. Chen and R. N. Sudan, *Phys. Rev. Lett.* **70**, 2082 (1993).

[54] .E. Esarey and A. Ting, *Phys. Rev. Lett.* **65**, 1961 (1990).

[55] J. M. Dawson, *Phys. Fluids* **5**, 445 (1962).

[56] C. K. Birdsall and A. B. Langdon, *Plasma Physics via Computer Simulation*, McGraw-Hill, New York (1985).

[57] J. M. Dawson, *Rev. Mod. Phys*. **55**, 403 (1983).

[58] R. W. Hockney and J. W. Eastwood, *Computer simulation using particles*, Adam Hilger Publishers, Bristol (1988).

[59] A. B. Langdon and C. K. Birdsall, *Phys. Fluids* **13**, 2115 (1970).

[60] G. Lapenta and S. Markidis, *Phys. Plasmas* **18**, 072101 (2011).

[61] R. Polanek, Nasr A. M. Hafz, Zs. Lécz, D. Papp, C. Kamperidis, Sz. Brunner, E. R. Szabó, T. Tőkés, and K. Hideghéty, *Nucl. Instrum. Methods Phys. Res. Sec. B* **987**, 164841 (2021).

[62] O. Lundh, J. Lim, C. Rechatin, L. Ammoura, A. BenIsmaïl, X. Davoine G. Gallot, J. P. Goddet, E. Lefebvre, V. Malka , J. Faure, *Nat. Phys.* **7**, 219 (2011).

[63] Zhu, Xing-Long, Min Chen, Su-Ming Weng, Tong-Pu Yu, Wei-Min Wang, Feng He, Zheng-Ming Sheng, Paul McKenna, Dino A. Jaroszynski, and Jie Zhang, *Sci. Adv.* **6**, eaaz7240 (2020).

2

LASER WAKEFIELD ACCELERATION OF ELECTRONS IN BUBBLE REGIME

2.1 Brief outline of the chapter

The bubble regime of the laser wakefield acceleration is one of the promising mechanisms for generating quasi-monoenergetic electron beams. In this chapter, we explore the dynamics of bubble structure in petawatt regime. The dependence of the beam energy and beam quality on the shape of the bubble is one of the main motivations behind this work. The bubble length and bubble shape are investigated using two-dimensional particle-in-cell (2D-PIC) simulations. The evolution of bubble with time, and the correlation of bubble length (longitudinal and transverse radius) with the intensity of laser pulse are revealed. The change of bubble dimensions can be estimated by various determining factors such as the laser pulse focusing, the beam loading, the residual electrons, and the bubble velocity. Consequently, the self-injection of plasma electrons in the bubble is seriously affected by the bubble evolution. Various scaling laws for electron beam energy estimations are predicted in this investigation. High quality electron beam can be obtained by controlling the bubble evolution, which may have significant applications in future coherent light sources, biomedical, condensed matter physics, and X-ray generation by table-top free electron laser (FEL).

2.2 Introduction

Laser wakefield acceleration (LWFA) is one of the most promising acceleration mechanisms in present since it was first proposed in 1979 by Tajima and Dawson [1]. It is due to their ability to generate quasi-monoenergetic electron bunches with upto GeV energies in millimetre/centimetre length plasmas [2-5]. The development in this field has been made possible by the progress in ultra-intense laser technology. Currently, based on chirped pulse amplification (CPA) technique, ultra-high intensity lasers with peak powers in hundreds of terrawatt (TW) or even pettawatt (PW) regime [6,7] have been demonstrated all over the world. A PW laser system is able to generate a focused intensity of 10^{20} to 10^{22} W/cm^2. A compressed pulse with pulse duration shorter than 20 fs and peak power of approximately 5 PW has been achieved on multi-petawatt 3-cascaded all-optical parametric chirped-pulse amplification laser facility [8]. Due to these great achievements in laser technology, it has become convenient to carry out researches in LWFA in highly non-linear regime (bubble or blow-out regime) [9-12]. The bubble is a wake structure formed when the driver pulse is intense enough to expel out all the electrons radially outward leaving a cavitated region behind the driver, surrounded by a sheath of relativistic high density electrons. It propagates behind the intense and tightly-focused laser pulse with nearly relativistic speed. The optimum conditions for the realization of bubble is $k_pR \approx 2\sqrt{a_0}$, where $k_p = \omega_p/c$, k_p is the plasma wave vector, ω_p is the plasma frequency, c is the speed of light, R is the focal spot size, and $a_0 \gg 1$ (a_0 is the peak normalized vector potential of the laser) [13].

It has been reported in various previous papers that sometimes electrons from the background plasma can be self-injected at the back of the bubble and get accelerated by the longitudinal space charge field of the bubble. Although, several techniques have been developed to induce the electron injection in the bubble such as colliding pulse injection [14,15] , ionization induced injection [16,17], density transitions [18,19] etc. But it is highly desirable to get the

electrons self-injected in the bubble, realizing the experimental challenges related to small spatial and temporal scales of laser wakefield acceleration. The evolution of the driver pulse causes various changes in the bubble geometry [20] and wake potential [21,22]. Previously, it was suggested that the bubble formation is not enough for the generation of mono-energetic beam. The collimation of the electron bunch has a dependence on the variation of the geometry of the bubble during its propagation. Therefore, understanding the mechanism of self-injection and its relation with the bubble dynamics is of key importance to control and improve the performance of laser wakefield acceleration in terms of beam energy and beam quality. Kostyukov *et al.* [23] first proposed the theory for electromagnetic fields in the bubble and its geometry. The bubble shape was assumed to be spherical in their study. The slower bubble velocities and the impact of residual electrons were ignored by Kostyukov *et al.* [23] Sadighi-Bonabi *et al.* [24] presented the ellipsoidal cavity model and found it more consistent to explain the monoenergetic electron trajectory in relativistic regime. Wu *et al.* [25] modified the theory by taking only residual electrons in to account. The change in the bubble shape to ellipsoid was shown in the study. Kalmykov *et al.* [26,27] discussed that the self-injection mechanism is majorly governed by the driver evolution. Hence, it may cause uninterrupted self-injection causing degraded electron beam quality. Benedetti *et al.* [28] presented a study of self-injection process, providing a better insight into the relation between self-injection and wake properties like wake velocity, wake amplitude etc. In 2015, Li *et al.* [29] presented the solution for the electromagnetic fields in the non-linear bubble wake and bubble shape, taking the ellipsoidal assumption. Slower bubble velocities and residual electrons were taken in to account while obtaining the general solution.

In this chapter, bubble dynamics has been studied in a systematic way. Quantitative information has been provided for the bubble geometry using 2D-PIC simulations [30,31]. It is shown that self-injection cannot be studied by taking a fixed bubble geometry, either spherical or ellipsoidal as the bubble geometry cannot be considered a constant in time (non-evolving). The bubble continuously changes depending on the wake properties such as wake velocity, wake amplitude, residual electrons etc. As the wake properties vary with time,

bubble also evolves. The electron beam quality is associated with the self-injection of electrons, and hence the bubble dynamics. Plasma parameter (density) is used as a controlling parameter to produce a high quality electron beam. The improvement in beam properties resulting from this is likely to be very significant in biomedical imaging, high energy density science, and ultrafast condensed matter [32,33]. In this chapter, we explore the geometry (shape/size) of the bubble using Particle-in-cell simulation method. The longitudinal and transverse bubble radius evolution with time and its dependence on laser pulse evolution is shown. A qualitative discussion on the influence of laser strength parameter (a_0) on bubble radii and the maximum energy gain is presented. The varying bubble shape estimation is also reported in this chapter. The self-injection of electrons in bubble as a function of bubble size and shape is discussed. The controlling and improving of the electron beam quality by optimizing the plasma density is reported. In the last section, a result summary is put forward.

2.3 Simulation model

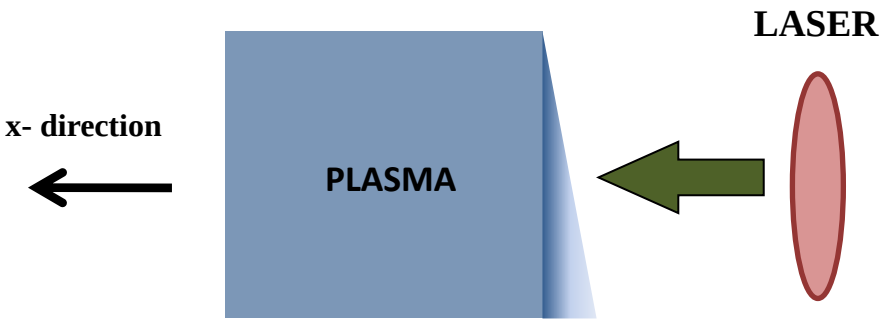

Fig. 2.1. Schematic of the laser pulse launched in plasma with plasma length of 1.2 mm.

In order to observe the shape and size of the bubble, 2D-PIC simulations have been performed on a relativistic and self-consistent plasma simulation code. A Gaussian laser pulse, linearly polarized in y-direction, of pulse duration $\tau = 20\ fs$, laser spot size $r_0 = 12\ \mu m$, laser wavelength $\lambda = 1\ \mu m$, and power in

petawatt regime is propagated in an underdense plasma. The simulation is run for approximately 1.2 mm propagation length. The laser pulse is launched in the x-direction and is channel-guided. The plasma density considered in the simulations is 10^{19} cm^{-3}. The schematic diagram illustrating laser pulse launched in plasma is shown in Fig. 2.1. The longitudinal and transverse resolution of the simulation are $\lambda/30$ and $\lambda/8$, respectively. A moving window of size 100 × 65 μm^2 is considered moving with the velocity of light. 3000× 292 cells have been used with two particles per cell. And the background of ions is considered immobile in the simulations.

2.4 2-Dimensional PIC Simulation Results

(a) Evolution of bubble radius

As the process of self-injection of electrons in bubble wake is closely related to the evolution of bubble. Thus it is crucial to understand the dynamic process of bubble lengthening. Bubble shape is basically characterized by longitudinal (r_{bl}) and transverse radii (r_{bt}). The longitudinal radius can be measured as the length of the accelerating part of the wake. The transverse radius can be calculated from the centre of the bubble to the electron sheath (where the electron density equals the background density).

The bubble radii are estimated using density plots obtained from the simulations. The bubble radii (longitudinal and transverse) as taken from the simulations at different time during the evolution are shown in Fig. 2.2 (a) and 2.2 (b). The bubble evolution has been studied for three different values of a_0 (i.e., a_0=10, 15, 21 for the corresponding laser intensities 1.37 ×10^{20}, 3.1×10^{20}, 6.4 ×10^{20} W/cm^2, respectively) to confirm the consistency of the results. The simulations show that the trend of the evolution of radius reported for three different laser intensity parameters is identical. The change in bubble wake dimensions is primarily dependent on the evolution of laser pulse in plasmas. Fig. 2.2 (a) shows the bubble longitudinal radius with the propagation time during bubble evolution for different laser intensity parameters. Initially, the

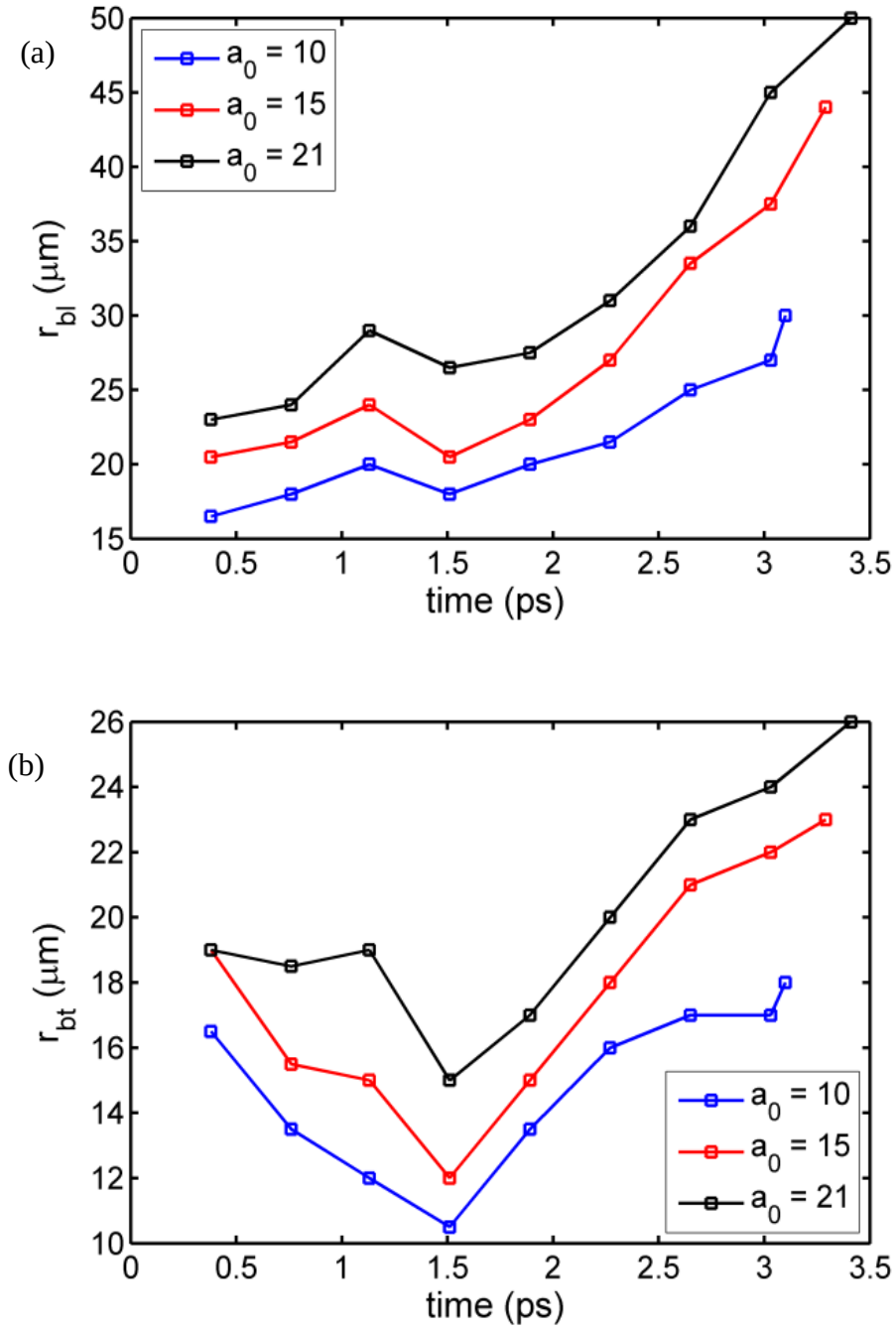

Fig. 2.2. (a) Variation of longitudinal bubble radius (r_{bl} in micron) with time (in picosecond) for different values of normalized laser strength parameter a_0=10, 15, 21. (b) Variation of transverse bubble radius (r_{bt} in micron) with time (in picosecond) for different values of normalized laser strength parameter a_0 as used for estimation of the longitudinal bubble radius. Other laser-plasma parameters considered in these simulations are as follows: laser pulse duration τ

laser spot size r_0= 12 μm, laser wavelength λ = 1 μm, and plasma density of 10^{19} cm^{-3}

longitudinal bubble radius increases with time and starts to fall at a time of t =1.2 ps. The initial lengthening of bubble is due to the intensity amplification of the pulse in plasmas. Pulse compression and self-steepening of the laser pulse are the responsible factors for laser pulse intensity enhancement. The longitudinal growth of the bubble is followed by the self-compression of the laser pulse. Physically, it can easily be understood as follows: as the plasma electrons are pushed outwards with high velocities to accelerate by the ponderomotive force of the compressed pulse front, a charge separation is created just behind the pulse. And a large electric field is created. As, the electrons behind the pulse receive a larger kick due to the compressed pulse front. Consequently, the electrons of the sheath take longer duration to return to the axis. This describes the bubble elongation process. The bubble wake evolution is therefore associated with the laser pulse evolution. The results show that the bubble longitudinal radius gets minima around t = 1.5 ps. As the laser pulse stars to focus beyond this time, the wakefield bubble evolution also starts rapidly to increase the bubble radius. The enhanced intensity of the focused laser pulse assists in bubble evolution. The transverse radius of the bubble shows the similar behaviour as shown in Fig. 2.2 (b). However, the transverse radius gets minima at larger propagation time. It is obvious due to the bubble evolution corresponding to the wakefield excitation by a Gaussian laser pulse in plasmas. This may be understood using the laser intensity curve in Fig. 3. Figure 2.3 shows variation of laser peak intensity and bubble radius with propagation time. It corresponds to the oscillation of the laser longitudinal spot size. The laser intensity falls leading to the shrinkage of the bubble. The laser intensity falls and then gradually rises, leading to further elongation of bubble longitudinal radius after 1.5 ps. Further increase in the length of the bubble might be due to other factors such as the beam loading. The transverse bubble radius evolution shows a slightly different trend from that of the longitudinal bubble radius evolution. This might be due to the evolution of transverse spot

size. The laser evolves differently in the transverse direction leading to a different evolution pattern of transverse bubble radius.

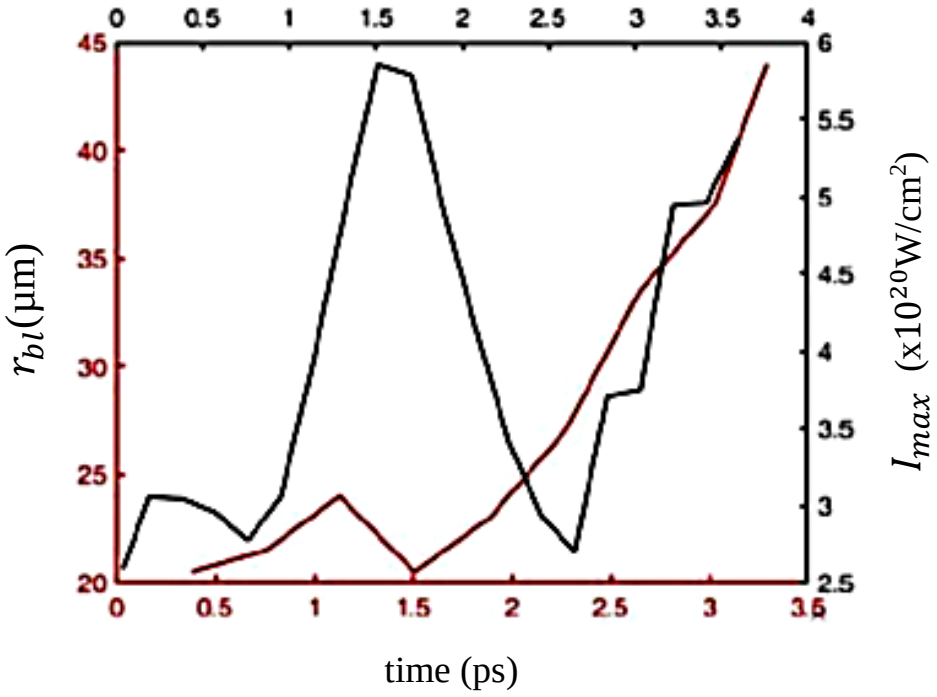

Fig. 2.3. The black curve represents the variation in peak laser intensity ($I_{max.}$ in W/cm^2) and the red curve represents the variation in bubble length (in micron) estimated with the propagation time (in picosecond).

These findings show that the bubble radius is strongly dependent on laser intensity. This may be confirmed from Fig. 2.4, where the longitudinal bubble radius is plotted with the laser intensity parameters for different propagation time. The bubble radius increased linearly with the laser intensity parameter (a_0). This effect becomes more profound at larger propagation time due to strong wakefield evolution. This linear dependence of longitudinal radius on laser intensity parameter (a_0) can also be deduced using the theoretical models proposed by Benedetti *et al.* [27] and Tossi *et al.* [33]. We validate our results using the theory proposed in these references as follows: assuming a spherical ion cavity of radius r_{bl}, the longitudinal wakefield in the plasma wake is given by: $E_z \approx (k_p \zeta/2)E_0$, where ζ is measured from the centre of the bubble. The longitudinal field is maximum for $= r_{bl}$, where r_{bl} is given by

$(2/k_p)\sqrt{a_0}$. The diameter of the bubble is approximately equal to the plasma wavelength in non-linear regime i.e. $\lambda_{nl} \approx (2\sqrt{a_0/\pi})\lambda_p$, which concludes that $r_{bl} \approx \lambda_{nl}/2$ (i.e. the longitudinal bubble radius is proportional to a_0). Therefore, the maximum field at the back of the bubble is given by $E_{zmax.} \approx r_{bl}/2$. Also, for $a_0 \geq 1$, the maximum electric field of the wake is $E_{zmax.\sim} a_0$. However, our simulation results show that r_{bl} has a linear dependence on a_0. The results shown in Fig. 2.3 are corresponding to this outcome. The bubble radius increases with the laser intensity parameter a_0. This behaviour is more severe for large propagation time, which is obvious due to strong wakefield evolution. The results have been compared with some previous studies and are found in agreement with the 2D simulation results obtained by Benedetti *et al.* [28] and Toosi *et al.* [34]. As the bubble expands, the electrons trapped at the back of the bubble experience a strong field gradient and get accelerated. A maximum energy is attained by the electrons before entering the decelerating phase. As observed previously that the bubble radius is strongly sensitive with the laser strength parameters. Thus the maximum electron energy gain should be laser intensity dependent.

(b) Dependence of electron energy on laser intensity parameter

To show these findings, we obtained the maximum electron energy ($\gamma_{max.}$) for different values of normalized laser strength parameter (a_0) in Fig. 2.3 (red curve). Five sets of simulation have been performed for different laser intensity parameters (a_0=10, 12.5, 15, 18 and 21). The electrons gain maximum energy about 0.65 GeV, 0.7 GeV, 0.79 GeV, 0.85 GeV, and 0.9 GeV for the corresponding laser intensity parameters of a_0=10, 12.5, 15, 18 and 21, respectively. The energy gain in LWFA depends on the maximum wakefield amplitude and the accelerating length. As one sees in Fig. 2.4 that the longitudinal bubble radius increases with a_0, which indicates the larger accelerating phase for electron acceleration. As dephasing length is proportional to $\sqrt{a_0}$, therefore, the trapped electrons traverse larger distance before getting dephased. A systematic tabulation of simulation parameters for bubble evolution is reported in Table 2.1. Our results clearly shows that, by varying the laser

intensity parameter, the bubble evolution can be examined for electron energy gain estimation in LWFA. Using these simulation results, one may predict the electron energy gain from LWFA in petawatt regime, where the bubble evolution is crucial in determination of wakefield strength.

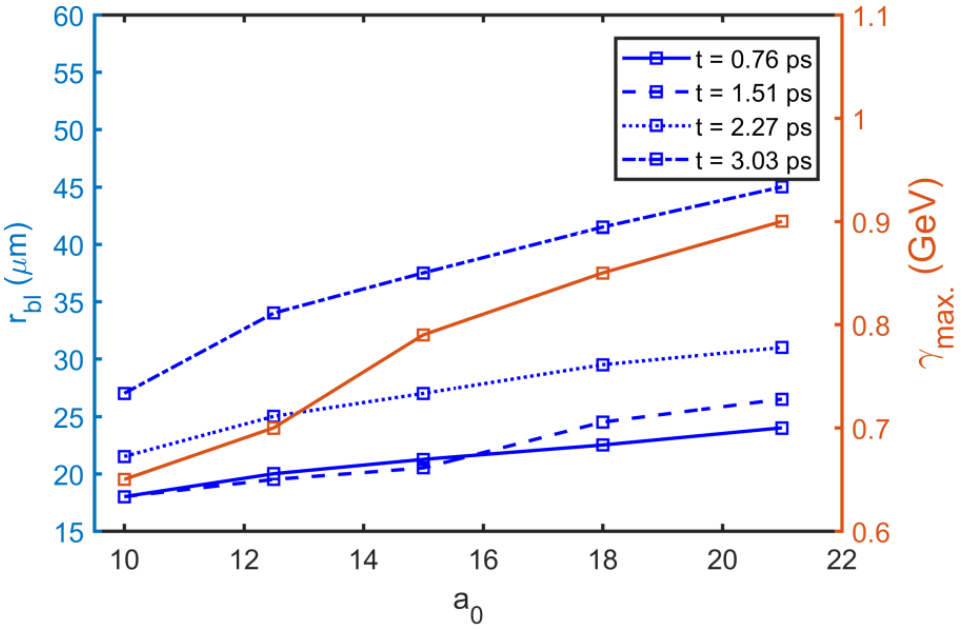

Fig. 2.4. Scaling of the longitudinal bubble radius (r_{bl}) with normalized strength parameter (a_0). Different line styles show the variation of r_{bl} with a_0 for different propagation times (t = 0.76, 1.51, 2.27, and 3.03 ps) and maximum electron energy gain with a_0 is shown (red curve). All other laser plasma parameters used in these simulations are same as used in Fig. 2.1.

a_0	I_0 ($\times 10^{20}$ W/cm^2)	K.E$_{(max)}$ (GeV)	$r_{bl(max)}$ (μm)	t (ps) for $r_{bl(max)}$
10	1.37	0.65	29	3.10
15	3.1	0.79	44	3.29
21	6.4	0.9	50	3.41

Table 2.1. A systemic tabulation of simulation results of LWFA for a_0= 10, 15, 21.

(c) Evolution of bubble shape

The bubble radii and their evolution have already been discussed. But in order to explore the shape of the bubble, both longitudinal and transverse radii have to be considered collectively. Hence, the ratio of longitudinal to transverse radius (r_{bl}/r_{bt}) has been evaluated to study the bubble geometry. The evolution of the ratio of longitudinal to transverse bubble radius for various laser intensity parameters at different propagation time is shown in Figure 2.5. Initially, the bubble shape is almost spherical. But as the bubble traverses behind the laser in plasmas, its shape starts evolving. Shape gradually changes from spherical to elliptical (longitudinally). This can easily be understood using the results reported in Fig. 2.2. The longitudinal radius increases till 1.2 picosecond, while the transverse radius continues to fall till 1.5 picosecond. This indicates the enhanced longitudinal to transverse radius ratio (r_{bl}/r_{bt}). Eccentricity is maximum at 1.51 picosecond time. After this point, the ratio of longitudinal to transverse radius starts decreasing because of the increasing trend of transverse bubble radius beyond 1.5 picosecond time. After that the transverse radius increases slowly compared with the longitudinal radius and the bubble remains more elliptical in shape. The bubble shape and size both depend on laser pulse intensity and plasma density.

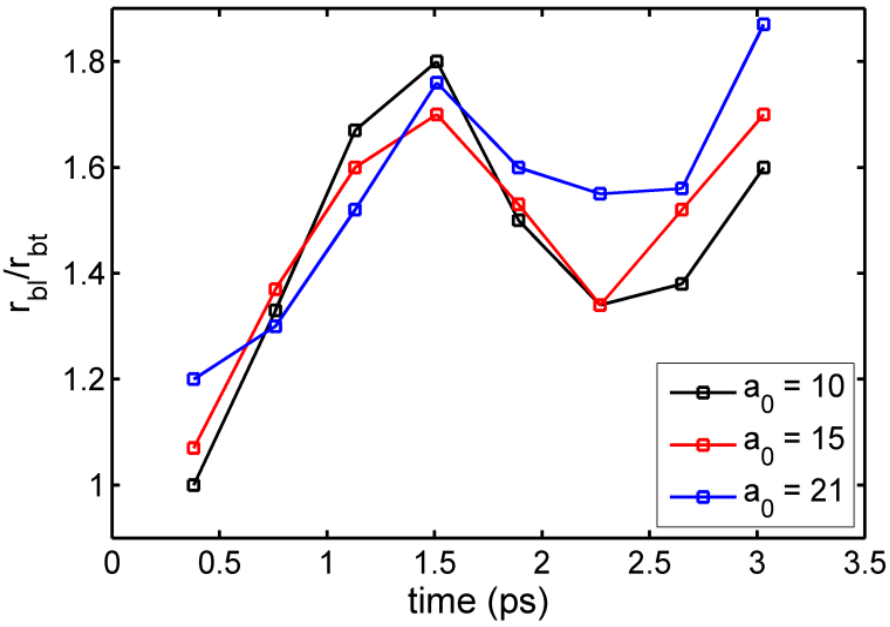

Monika Yadav, Department of Applied Physics, Delhi Technological University, Delhi, India

Fig. 2.5. Variation of ratio of longitudinal to transverse bubble radius (r_{bl} /r_{bt}) at different propagation time (in picosecond) for 3 different values of a_0 (a_0= 10, 15, 21). Other laser-plasma parameters are same as used in Fig. 2.1.

Our simulation results are in reasonable agreement with the previously proposed outcomes [13,28,34]. The bubble becomes less longitudinal ellipsoidal from its previous shape (which was more longitudinal ellipsoidal) due to increase in residual electrons and slower bubble velocity. As the laser intensity curve shows in Fig. 2.3, the laser intensity first increases up to 1.5 ps and then oscillates. The residual electrons inside the bubble alter the electromagnetic fields in the bubble as they carry certain charge and current densities. The slope of the transverse field was found to be reduced, while the slope of longitudinal field remained same. It leads to the increase in the longitudinal radius as compared to the transverse one. In this paper, our results show that the residual electrons decreases initially due to the increase in laser intensity as a result of their inverse relation. Therefore, the residual electron decreases in the beginning, which consequently leads to increase in the eccentricity of the ellipsoidal bubble up to 1.51 picosecond propagation time. Furthermore, it has been observed that the velocity of bubble is not equal to *c* (velocity of light) during the entire propagation length. As the laser pulse excites the plasma wake, it starts losing energy to the plasma wave. The front of the laser pulse etches back due to pump depletion with an etching velocity. Hence, the phase velocity of the wake is modified. It is less than the speed of light and also varying with time [36]. Therefore, this may also be a responsible factor for bubble shape evolution. And, of course, this effect may be crucial in petawatt regime. Thus, understanding the evolution of bubble provides an opportunity to explore various ways to control the bubble geometry and, therefore, improve the energy gain and the beam quality in LWFA. So, unlike previous studies, bubble shape cannot be considered to be constant. It continuously evolves with time as shown in Fig. 2.5. Hence, the results depicted in Fig. 2.5 can be used for the scaling of bubble dimension with the laser intensity for controlling and optimization of electron beam quality in LWFA. The previous studies involving bubble dimensions might get affected because of the evolving bubble shape. Hence,

considering the variable shape of the bubble in further blow-out region studies is highly desirable to obtain more realistic results.

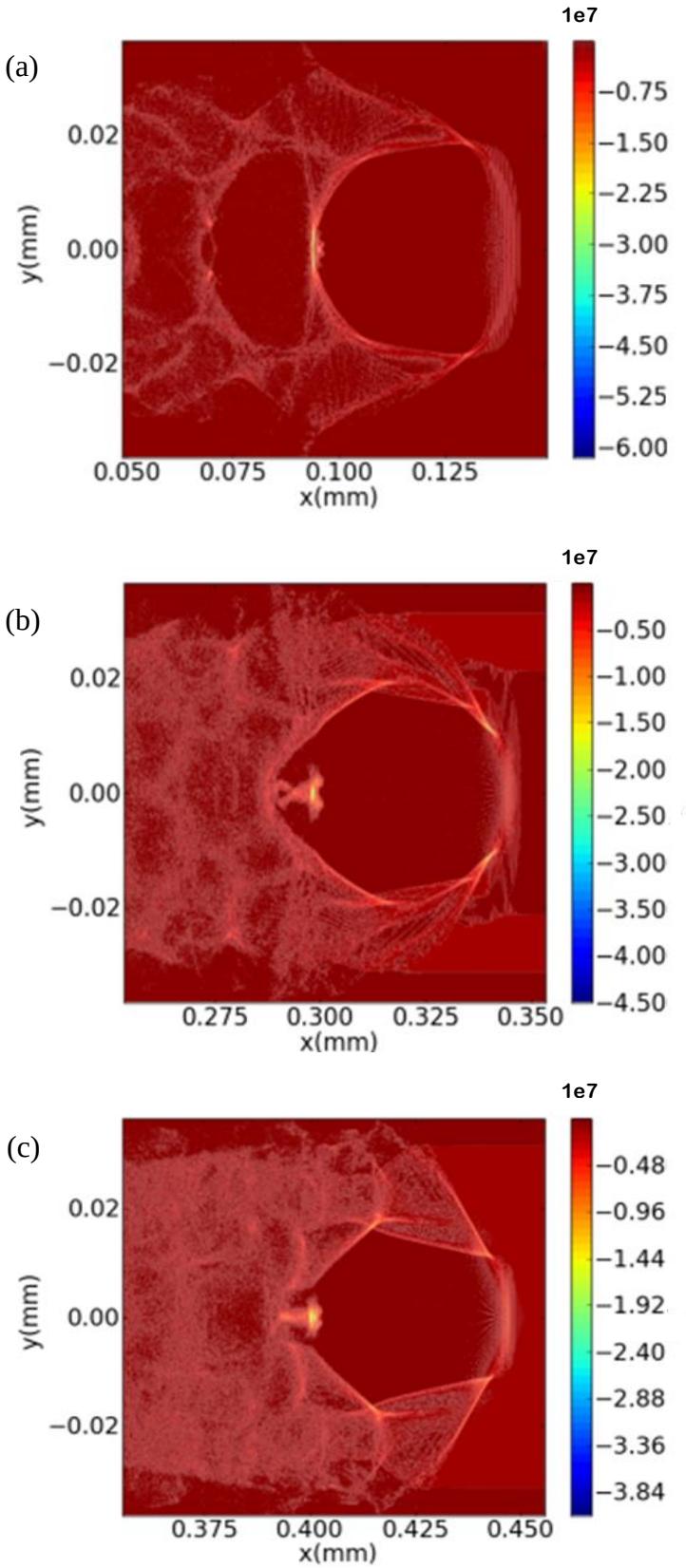

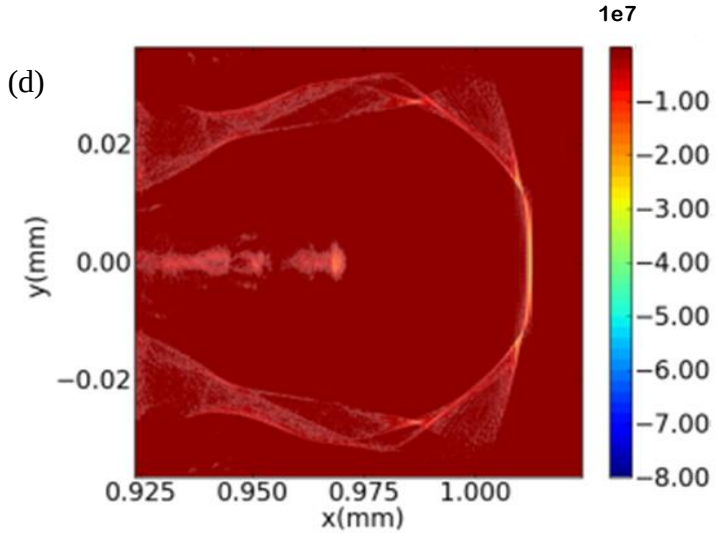

Fig. 2.6. Electron density distribution plots derived from PIC simulation at different propagation time (a) t= 0.5 ps, (b) t = 1.2 ps, (c) t = 1.5 ps, and (d) t = 3.4 ps. The laser strength parameter $a_0$considered for this simulation is 21.

Details of bubble evolution describe the mechanism of self-injection, which in turn describes key properties of electron beam such as energy spread, angular divergence, emittance etc. The density plots shown in Fig. 2.6 shows that the self-injection of plasma electrons in the bubble is seriously affected by the bubble evolution. It can be observed from Figs. 2.2 and 2.6 that no substantial injection of charge is visible as the bubble has not started to expand yet at 0.5 picosecond time. As the longitudinal radius starts to grow due to laser self-focusing, the self-injection of charge becomes noticeable at propagation time of 1.2 ps. At t = 1.5 ps, the longitudinal bubble radius falls and the corresponding injected charge in the bubble reduces. This is due to the fact that as the bubble size decreases the injected electrons gets de-trapped from the bubble. A significant amount of charge is injected into the wake only after the bubble radius has started to increase significantly (for example after the time of 1.5 ps in our case). Beyond the propagation time of 1.5 ps, however, the bubble radius continues to increase due to beam loading effect. The simulation results also show the self-injection of electrons during bubble expansion. High energy electron beam can be obtained by running the simulations up to dephasing limit

but the beam quality and charge is compromised due to uncontrolled injection. Understanding the mechanism of electron injection in the bubble is crucial to control the beam quality by controlling the injection. This undesirable effect can be avoided if injection is made a one-time event. In this particular paper, the main focus was to investigate the evolution of bubble (blow-out regime) structure in laser wakefield acceleration scheme. Certain optimized parameters were chosen to run the simulation. The plasma density equals to 5×10^{18} cm^{-3} was used to observe the blow-out regime. The injection of electrons in the bubble and formation of electron bunch was noticeable in the simulation results.

(d) Electron energy spectra

Extending our work to obtain even better quality and higher charged electron bunch, further simulations were carried out by varying plasma density, keeping all other parameters same. The value of plasma density is optimized to obtain a better quality quasi-monoenergetic electron beam, as shown in Fig. 2.7. We obtain the electron energy spectra for different plasma densities (n = 6×10^{18} and 4×10^{18} cm^{-3}). It has been observed that lowering the plasma density reduces the electron energy gain but assists in electron number enhancement. It is due to the reason that the self-injection terminates at a point of shrinkage of bubble and the bunch shortens. The electrons injected later are closer to the bubble axis and are, therefore, seen higher accelerating gradient. The back part of the bunch matches up with the front part in energy and thus, reducing the energy spread. The final energy of the electron bunch can be estimated about 1.3 GeV approximately over a length of 2.5 mm. (considering the accelerating gradient be preserved over the dephasing length).

We predict that the plasma density of 4×10^{18} cm^{-3} produces a highly mono-energetic beam and no secondary injections are observed. A monoenergetic electron bunch obtained of peak energy 0.72 GeV and 0.35 GeV has been obtained for plasma density 6×10^{18} cm^{-3} and 4×10^{18} cm^{-3}, respectively.

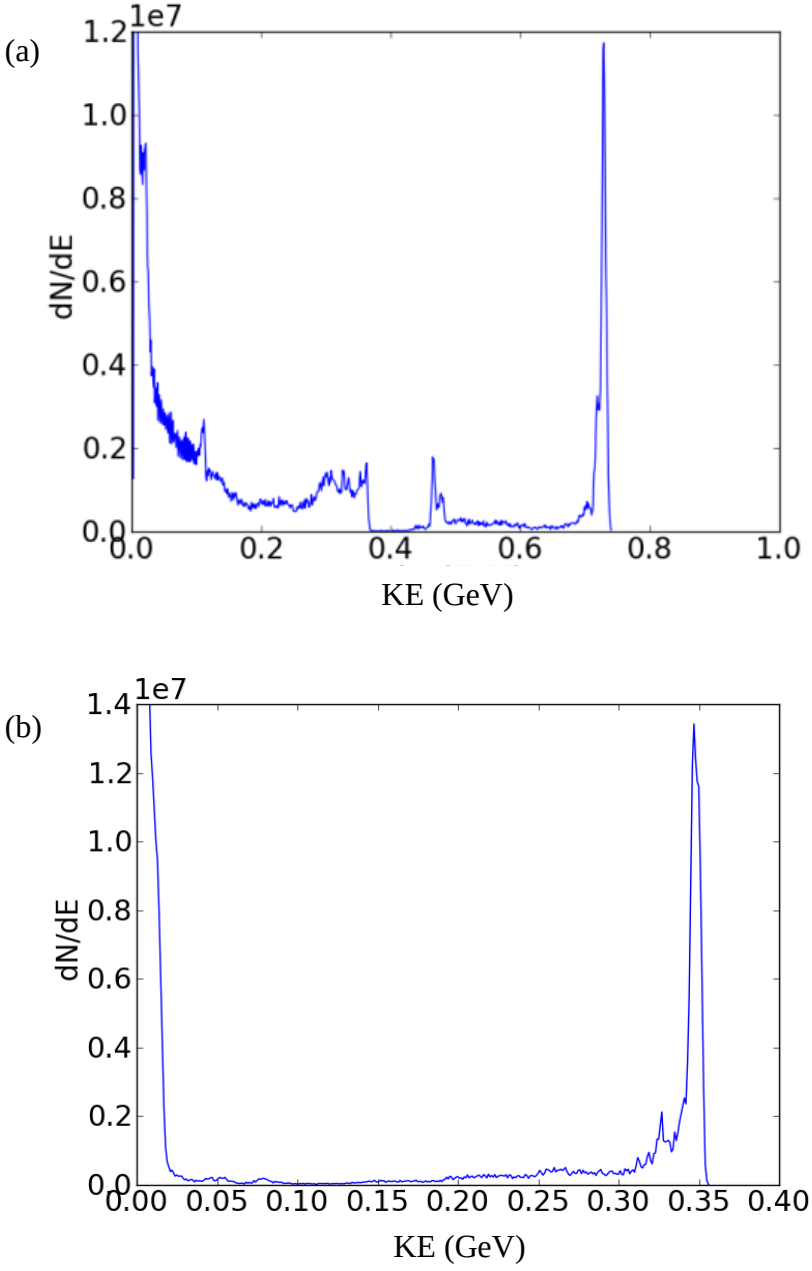

Fig. 2.7. Electron energy spectra for (a) plasma density 6×10^{18} cm^{-3} and (b) 4×10^{18} cm^{-3} for laser intensity parameter a_0= 21. Other laser parameters used are: laser pulse duration τ = 20 fs, laser spot size r_0= 12 μm, and laser wavelength $\lambda = 1$ μm.

The computed charge of the electron bunch for density of 6×10^{18} cm^{-3} is approximately 294 pC corresponding to the peak energy. This charge estimation for plasma density of 4×10^{18} cm^{-3} is about 356 pC. However, the energy spread

in both the cases is calculated to be less than 1%. The electron bunch charge delivered by the lower plasma density case is found to be greater than the higher plasma density case. For a_0=21, the normalized transverse emittance of the electron beam computes to about 1.59 and 0.87 π mm mrad for 4×10^{18} cm^{-3} and 6×10^{18} cm^{-3}, respectively. Usually, the beam emittance varies with both the bubble size and plasma density. The transverse emittance of the beam reduces for lower plasma density, which is justified with the scaling laws provided by Kneip *et al.* [36]. The electron beam parameters for both the plasma densities are collectively presented in Table 2.2.

Plasma density	6×10^{18} cm^{-3}	4×10^{18} cm^{-3}
Bunch charge (pC)	294	356
Tran. Emittance (π mm mrad)	0.87	1.59
Energy spread (%)	<1	<1
Peak energy (GeV)	0.72	0.35

Table 2.2. Electron beam parameters for different plasma densities (6×10^{18} cm^{-3} and 4×10^{18} cm^{-3}).

Such electron beams can be of great use for a number of applications requiring high charged electron beam like in seeding high-flux γ-ray, electron radiography, radiobiology and in the fast ignition scheme and so on.

2.5 Conclusion

In this chapter, the bubble evolution in laser wakefield acceleration has been predicted via 2D-PIC simulations. The evolution of bubble has been shown to be dependent on driver evolution. The self-injection dynamics and its relation with the bubble evolution have been discussed. Injection is facilitated by bubble expansion and contraction suppresses it. As beam energy and the beam quality is determined by the electron injection, hence, it is necessary to

understand the bubble evolution. It has also been demonstrated that continuous injection sometimes degrades the beam quality, therefore controlling injection is fundamental. Plasma density optimization has been done to obtain the improved beam quality. It has been presented that low plasma density leads to the increase in the bunch charge but at the cost of beam energy. It may be quite significant for various applications demanding high charge and low energy beam such as non-destructive-testing, condensed matter physics, radiolysis, radiotherapy etc.

References

[1] T. Tajima and J. M. Dawson, *Phys. Rev. Lett.* **43**, 267 (1979).

[2] J. Faure, Y. Glinec, A. Pukhov, S. Kiselev, S. Gordienko, Lefebvre E, J. P. Rousseau, F. Burgy and V. Malka, *Nature* **431**, 541(2004).

[3] C. G. R. Geddes, C. Toth, J. V. Tilborg, E. Esarey, C. B. Schroeder, D. Bruhwiler, C. Nieter, J. Cary and W. P. Leemans, *Nature* **431**, 538 (2004).

[4] W. P. Leemans, B. Nagler, A. J. Gonsalves, C. Toth, K. Nakamura, C. G. R. Geddes, E. Esarey, C. B. Schroeder and S. M. Hooker, *Nature Phys*., **2**, 696 (2006).

[5] K. Gopal and D. N. Gupta, *Phys. Plasmas* **24**, 103101(2017).

[6] X. Zeng, K. Zhou, Y. Zou, Q. Zhu, J. Su, X. Wang, X. Wang, X.Huang, X. Jiang, D. Jiang, Y. Guo, N. Xie, S. Zhou, Z. Wu, J. Mu, H. Peng, and F.Jing, *Opt. Lett.* **42**, 2014 (2017).

[7] T. J. Yu, S. K. Lee, J. H. Sung, J. W. Yoon, T. M. Jeong, and J. Lee, *Opt. Exp.* **20**, 163054 (2012).

[8] J. H. Sung, S. K. Lee, J. Y. Yoo, J. W. Yoon, C. W. Lee, J. M. Yang, Y. J. Son, Y. H. Jang, S. K. Lee and C. H. Nam, *Opt. Lett.* **42**, 2058 (2017).

[9] A. Pukhov and J. Meyer-ter-vehn, *Appl. Phys. B* **74**, 355 (2002).

[10] J. B. Rosenzweig, B. Breizman, T. Katsouleas, and J. J. Su, *Phys. Rev. A* **44**, R6189 (1991).

[11] P. Mora and T. M. Antonsen, *Phys. Rev. A* **44**, R6189 (1991).

[12] S. Gordienko, and A. Pukhov, *Phys. Plasmas* **12**, 043109 (2005).

[13] W. Lu, C. Huang, M. Zhou, and M. Tzoufras, *Phys. Plasmas* **13**, 056709 (2006).

[14] E. Esarey, R. F. Hubbard, W. P. Leemans, A. Ting, and P. Sprangle, *Phys. Rev. Lett.* **79**, 2682 (1997).

[15] J. Faure, C. Rechatin, A. Norlin, A. Lifschitz, Y. Glinec and V. Malka, *Nature* **444**, 737 (2006).

[16] S. Bulanov, N. Naumova, F. Pegoraro, and J. Sakai, *Phys. Rev. E* **58** R5, 257 (1998).

[17] C. G. R. Geddes, K. Nakamura, G. R. Plateau, C. Toth, E. Cormier-Michel, E. Esarey, C. B. Schroeder, J. R. Cary and W. P. Leemans, *Phys. Rev. Lett.* **100**, 215004 (2008).

[18] A. J. Gonsalves, K. Nakamura, C. Lin, D. Panasenko, S. Shiraishi,, T. Sokollik, C. Benedetti, C. B. Schroeder, C. G. R. Geddes, J. van Tilborg, J. Osterhoff, E. Esarey, C. Toth & W. P. Leemans ,*Nature Phys.* **7** , 862 (2011).

[19] S. Kalmykov, S. A. Yi, V. Khudik, and G. Shvets, *Phys. Rev. Lett.* **103**, 135004 (2009).

[20] A. Sävert, S. P. D. Mangles, M. Schnell, E. Siminos, J. M. Cole, M. Leier, M. Reuter, M. B. Schwab, M. Möller, K. Poder, O. Jäckel, G. G. Paulus, C. Spielmann, S. Skupin, Z. Najmudin, and M. C. Kaluza, *Phys. Rev. Lett.* **115**, 055002 (2015).

[21] B. S. Xie, H. C. Wu, H. Wang, N. Y. Yang, and M. Y. Yu, *Phys. Plasmas* **14**, 073103 (2007).

[22] M. Yadav, D. N. Gupta, S. C. Sharma and Hyyong Suk, *Laser Phys. Lett.* **17**, 076001(2020).

[23] I. Kostyukov, A. Pukhov, and S. Kiselev, *Phys. Plasmas* **11**, 5256 (2004).

[24] R. Sadighi-Bonabi and S. H. Rahmatollahpur, *Phys. Plasmas* **17**, 033105 (2010).

[25] H. C. Wu, B. S. Xie, S. Zhang, X. R. Hong, X. Y. Zhao, and M. P. Liu, *Phys. Plasmas* **17**, 113103 (2010).

[26] S. Y. Kalmykov, A. Beck, S. A. Yi, V. N. Khudik, M. C. Downer, E. Lefebvre, B. A. Shadwick, and D. P. Umstadter, *Phys. Plasmas* **18**, 056704 (2011).

[27] S. Kalmykov, S. A. Reed, S. A. Yi, A. Beck, A. F. Lifschitz, X. Davoine, E. Lefebvre, V. Khudik, G. Shvets, P. Don, X. Wang, D. Du, S. Bedacht, Y. Zhao, W. Henderson, A. Bernstein, G. Dyer, M. Martinez, E. Gaul, T. Ditmire, M.C. Downer, *High Energy Density Phys.* **6**, 200 (2010).

[28] C. Benedetti, C. B. Schroeder, E. Esarey, F. Rossi, and W. P. Leemans, *Phys. Plasmas* **20**, 103108 (2013).

[29] X. F. Li, Q. Yu, Y. J. Gu, S. Huang, Q. Kong, and S. Kawata, *Phys. Plasmas* **22**, 083112 (2015).

[30] C. K. Birdsall, A. B. Langdon, V. Vehedi, and J. P. Verboncoeur, *Plasma Physics via Computer Simulation (*2004) CRC Press.

[31] J. M. Dawson, *Rev. Mod. Phys.* **55**, 403 (1983).

[32] V. Malka, J. Faure, Y. A. Gauduel, E. Lefebvre, A . Rousse, and A. K. T. Phuoc, *Nature Phys.* **4**, 447 (2008).

[33] F. Albert, A. G. R. Thomas, *Plasma Phys. Control. Fusion* **58**, 103001 (2016).

[34] E. S. Toosi, S. Mirzanejhad, and D. Dorranian, *Laser Part. Beams* **34**, 193 (2016).

[35] W. Lu, M. Tzoufras, C. Joshi, F. S. Tsung, and W. B. Mori, *Phys. Rev. ST Accel. Beams* **10**, 061301 (2007).

[36] S. Kneip, C. McGuffey, J. L. Martins M. S. Bloom, V. Chvykov, F. Dollar, R. Fonseca, S. Jolly, G. Kalintchenko, K. Krushelnick, A. Maksimchuk, S. P. D. Mangles, Z. Najmudin, C. A. J. Palmer, K. Ta Phuoc, W. Schumaker, L. O. Silva, J. Vieira, V. Yanovsky, and A. G. R. Thomas, *Phys. Rev. ST Accel. Beams* **15**, 021302 (2012).

3

CONTROLLED ELECTRON BUNCH CHARGE USING FLATTENED GAUSSIAN LASER

3.1 Brief outline of the chapter

We demonstrate the generation of electron bunch charge enhancement in laser wakefield acceleration using a flattened Gaussian laser pulse. The change in the laser pulse intensity profile in laser wakefield acceleration scheme affects the diffraction pattern, resulting variation in laser intensity distribution during propagation in plasmas. We employ a flattened Gaussian laser pulse to excite the wakefield for electron accelerations. Central flattened region of the flattened Gaussian laser pulse helps to preserve the pulse shape due to maintaining the stronger energy density within the pulse. The quasi- three-dimensional PIC simulations show that the flattened Gaussian laser pulse is capable to generate stronger wakefield, which triggers the electron injection. Choosing a flattened Gaussian laser pulse with $N = 6$ (where N is the order of the super Gaussian shape) yields high quality electron bunch retaining relatively higher beam charge of about 189 pC. This charge of electron bunch is about 5 times than the charge obtained by the ordinary Gaussian laser pulse (39 pC). The simulation results are well supported by the theoretical model. The high charge electron bunch may be a promising candidate to drive next-generation compact free-electron lasers with unique X-ray properties.

3.2 Introduction

High-intensity ultra-short laser pulses [1,2] have created novel scientific phenomena on atomic and molecular dynamics in strong fields, ionization dynamics, higher harmonic generation, coherent X-ray radiation, and particle acceleration [3–10]. Laser wakefield accelerators (LWFA) have been proposed as a next generation compact accelerator, which can sustain accelerating fields of hundreds of GV/m [11]. However, the accelerating electric fields in conventional accelerators are limited to orders of tens of MV/m due to material breakdown issue. During the past two decades, LWFA has been used to accelerate electrons to first some hundreds of MeV [12–14] and recently reaching to multi GeV energy level [15, 16].

In LWFA, a high-power laser pulse pushes electrons aside due to ponderomotive force, which is proportional to laser pulse intensity gradient. As laser pulse passes, a space charge field is created which made electrons to oscillate around the ions at plasma frequency, which results in a plasma wave trailing the laser pulse defined as laser wakefield. In a highly nonlinear case, ion cavity of spherical shape surrounded by an electron sheath is formed behind a strong driving laser pulse, this regime is commonly referred to as bubble or blow-out regime [17]. Electrons can be injected in this accelerating structure if they are located at the appropriate phase of the wake having sufficient initial kinetic energy. Electron bunch properties are determine by the injection process. Self-injection is the most commonly used mechanism and least experimentally demanding [18].

In this chapter, it is shown that electron injection can also be enhanced by flattened Gaussian laser pulse. The basic idea behind flattened Gaussian profiles and its propagation was initially proposed by F. Gori in 1993 [19]. The super-Gaussian model has also proved to be very useful for laser cavities with variable reflectivity mirrors. The production of flattened Gaussian beams have been reported experimentally also with elaborating the main features regarding its field distribution [20,21]. The profile/shape of the laser pulse is a significant factor to control the parameters of electron beam generated by LWFA. Various researchers

have examined the effect of frequency chirp and temporal laser pulse shape on wake excitation theoretically as well as experimentally [22-26]. The influence of laser frequency chirp on electron acceleration has been studied theoretically using different laser pulse profiles such as Gaussian, super-Gaussian and Cosine-Gaussian profiles [27]. Ostermayr *et al.* employed the super-Gaussian laser pulse to investigate the wakefield and electron beam dynamics in LWFA and also, analyzed transverse betatron oscillations [28]. Using 2D Particle-in-cell (PIC) simulations, a remarkable increment in the wakefield amplitude generated by super-Gaussian laser pulse was observed as compared to the Gaussian laser pulse [29]. Despite the work already been done in the field of laser wakefield acceleration, the charge of the electron beam and the beam quality are still of major concern.

In flat Gaussian pulse case, the flatness in the laser pulse makes flat gradient in shape. The flattened region of the flattened Gaussian laser pulse can reduce the effect of intensity variation and simultaneously minimize the shape distortion. Moreover, the flat portion of the pulse can allow to retain more energy within the pulse volume. Our results suggest that self-focusing of flattened Gaussian laser is considerable higher than the Gaussian laser pulse. The specific evolution of flat Gaussian pulse enhances self-injection which leads to copious amount of electrons into the accelerating field. The bunch charge in case of flattened Gaussian gets approximately five-folds the beam charge obtained by Gaussian laser pulse. Here, it is demonstrated that using FGP could lead to high-charge electron beam in the nonlinear regime of laser wakefield acceleration (LWFA). High electron beam charge is of great interest in number of applications like radiography, radiobiology, sub-10 *fs* jitter-free ultrafast electron diffraction experiments, high charge injector in conventional accelerators, allows single shot imaging by increasing the signal to noise ratio, produces bright gamma rays to probe dense materials and so on [30-35]. This supports that the beam charge is a crucial parameter of the generated electron beam in LWFA.

We provide particle-in-cell (PIC) simulation results supported by the theoretical model for laser wakefield acceleration of electrons using flattened Gaussian laser pulse. The advantage of large bandwidth of flattened Gaussian laser pulse for electron beam parameter optimization through LWFA is

investigated. For current laser-plasma parameters, based on this proposal, we suggest to employ a flattened Gaussian laser pulse for electron beam quality enhancement. A theoretical model for this problem is formulated in next section.. The PIC simulation results are put forward in the next Section. Finally, a short summary of this work is given in the last of this chapter.

3.3 Analytical model

Considering a laser pulse with electric field amplitude E_0, pulse length L, and wavelength λ_0, propagating in the z-direction in a plasma with density n_0. The laser pulse exerts a ponderomotive force on the plasma electrons and excites a wakefield E_w. We write the quasistatic fluid momentum and continuity equation as

$$\frac{\partial n_e}{\partial t} + \nabla.(n_e v) = 0, \tag{3.1}$$

$$\frac{d\boldsymbol{p}}{dt} = -e\boldsymbol{E} - \frac{e}{c}(\boldsymbol{v} \times \boldsymbol{B}), \tag{3.2}$$

where $n_e = n_0 + \delta n$ is the electron density and δn is the perturbed density. Also, we write the Poisson equation for the wakefield as

$$\epsilon_0 \nabla^2 \phi_w = e\delta n. \tag{3.3}$$

We consider all the quantities depend on $\xi = z - v_g t$, where $v_g = c\left(1 - \omega_p^2/\omega^2\right)$ is the group velocity of the laser pulse in plasma, $\omega_p^2 = 4\pi n_0 e^2/m'$ is the electron plasma frequency, and ω is the laser frequency. Ions are considered immobile. Using the standard perturbation approximation, the equation for wakefield can be obtained as

$$\frac{\partial^2 \phi_w}{\partial \xi^2} + k_p^2 \phi_w - \frac{ec^2 \boldsymbol{E}^2(\xi)}{2m' v_g^4} = 0, \tag{3..4}$$

where ϕ_w is the wakefield potential and $\boldsymbol{E}(\xi)$ is the laser electric field.

Monika Yadav, *Department of Applied Physics, Delhi Technological University, Delhi, India*

This is a general equation for wakefield excitation in plasmas. The third-term of Eq. (3.4) is the ponderomotive force term that drives the wakefield.

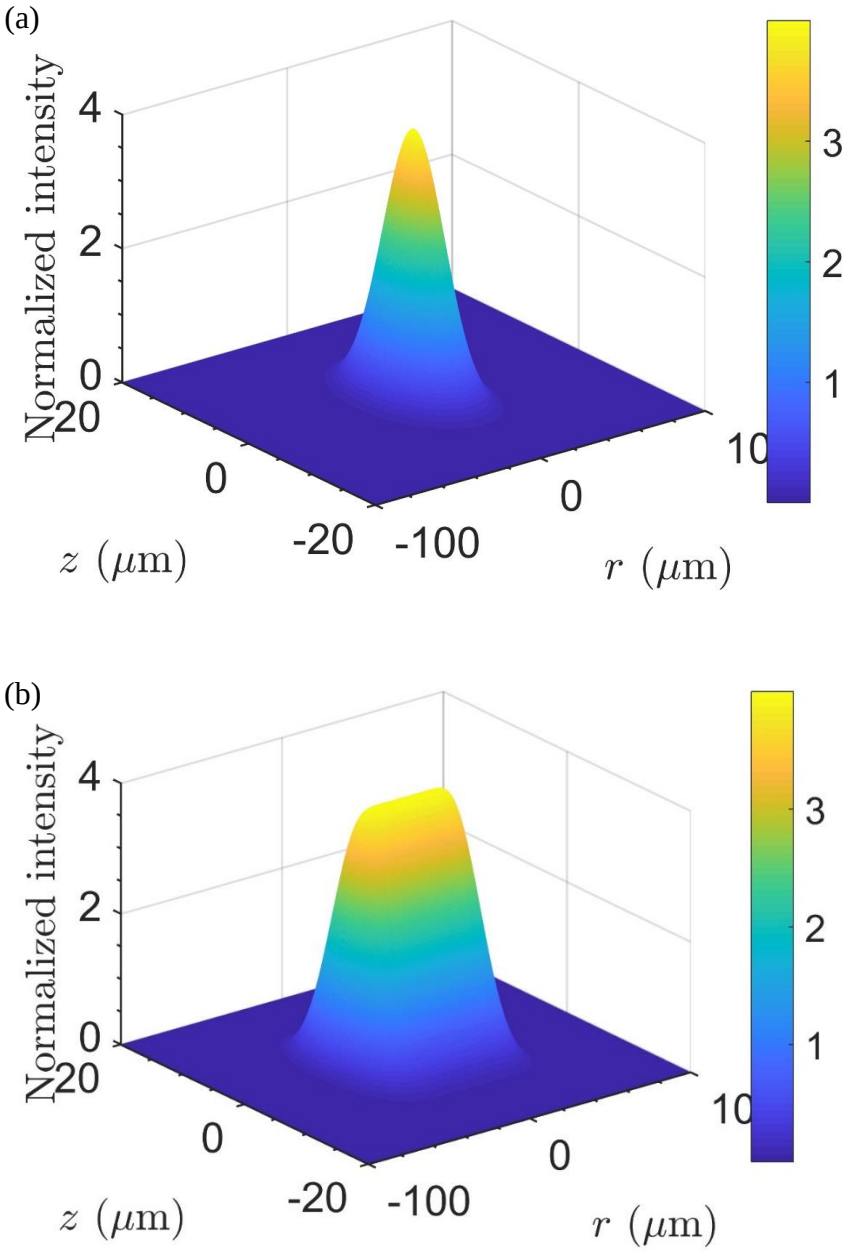

Fig. 3.1. Three-dimensional spatial intensity profile of a (a) Gaussian laser pulse ($N = 0$) and (b) flattened-Gaussian laser pulse ($N = 6$) for $a_0 = 2.0$.

The plasma density variation associated with the wakefield can be expressed as

$$\frac{\delta n}{n_0} = \frac{\gamma_\perp^2 + (1+\phi_w)^2}{2(1+\phi_w)^2}, \tag{3.5}$$

where $\gamma_\perp^2 = 1 + a_0^2$ and a_0 is the laser strength parameter.

The wakefield equation given above shows that the wakefield excitation basically depends on the laser electric field. The laser pulse shape plays a crucial role in determining the wakefield in a plasma. In this particular work, we focus on two different spatial profiles i.e. Gaussian and flattened Gaussian. For a linearly polarized Gaussian laser pulse, we consider the electric field as

$$\boldsymbol{E}(x,t) = \boldsymbol{E}_0 exp\left(\frac{-r^2}{w_0^2} - \frac{(z-z_0-ct)^2}{c^2\tau^2}\right)\cos[k_0(z-z_0-ct)]. \tag{3.6}$$

For flattened Gaussian laser profile, the electric field expression can be given as

$$\boldsymbol{E}(x,t) \propto exp\left(-\frac{(N+1)r^2}{w(z)^2}\right)\sum_{n=0}^{N}\frac{1}{n!}\left(\frac{(N+1)r^2}{w(z)^2}\right)^n, \tag{3.7}$$

where $k_0 = 2\pi/\lambda_0$ is the wave vector, $a_0 = eE_0/m'c\omega$ is the normalized peak amplitude, E_0 is the peak laser field amplitude, w_0 is the laser spot size, τ is the pulse duration, z_0 is the initial position of pulse centroid, $w(z) = \frac{\lambda_0}{\pi w_0}|z - z_{foc}|$ z_{foc} is the position of the focal plane. Here, N is defined as the laser pulse shape parameter, which defines the flatness of the laser transverse profile. For $N = 0$, we obtain a Gaussian pulse (GP) and for $N = \infty$, we obtain a flattened Gaussian pulse (FGP).

Eqs. 3.6 and 3.7 are plotted to obtain the intensity profiles of the flattened-Gaussian $(N = 6)$ and Gaussian $(N = 0)$ laser pulse for the laser parameters: $a_0 = 2.0$, $\tau = 30\ fs$, $w_0 = 24\ \mu m$, and $\lambda_p = 15.6\ \mu m$.

Monika Yadav, *Department of Applied Physics, Delhi Technological University, Delhi, India*

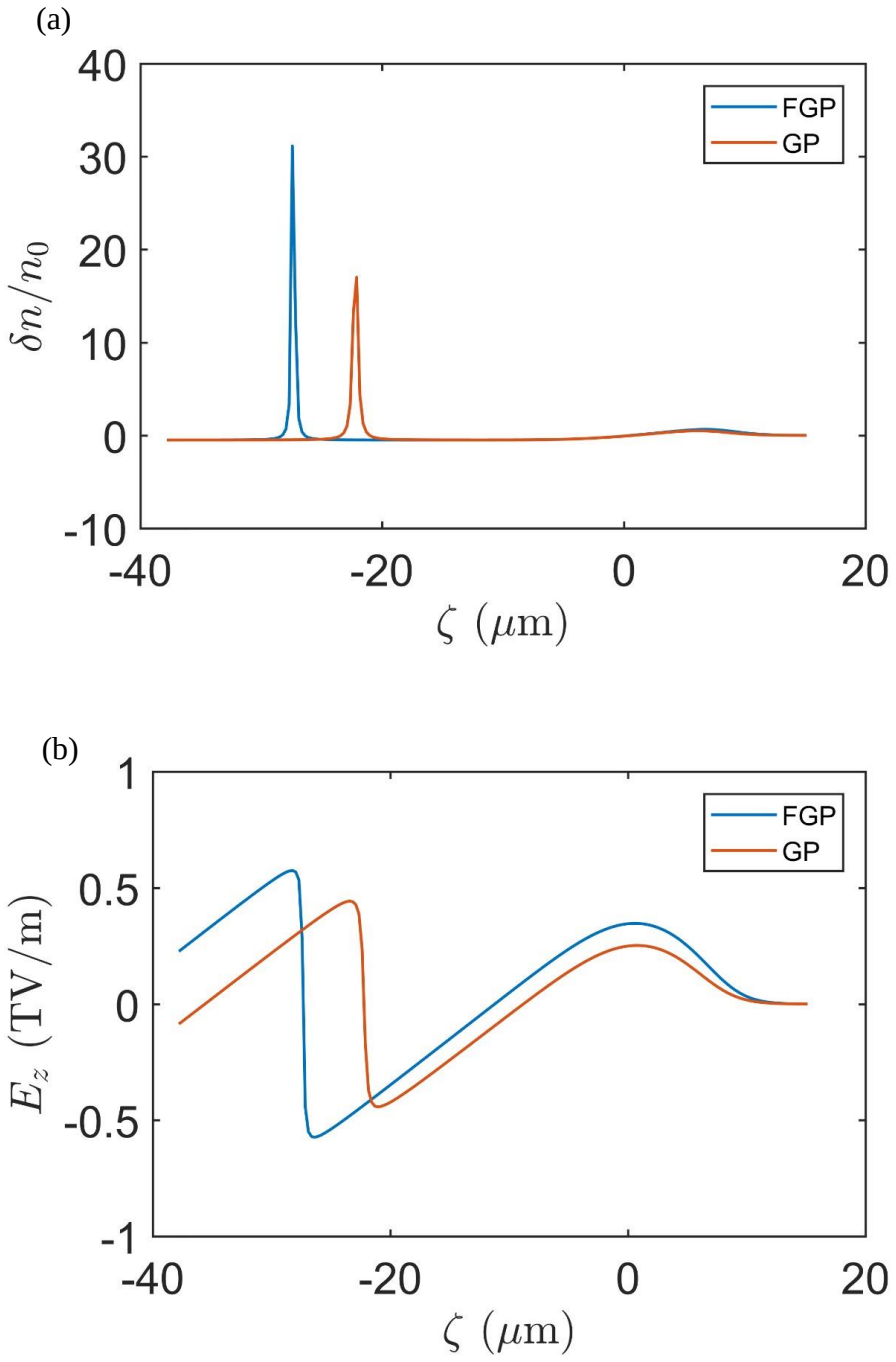

Fig 3.2. Plasma electron density perturbation and (b) the corresponding longitudinal electric field associated with the laser wakefield driven by Gaussian pulse (GP) (red curve) and flattened-Gaussian pulse (FGP) (blue curve) for $a_0 = 2.0$ with plasma density $n_0 = 4.45 \times 10^{18} cm^{-3}$.

Fig. 3.1 displays the 3-dimensional view of the spatial intensity distribution for both Gaussian as well as flattened-Gaussian laser pulse. As compared to the ordinary Gaussian intensity, the flattened intensity profile behaves like an energy step function with the enhanced pulse energy. The flat edges of the pulse profile results in enhanced energy density of the pulse. The flatness in super-Gaussian laser pulse makes flat gradient in shape. The distribution of laser intensities of both types of the pulse is depicted in Figure 3.1. The flattened region of the FGP can reduce the effect of intensity variation and simultaneously minimize the shape distortion. Moreover, the flat portion of the pulse can allow to retain more energy within the pulse volume. These unique properties of the FGP can be utilized to generate efficient wakefield for electron accelerations. The FGP can be generated by combining laser pulse shaping with ultrafast electro-optics sampling technique [36]. The pulse shape can also be flattened by using a positive and moderate nonlinear light induced change of the refractive index in a transparent material followed by a simple optical system [37].

Eqs. 3.6 and 3.7 are used in Eq. 3.4 to obtain the longitudinal wakefield excited by different laser profiles. Fig. 3.2 (a) displays the normalized electron density perturbation associated with the wakefield driven by flattened-Gaussian and Gaussian laser pulse. As noticed from the perturbed density curves, the density perturbation created behind the flattened-Gaussian laser pulse is considerably higher than the Gaussian laser pulse case. An enhancement of approximately 50% is figured for the flattened-Gaussian laser case. Fig. 3.2 (b) shows the longitudinal wakefield in *TV/m* generated by both the laser profiles. It is observed that the flattened-Gaussian laser pulse drives a stronger wakefield as compared to the Gaussian pulse. The amplitude of the wakefield in flattened-Gaussian case is approximately 33% greater than the wakefield driven by Gaussian pulse. These numerical estimations clearly show that the FGP may be better for wakefield excitation in plasmas. The large energy density of the FGP contributes effectively to excite the wakefield.

3.4 Simulation Results

To extend our insight in the laser wakefield acceleration scheme by utilizing a flattened Gaussian laser pulse, PIC simulations have been performed using FBPIC (a quasi-3D simulation code) [36]. A comparative study of laser wakefield acceleration using Gaussian and flattened Gaussian laser pulse is presented. The simulations showed that the flattened Gaussian laser pulse is more suitable for applications demanding high charge electron beam. In this study, linearly polarized Gaussian and flattened Gaussian laser pulses are considered with wavelength $\lambda_p = 0.8\,\mu m$. The LWFA simulations for both the laser profiles are carried out separately for the optimized values of laser and plasma parameters. Parameters are selected as follow: normalized laser strength parameter $a_0 = 2.0$, pulse duration $\tau = 30\,fs$, and spot size $w_0 = 24\,\mu m$. A 6th order ($N = 6$) flattened-Gaussian laser pulse is considered for these simulations. The pulse is introduced in a plasma from the left boundary of a moving window. The plasma density $n_0 = 4.45 \times 10^{18} cm^{-3}$ is considered for these simulations. The plasma wavelength is calculated to be $\lambda_p \cong 15.6\,\mu m$. A density ramp of $50\,\mu m$ is taken at the entrance with the density varying from 0 to n_0. The optimized set of laser and plasma parameters are used to obtain considerable electron injection to the wakefield. The simulation box of $60\,\mu m \times 80\,\mu m$ is considered in the longitudinal and transverse directions, respectively. The grid size is chosen as $\Delta z = 0.04\,\mu m$, $\Delta r = 0.064\,\mu m$ with 4 particles per cell. The grid size is able to resolve both laser as well as plasma wave popagation.

(a) Evolution of laser pulse

As the evolution of wakefield has a strong dependence on laser pulse evolution. Hence, it is crucial to investigate the evolution dynamics of both Gaussian as well as flattened Gaussian laser pulse in a plasma. Fig. 3.3 shows the variation of normalized laser peak amplitude a_0 as a function of propagation distance z. During the propagation of the laser pulse, the laser amplitude of flattened Gaussian laser exceeds the Gaussian laser amplitude due to the combined outcome of self-focusing and self-compression effects. The enhanced

self focusing of fattened Gaussian pulse significantly affects self-injection process.

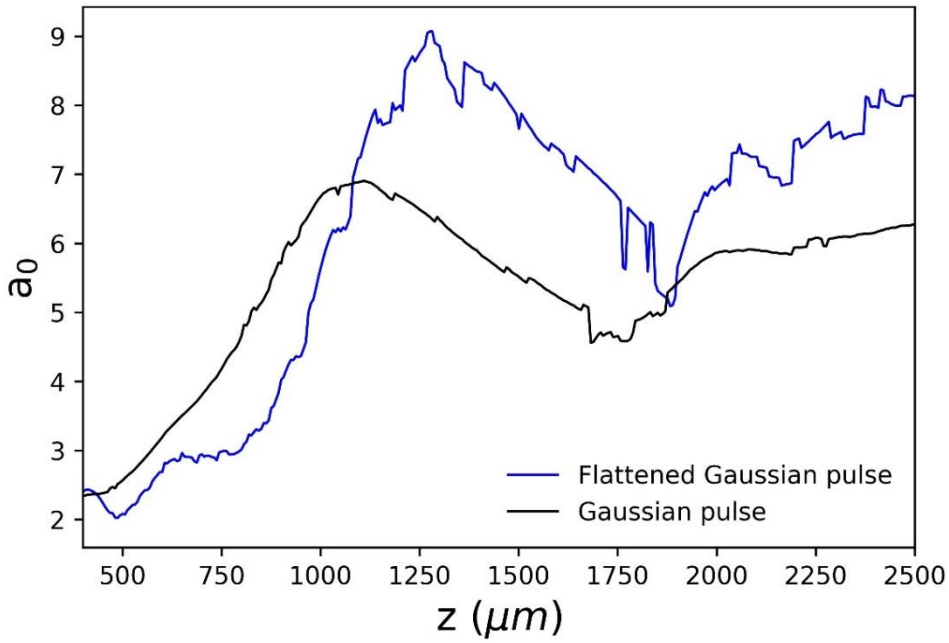

Fig. 3.3. The evolution of on-axis normalized laser peak amplitude with the propagation distance (z) for Gaussian (black curve) and flattened Gaussian (blue curve) laser pulse. The laser intensity parameter $a_0 = 2.0$ is used for these results.

(b) Wakefield evolution (depending on laser intensity)

The laser wakefield acceleration simulations are run for both Gaussian and flattened Gaussian laser pulse profiles using same parameters. In Fig. 3.4, the laser wakefield (E_z) generated by the Gaussian and flattened Gaussian laser pulse is investigated. Fig. 3.4 shows the comparison of the electron density distribution and the corresponding longitudinal accelerating field driven by Gaussian and flattened Gaussian laser pulse at a distance $z \approx 1.2\, mm$ travelled by the laser pulse. The wakefield results shown in Figure 3.4 is found to be in good agreement with the wakefield estimations obtained from numerical study (Fig. 3.2). Simulation as well as theoretical results both supports the prediction that flattened-Gaussian laser pulse excites a larger amplitude plasma wave (or wakefield). From the calculations, we found that the longitudinal electric field of

the FGP in plasma is about 27% higher than the Gaussian laser pulse case (Figure 3.4). Efficient excitation of the wakefield is observed for flattened Gaussian laser pulse as compared to the Gaussian laser pulse.

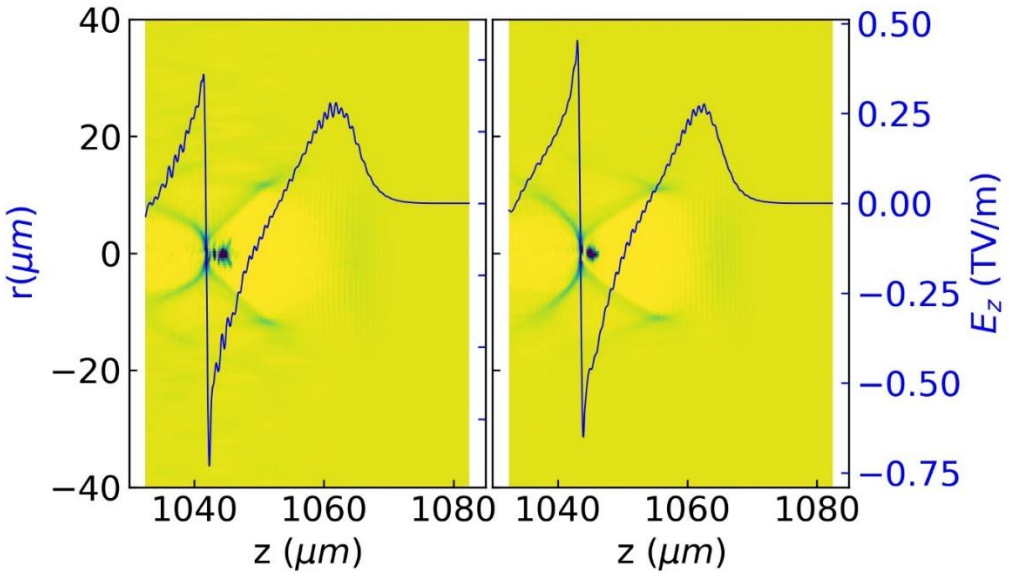

Fig. 3.4. Density distribution of the electrons and line plot of wakefield along the z-axis for flattened Gaussian pulse (FGP) (left) and Gaussian pulse (GP) (right) pulse. Longitudinal electric field E_z is increased for FGP due to enhanced self-focusing of laser pulse as it propagates through the plasma.

(c) Wakefield evolution (depending on beam loading)

Figure 3.5 shows a comparative study of total injected charge in the wake excited by Gaussian and flattened-Gaussian laser profiles. The total charge injected in flattened-Gaussian case is approximately 0.8 nC as compared to the charge injection of 0.4 nC in Gaussian case. An enhanced electron injection in case of flattened-Gaussian laser is clearly visible in Figure 4.5. Hence, the beam is loaded more in case of flattened-Gaussian profile case. It is a known fact that beam loading perturbs the wakefield. The charge accelerated in the bubble wake drives a plasma wave which tends to negate the laser wakefield [38].

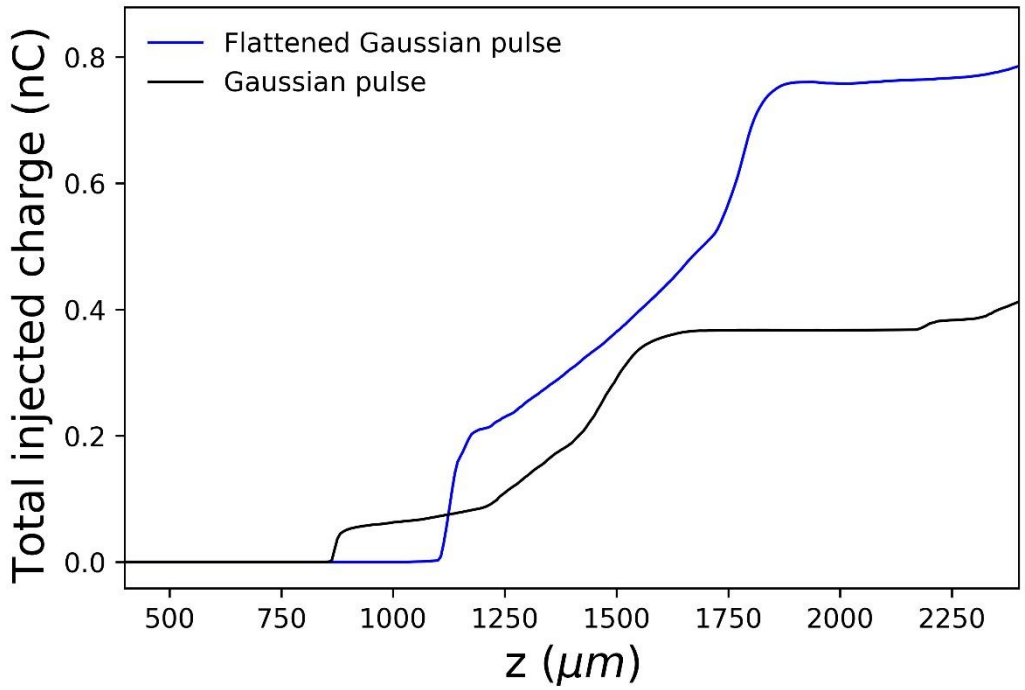

Fig. 3.5. Total injected charge (in nC) with the propagation distance (z) for the Gaussian (black curve) and flattened Gaussian (blue curve) laser profiles.

The suppression of the longitudinal electric field E_z can be clearly observed with increasing injected charge for flat Gaussian pulse in Figure 3.6. Moreover, an easing of the accelerating field slope along the injected charge can also be observed. This field change subsequently affect the electron momentum phase space distribution, resulting in reduction of peak energy and energy spread. The effect of beam loading is also clearly illustrated in the electron energy distribution for 0.8 nC (FGP) and 0.4 nC (GP) in Figure 3.7. Electron energy spectra for Gaussian and flattened Gaussian laser profiles at propagation distance $z \approx 2.2\, mm$ is depicted in Figure 3.7. A quasi monoenergetic electron beam is easily distinguishable in the figure, followed by trailing electrons. However, the electron beam generated using different profiles are found to have different beam quality and peak energies. The electron beam generated by the wakefield driven by flattened Gaussian profile is observed to have lower peak energy as compared to the Gaussian laser pulse. In case of flattened Gaussian pulse, the electrons are accelerated to a final energy (at $z \approx 2.2\, mm$) of approximately 550 MeV, while in Gaussian pulse case, electrons reached to higher energy of around 700 MeV. The decrease in peak energy is the consequence of beam loading [39,40].

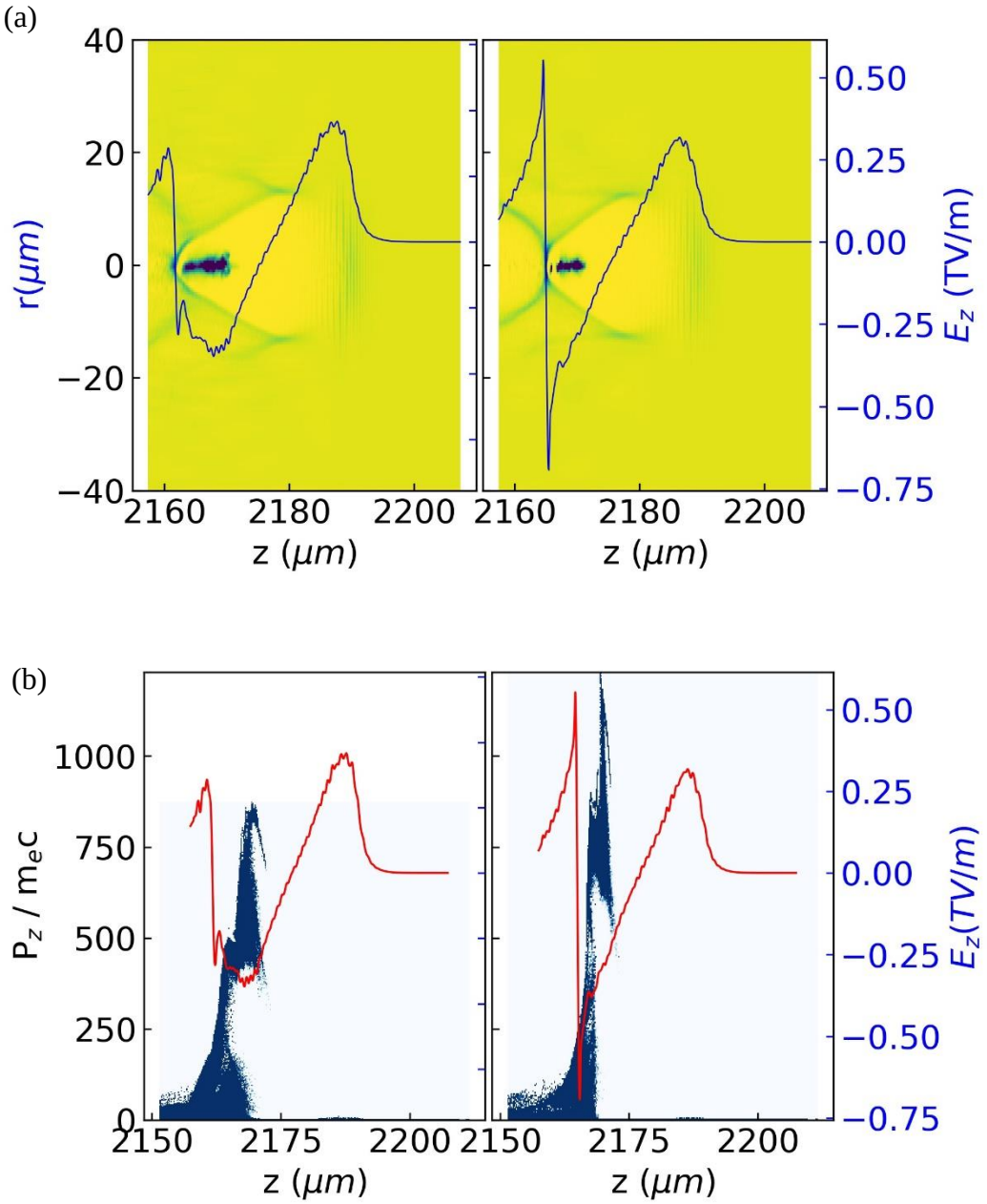

Fig. 3.6. Beam loading effect. (a) shows the wakefield line out plot along with density distribution plot by flattened Gaussian laser (left) and Gaussian laser pulse (right).(b) shows the wakefield line out plot along with phase space distribution for FGP (left) and GP (right).

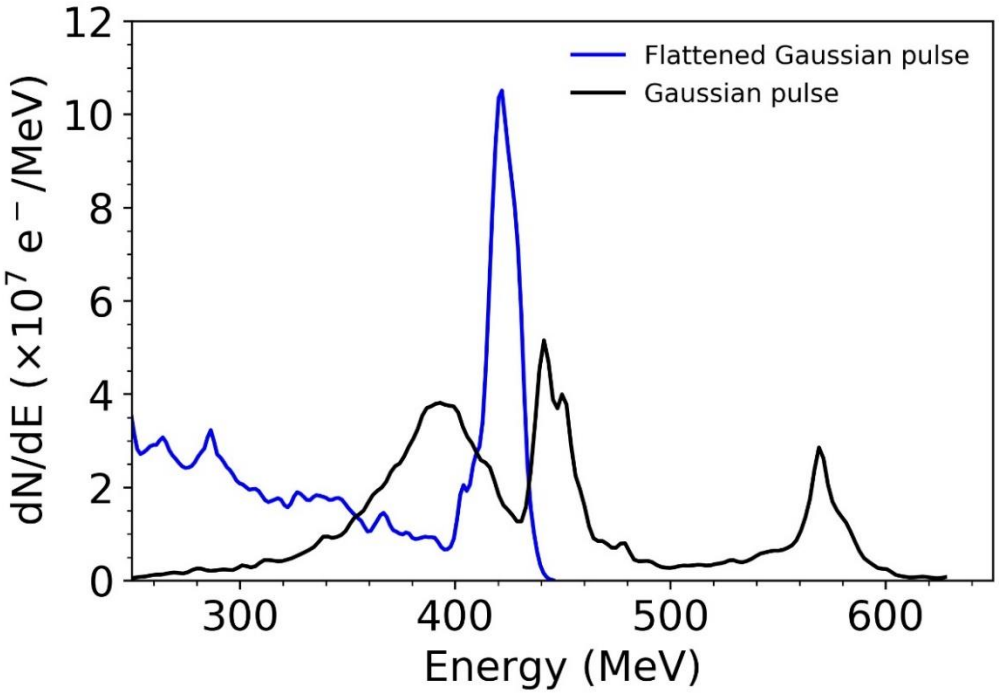

Fig. 3.7. Electron energy spectra for Gaussian (in black) and Flattened Gaussian laser pulse (in blue) at distance $z \approx 2.2\, mm$.

(d) Comparison of electron beam parameters using GP and FGP

The quality of the electron beam is characterized by beam charge, peak current, energy spread, emittance etc. Hence, the beam parameters are estimated for both the profiles using simulation results. The final charge of the bunch accelerated by Gaussian laser pulse is found to be 39 pC ($z \approx 2.2\, mm$). At the same distance, the flattened Gaussian accelerator delivers a bunch charge of nearly 187 pC, which is roughly five-fold the charge delivered by Gaussian accelerator. Figure 3.8 features the current profile of the injected electron beam for both Gaussian and flattened-Gaussian laser cases. The higher value of peak current (approximately 50 kA) in flattened-Gaussian case as compared to the peak current of approximately 20 kA in Gaussian case, is manifested in Figure 3.8. The electron bunch accelerated in wakefield excited by flattened-Gaussian laser profile exhibits a mean energy of 490.5 MeV with an energy spread of 15.9

MeV. While in Gaussian profile case, mean energy is found to be 634.5 MeV with an energy spread of 32.5 MeV.

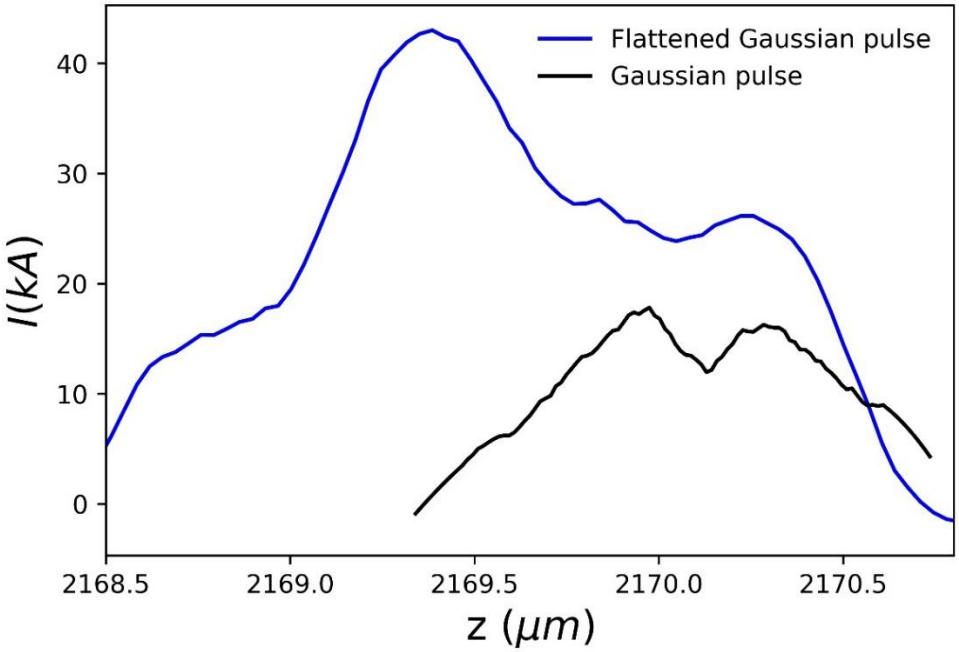

Fig. 3.8. Instantaneous current along the z-axis for the injected electron beam for both Gaussian (black curve) and flattened Gaussian laser case (blue curve).

(e) Dependence of electron beam parameters on laser strength for FGP

In order to further explore the physics behind lower value of maximum electron energy in case of flattened Gaussian laser pulse, simulations are performed for different values of laser strength parameter (a_0=1.8, 2.0, 2.2, 2.4) of flattened Gaussian laser. Table 3.1 incorporates the parameters of the electrons injected in the wakefield induced by the flattened Gaussian laser pulse of different intensities. The impact of higher charge injection can be easily associated with the maximum attainable electron energy as illustrated in Table 3.1. As the total injected charge is increased, the beam loading effect dominates. A decrement in the accelerating field is observed in the simulation results as the injected electrons are increased. The decrease in the maximum attainable electron energy also suggests the decline in the accelerating field. As recorded in the

Table 1, the maximum electron energy falls from approximately 590 MeV to 500 MeV as the electron injection in the wakefield hikes from 0.55 nC to 1.37 nC with increasing a_0 as a result of beam loading. Hence, a highly charged electron beam with low energy spread is obtained using flattened-Gaussian laser profile. Such a highly charged electron beam can have numerous applications in radiotherapy, radiobiology, and generation of intense X-rays, and gamma rays via the bremsstrahlung or inverse-scattering processes.

a_0	Maximum electron energy (MeV)	Energy spread (MeV)	Total injected charge (nC)	Bunch charge (pC)
1.8	590	30.6	0.55	90
2.0	526	28.7	0.82	187
2.2	510	27.5	1.09	280
2.4	500	26.4	1.37	397

Table. 3.1. Parameters of the injected electron bunch for different peak laser amplitude a_0 of flattened Gaussian laser pulse ($N = 6$).

3.5 Conclusion

In conclusion, we have explored the effect of laser pulse profile on the electron bunch quality in LWFA scheme. The comparison of bunch energy and quality using Gaussian and flattened-Gaussian pulse profile is presented and discussed in the chapter. Both, numerical study as well as simulations are carried out to validate the concept. The evolution of laser strength parameter for both the laser profiles is investigated to understand the wakefield evolution. It is found that the wakefield excited by the flattened-Gaussian laser pulse is stronger as compared to the Gaussian pulse till the effect of beam loading dominates. The

total injected charge in flattened-Gaussian case is almost twice the Gaussian case. Therefore, the perturbation of wakefield due to beam loading is substantial in the case of flattened-Gaussian laser pulse. The peak energy of the electron bunch is also affected to a large extent due to large beam load. However, it is noteworthy that the bunch charge obtained using flattened-Gaussian laser is significantly higher than the Gaussian case. The peak current of the injected electron beam in flattened-Gaussian case is also better by a factor of two. The energy spread in flattened-Gaussian case also displayed a modest improvement. Such a high charge, low energy spread electron beam makes the replacement of Gaussian laser profile by flattened-Gaussian laser profile desirable, depending on the requirement of the applications.

References

[1] X. Zeng, K. Zhou, Y. Zuo, Q. Zhu, J. Su, X. Wang, X. Wang, X. Huang, X. Jiang, D. Jiang, Y. Guo, N. Xie, S. Zhou, Z. Wu, J. Mu, H. Peng, and F. Jing, *Opt. Lett.* **42**, 2014 (2017).

[2] T. J. Yu, S. K. Lee, J. H. Sung, J. W. Yoon, T. M. Jeong, and J. Lee, *Opt. Exp.* **20**,10807 (2012).

[3] E. Esarey, S. K. Ride, and P. Sprangle, *Phys. Rev. E* **48**, 3003 (1993).

[4] P. Amendt, D. C. Eder, and S. C. Wilks, *Phys. Rev. Lett.* **66**, 2589 (1991).

[5] A. Rousse, K. T. Phuoc, R. Shah, A. Pukhov, E. Lefebvre, V. Malka, S. Kiselev, F. Burgy, J. P. Rousseau, D. Umstadter, and D. Hulin, *Phys. Rev. Lett.* **93**, 135005 (2004).

[6] S. Corde, K. T. Phuoc, G. Lambert, R. Fitour, V. Malka, A. Rousse, A. Beck, and E. Lefebvre, *Rev. Mod. Phys.* **85**, 1 (2013).

[7] C. Gahn, G. Tsakiris, A. Pukhov, J. Meyer-ter Vehn, G. Pretzler, P. Thirolf, D. Habs, and K. Witte, *Phys. Rev. Lett.* **83**, 4772 (1999).

[8] C. Clayton, K. Marsh, A. Dyson, M. Everett, A. Lal, W. Leemans, R. Williams, and C. Joshi, *Phys. Rev. Lett.* **70**, 37 (1993).

[9] D. N. Gupta, N. Kant, D. Kim, and H. Suk, *Phys. Lett. A* **368**, 402 (2007).

[10] D. Gupta, K. Gopal, I. Nam, V. Kulagin, and H. Suk, *Laser Part. Beams* **32**, 449 (2014).

[11] T. Tajima, and J. M. Dawson, *Phys. Rev. Lett.* 43, 267 (1979).

[12] J. Faure, Y. Glinec, A. Pukhov, S. Kiselev, S. Gordienko, E. Lefebvre, J.-P. Rousseau, F. Burgy, and V. Malka, *Nature* **431**, 541 (2004).

[13] C. Geddes, C. Toth, J. Van Tilborg, E. Esarey, C. Schroeder, D. Bruhwiler, C. Nieter, J. Cary, W. Leemans, *Nature* **431**, 538 (2004).

[14] S. P. Mangles, C. Murphy, Z. Najmudin, A. G. R. Thomas, J. Collier, A. E. Dangor, E. Divall, P. Foster, J. Gallacher, C. Hooker, D. A. Jaroszynski, A. J. Langley, W. B. Mori, P. A. Norreys, F. S. Tsung, R. Viskup, B. R. Walton, and K. Krushelnick, *Nature* **431**, 535 (2004).

[15] K. Nakamura, B. Nagler, C. Tóth, C. Geddes, C. Schroeder, E. Esarey, W. Leemans, A. Gonsalves, and S. Hooker, *Phys. Plasmas* **14**, 056708 (2007).

[16] A. J. Gonsalves, K. Nakamura, J. Daniels, C. Benedetti, C. Pieronek, T. C. H. de Raadt, S. Steinke, J. H. Bin, S. S. Bulanov, J. van Tilborg, C. G. R. Geddes, C. B. Schroeder, C. Tóth, E. Esarey, K. Swanson, L. Fan-Chiang, G. Bagdasarov, N. Bobrova, V. Gasilov, G. Korn, P. Sasorov, and W. P. Leemans, *Phys. Rev. Lett.* **122**, 084801 (2019).

[17] A. Pukhov, and J. Meyer-Ter-Vehn, *App. Phys. B: Lasers Opt.* 74, 355 (2002).

[18] C. Benedetti, C. B. Schroeder, E. Esarey, F. Rossi, and W. P. Leemans, *Phys. Plasmas* **20**, 103108 (2013).

[19] F. Gori, *Opt. Commun.* **107**, 335 (1994).

[20] M. Santarsiero, D. Aiello, R. Borghi, and S. Vicalvi, *J. Mod. Opt.* **44**, 633 (1997).

[21] V. Bagini, R. Borghi, F. Gori, A. Pacileo, M. Santarsiero, D. Ambrosini, and G. S. Spagnolo, *JOSA A* **13**, 1385 (1996).

[22] V. B. Pathak, J. Vieira, R. Fonseca, and L. Silva, *New J. Phys.* **14**, 023057 (2012).

[23] C. Schroeder, E. Esarey, C. Geddes, C. Toth, B. Shadwick, J. Van Tilborg, J. Faure, and W. Leemans, *Phys. Plasmas* **10**, 2039 (2003).

[24] X. Zhang, B. Shen, L. Ji, W. Wang, J. Xu, Y. Yu, L. Yi, X. Wang, N. A. Hafz, and V. Kulagin, *Phys. Plasmas* **19**, 053103 (2012).

[25] A. K. Upadhyay, S. A. Samant, and S. Krishnagopal, *Phys. Plasmas* **20**, 013106 (2013).

[26] K. Gopal, and D. Gupta, *Phys. Plasmas* **24**, 103101 (2017).

[27] R. Fallah, and S. M. Khorashadizadeh, *IEEE Trans. Plasma Sci.* **46,** 2085 (2018).

[28] T. Ostermayr, S. Petrovics, K. Iqbal, C. Klier, H. Ruhl, K. Nakajima, A. Deng, X. Zhang, B. Shen, J. Liu, R. Li, Z. Xu, and T. Tajima, *J. Plasma Phys*. **78**, 447 (2012).

[29] P. Jha, A. Saroch, and R. K. Mishra, *Laser Part. Beams* **31**, 583 (2013).

[30] C. Rechatin, X. Davoine, A. Lifschitz, A. B. Ismail, J. Lim, E. Lefebvre, J. Faure, and V. Malka, *Phys. Rev. Lett.* **103**, 194804 (2009).

[31] A. Ben Ismail, O. Lundh, C. Rechatin, J. Lim, J. Faure, S. Corde, and V. Malka, *App. Phys. Lett.* **98**, 264101 (2011).

[32] O. Rigaud, N. Fortunel, P. Vaigot, E. Cadio, M. Martin, O. Lundh, J. Faure, C. Rechatin, V. Malka, and Y. Gauduel, *Cell Death & Disease* **1**, e73 (2010).

[33] Z.-H. He, B. Beaurepaire, J. Nees, G. Gallé, S. Scott, J. S. Pérez, M. Lagally, K. Krushelnick, A. Thomas, and J. Faure, *Scientific Reports* **6**, 1 (2016).

[34] H. W. Kim, N. A. Vinokurov, I. H. Baek, K. Y. Oang, M. H. Kim, Y. C. Kim, K.-H. Jang, K. Lee, S. H. Park, S. Park, J. Shin, J. Kim, F. Rotermund, S. Cho, T. Feurer, and Y. Uk Jeong, *Nat. photonics* **14**, 245 (2020).

[35] P. Antici, A. Bacci, C. Benedetti, E. Chiadroni, M. Ferrario, A. Rossi, L. Lancia, M. Migliorati, A. Mostacci, L. Palumbo, and L. Serafini, *J. App. Phys.* **112**, 044902 (2012).

[36] M. G. Zhao, C. Xu, and M. Minty, *Progress in Electromagnetics Research* **64**, 35 (2018).

[37] B. Mercier, J. Rousseau, A. Jullien, and L. Antonucci, *Opt. Commun*. **283**, 2900 (2010).

[38] R. Lehe, M. Kirchen, I. A. Andriyash, B. B. Godfrey, and J.L. Vay, *Comp. Phys. Commun.* **203**, 66 (2016).

[39] C. Rechatin, X. Davoine, A. Lifschitz, A. B. Ismail, J. Lim, E. Lefebvre, J. Faure, and V. Malka, *Phys. Rev. Lett.* **103**, 194804 (2009).

[40] C. Rechatin, J. Faure, X. Davoine, O. Lundh, J. Lim, A. Ben-Ismaïl, F. Burgy, A. Tafzi, A. Lifschitz, E. Lefebvre, and V. Malka,, *New J. Phys.* **12**, 045023 (2010).

4

LASER WAKEFIELD EXCITATION AND ELECTRON ACCELERATION BY A Q-GAUSSIAN LASER BEAM

4.1 Brief outline of the chapter

A theoretical study is investigated to understand the propagation dynamics of a q-Gaussian laser beam in a plasma under the influence of relativistic and ponderomotive nonlinearities. A q-Gaussian laser beam exhibits unique characteristics while interacting with the plasma. On account of the interaction of the q-Gaussian laser beam, the plasma density distribution becomes more finite and leads to affect the self-focusing of the laser beam. A comparative study of self-focusing for Gaussian and q-Gaussian laser beam is reported. The results are illustrated with numerical analysis, revealing a strong self-focusing of the q-Gaussian laser beam in plasmas, which is desirable to excite a large amplitude plasma wave for electron accelerations by extending the interaction length. We then extended this study to investigate the electron plasma wave excitation by the q-Gaussian laser beam. The generation of electron plasma wave is seen to be modified by the self-focusing of q-Gaussian laser beam. It is evident from the results that the electron plasma wave field intensity is enhanced more than two-fold for q-Gaussian laser beam in comparison with the case of Gaussian laser beam. And consequently, the energy gained by the accelerated electrons trapped in the plasma wave is also found to be significantly enhanced for q-Gaussian laser beam case. The numerical analysis has been done for this study for the established set of laser and plasma parameters.

4.2 Introduction

During the past few decades, the laser technology development has drawn significant attention towards the unexplored area of laser-plasma interactions [1-3]. Its importance has been recognised in various areas such as electron acceleration [4-8], laser driven fusion [9], X-ray lasers [10,11], high harmonic generation [12] etc. For the realization of all these applications, the propagation of high-intensity laser pulse to a large distance without energy loss is highly desirable. The laser propagation without any energy loss is limited to a distance of approximately a Rayleigh length (without any optical guiding). This is due to the reason that laser pulse suffers Rayleigh diffraction in the absence of any optical guiding, in vacuum. The spot size varies as $w = w_0(1 + z^2/Z_R^2)$, where Z_R is the Rayleigh length. Hence, the laser-plasma interaction length is restricted by this diffraction to a few Rayleigh lengths only. Self-focusing is the process that can maintain the intense beam, focussed and collimated, during propagation. The laser self-focusing arises due to the modification of the dielectric property of a plasma when an intense laser propagates through it [13-15]. The refractive index for the small amplitude laser pulse in a uniform density plasma is given by $\eta(r) = \frac{c}{v_p} = \sqrt{1 - \frac{\omega_p^2}{\omega^2}}$, where v_p is the phase velocity of electromagnetic wave and c is the speed of light [16]. But, when the amplitude of the plasma wave increases, the plasma frequency is modified due to the electron density and mass variation. This is because when an intense laser pulse travels in an underdense plasma, the electrons start oscillating relativistically and therefore, their mass too increases relativistically. Hence, the refractive index term becomes intensity dependent i.e. $\omega_p^2 = \omega_{p0}^2/\gamma$, where $\gamma = \sqrt{1 + {a_0}^2}$.

As the laser beam used has a radially Gaussian profile, laser intensity peaks on axis ($\partial a^2/\partial r < 0$). This leads to the decrease in the phase velocity (and $\partial \eta/\partial r < 0$) of the pulse on-axis than off-axis. Hence, the plane wavefront gets curved and starts focusing to a smaller spot. This mechanism of self-focusing of laser pulse in plasma due to relativistic mass effect is *relativistic self-focusing* [17,18]. This occurs when the laser power (P) exceeds the critical power (P_c) [19], $\mathrm{P} \geq \mathrm{P_c} \approx 17.4\left(\omega^2/\omega_p^2\right)(GW)$. When a laser pulse propagates through

Monika Yadav, *Department of Applied Physics, Delhi Technological University, Delhi, India*

plasma, it exerts a radial ponderomotive force on electrons from high intensity region towards low intensity region. Hence a radial density gradient ($\partial(\delta n)/\partial r > 0$) is created, leading to negative transverse refractive index gradient ($\partial n/\partial r < 0$). This mechanism of self-focusing is termed as *ponderomotive self-focusing* [20,21]. Although, in case of $a_0 < 1$, for $P \geq P_c$, relativistic focusing dominates, but ponderomotive focusing enhances the total focusing effect.

The theoretical investigation of self-focussing phenomenon was reported by Akhmanov *et al.* [22] for the first time. It was later developed and extended by Sodha *et al.* [23,24] and Kaw *et al.* [25] to a variety of media. Research on self-focusing [26-28] and electron acceleration [29,30] was initially restricted to the Gaussian distribution of laser beams. However, various unexplored aspects of the beam propagation have also been revealed by the researchers by considering non-Gaussian profile. Authors have reported the self-focusing of laser beam with different spatial profiles such as super-Gaussian profile, Bessel profile, hollow Gaussian, elliptical Gaussian etc., theoretically and experimentally [31-42]. These different beams show different behaviour in plasmas. Patel *et al.* [43] and Nakatsutsumi *et al.* [44] have observed the intensity profile of the Vulcan petawatt laser and found it different from the Gaussian intensity distribution function. It was found that 20% energy contained within the FWHM of 6.9 μm and 50% within 16 μm on measuring the intensity distribution of Vulcan petawatt laser. The intensity distribution function of Vulcan petawatt laser was given as $I(r) = I(0)(1 + r^2 / qr_0^2)^{-q}$ (where the value of q and r_0 can be obtained by fitting the experimental data). Recently, Dwivedi and Malik [45] have studied the plasma channel formation by a q-Gaussian laser beam in low-intensity regime, where the ponderomotive nonlinearity was considered for laser dynamics. A q-Gaussian laser beam of intensity parameter a_0=0.01 of wavelength 10.6 μm was employed to calculate the density perturbation and subsequent self-focusing of the laser beam. At such a low-intensity, the relativistic effects are not important, hence, neglected in that study.

We extended the work for high-intensity laser case, where both the relativistic and ponderomotive effects may be operative and relevant to the laser

wakefield accelerations of electrons. Moreover, we emphasize the previous study to explore the propagation of a q-Gaussian laser beam for electron plasma wave excitation. The analytical study of the wakefield excitation has also been done by using different shaped electromagnetic pulses in plasmas [46,47]. We seek a possibility to consider the q-Gaussian laser beam for plasma wave acceleration of electrons [48]. A theoretical model supported by numerical analysis suggests employing a q-Gaussian laser beam for strong self-focusing as well large amplitude electron plasma wave excitation. The subsequent electron acceleration by the electron plasma wave for higher energy may be predicted from this model. The analytical model for derivation of the governing equations of the self-focusing of a q-Gaussian laser beam is developed. The modified wave equation for electron plasma wave excitation and subsequent electron acceleration is studied thereafter. The mathematical analysis and results are summarized in next section. The results of this work are then summarized and concluded in the last section of this chapter.

4.3 Theoretical Model

(a) Propagation of q-Gaussian Laser Beam

A q-Gaussian laser beam, polarized in the x-direction, propagates along the *z*-direction in a plasma. The distribution of electric field of q-Gaussian laser beam is given by $E(r,z,t)=\hat{x}A(r,z,t)\exp[-i(\omega t-kz)]$, where $\hat{x}$ is the unit vector along the x-axis, ω is the laser frequency, k is the laser wave vector, and A is the amplitude of the laser field which is a function of space (r,z) and time (t). The initial intensity profile of q-Gaussian laser beam at $z=0$ is given by $A^2=A_0{}^2(1+r^2/qr_0^2)^{-q}g(t)$, where $g(t)=\exp(-t^2/t_0^2)$, t_0 is the laser pulse duration, and r_0 is the laser spot size. Here, q is the parameter, which indicates the deviation of intensity distribution from the usual Gaussian profile. The smaller finite value of q represents strongly q-Gaussian profile, characterized by expanded tails. And, q tends to infinity gives the usual Gaussian distribution. It is clearly visible from Fig. 4.1 that as the value of q-parameter is increased, the

intensity distribution of the q-Gaussian laser pulse starts shifting towards the usual Gaussian curve.

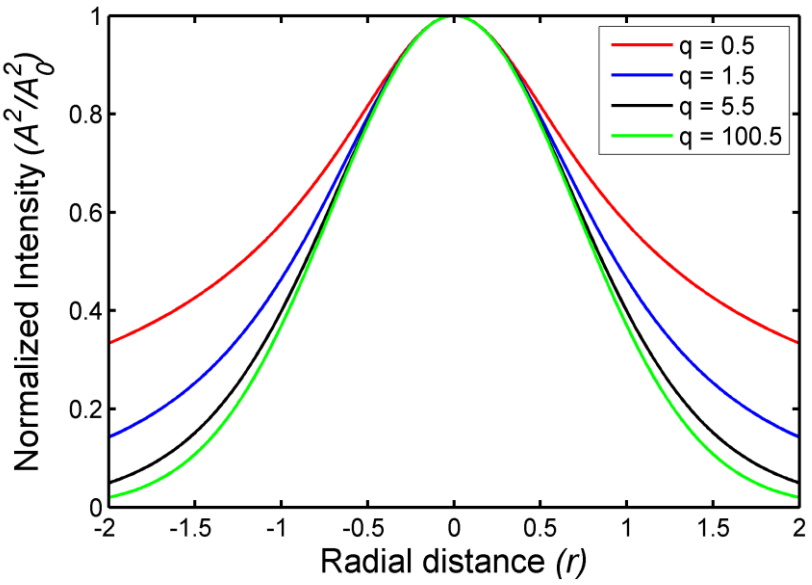

Fig. 4.1. Intensity profile of q-Gaussian laser beam for different values of q-parameter. Lower value of q-parameter shows more deviation from Gaussian curve.

The electric field of the laser beam is governed by the wave equation,

$$\nabla^2\mathbf{E} - \frac{\varepsilon}{c^2}\frac{\partial^2\mathbf{E}}{\partial t^2} = 0, \tag{4.1}$$

where $\varepsilon = 1-(\omega_p^2/\omega^2)+\phi(|E|^2)$, $\omega_p^2 = 4\pi n_0 e^2/m'$ is the plasma frequency, n is the electron density, e and m' represent the electron charge and mass, respectively. The radial component of the laser field pushes the plasma electrons outward on the time scale of plasma period ω_p^{-1}, which creates a radial space-charge field of $\mathbf{E}_s = -\nabla\phi_s$. Thus the distribution of electron density may be written as

$$n_e = n_0 + \frac{1}{4\pi e}\nabla^2\phi_s . \tag{4.2}$$

The ponderomotive potential associated with the ponderomotive force is given by $\phi_p = -(mc^2/e)[(1+a^2/2)^{1/2}-1]$. In quasi-steady state, $\phi_s = \phi_p$. Therefore, the electron density distribution can be rewritten as

$$n_e = n_0\left[1+\frac{1}{m\omega_p^2}\left\{mc^2\nabla^2\left(1+\frac{a^2}{2}\right)^{1/2}\right\}\right], \tag{4.3}$$

where $a^2 = (a_0^2/f^2)(1 + r^2/qr_0^2f^2)g(t)$, $a_0 = eA_0/m\omega_0 c$ and f is a dimensionless quality, which is defined as the beam width parameter of the laser beam. Here we have defined the laser beam width as $r_0 f$. The initial laser band width (spot size) can be obtained by taking $f = 1$. By estimating of f, one may find the variation of the corresponding spot size of the laser beam. For example, one can say that the laser spot size reduces by decreasing the value of f. The purpose to introduce f is to make the mathematics simple and convenient.

The effective dielectric constant of the plasma at frequency ω can be written as

$$\varepsilon = 1-\frac{\omega_p^2}{\omega^2}\frac{(n_e/n_0)}{\gamma}, \tag{4.4}$$

where $\gamma = (1+a^2/2)^{1/2}$. The dielectric constant can be expanded using Taylor expansion around $r = 0$ and can be expressed as $\varepsilon = \varepsilon_0 - \phi r^2/r_0^2$, where

$$\varepsilon_0 = 1-\frac{\omega_p^2}{\omega^2}\left(1+\frac{a_0^2}{f^2}\right)^{-1/2}\frac{a_0^2c^2}{r_0^2f^4\omega^2}\left(1+\frac{a_0^2}{2f^2}\right), \tag{4.5}$$

Monika Yadav, *Department of Applied Physics, Delhi Technological University, Delhi, India*

$$\phi = \frac{c^2 a_0^2}{\omega^2 r_0^2 f^6}\left(1+\frac{a_0^2}{2f^2}\right)^{-1}\left[-\frac{a_0^2}{4f^2}\left(1+\frac{a_0^2}{2f^2}\right)^{-1}+2\left(1+\frac{1}{q}\right)\right]. \qquad (4.6)$$

Following Akhmanov *et al.* [22] and Sodha *et al.* [23], the solution of the wave equation can be considered as $E = A(r,z)\exp(-ikz)$, where $A(r,z)$ is the amplitude of the laser electric field. Substituting the solution in wave equation, we get the parabolic equation

$$-2ik\frac{\partial A}{\partial z}+\frac{\partial^2 A}{\partial r}+\frac{1}{r}\frac{\partial A}{\partial r}+\frac{\omega^2}{c^2}\varepsilon A = 0\,. \qquad (4.7)$$

Using the paraxial and WKB approximations, we assume the solution of Eq. (4.7), as $A = A_0(r,z)\exp(-ikS)$, where A_0 and S are the real functions of r and z. Substituting this expression in Eq. (4.7) and separating the real and imaginary parts, we get

$$2\left(\frac{\partial S}{\partial z}\right)+\left(\frac{\partial S}{\partial r}\right)^2 = \frac{1}{k^2 A}\left(\frac{\partial^2 A}{\partial r^2}+\frac{\partial A}{r\partial r}\right)-r^2\frac{\phi}{\varepsilon_0}\,, \qquad (4.8)$$

$$\frac{\partial A^2}{\partial z}+\frac{\partial A^2}{\partial r}\frac{\partial S}{\partial r}+A^2\left(\frac{\partial S}{r\partial r}+\frac{\partial^2 A}{\partial r^2}\right)=0. \qquad (4.9)$$

To solve Eqs. (4.8) and (4.9), we assume the solutions as $S = (r^2/2)\beta(z)+\phi(z)$ and $A = (A_0/f)\left(1+r^2/qr_0^2 f^2\right)^{-q/2}$, where $\beta(z) = (1/f)df/dz$. Substituting these solutions in Eq. (4.9) and equating the coefficients of r^2, we obtain the expression for f as

$$\varepsilon_0\frac{d^2 f}{d\xi^2} = \frac{(q+4)}{q}\frac{1}{\rho^4 f^3}-\frac{\phi}{\rho^2}f\,, \qquad (4.10)$$

Monika Yadav, *Department of Applied Physics, Delhi Technological University, Delhi, India*

where $\xi = z\omega/c$ is the normalized distance and $\rho = r_0\omega/c$ is the normalized laser spot size.

In Eq. (4.10), the first term on right hand side is due to the diffraction effects and the second term is the nonlinear term that is responsible for laser self-focusing. In general case, we use the initial boundary conditions: f=1 and df/dz =0 at $z = 0$ (for initial plane wave-front) to solve this equation. For perfect guiding (where the laser spot size becomes constant), the two terms in beam width parameter equation representing diffraction and self-focusing effects balance each other exactly with f=1 giving the matched solution for laser spot size as $\rho^2 = (1 + 4/q)\phi$. However, we solve Eq. (4.10) for actual evolution of the laser beam width parameter. Eq. (4.10) is a non-linear differential equation, which governs self-focusing of a q-Gaussian laser beam when both the relativistic and ponderomotive nonlinearities are operative. We discuss the laser beam propagation characteristics using this equation. The set of laser and plasma parameters used for this calculation are as follows: $\omega = 1.8 \times 10^{15} s^{-1}$ (corresponding to the laser wavelength λ =1 μm), $r_0 = 9\,\mu m$, $\omega_p/\omega_0 = 0.09$ (corresponding to the plasma electron density $n = 8 \times 10^{18} cm^{-3}$), $v_{th}/c = 0.1$ and $a_0 = 1 - 3$ (corresponding to the laser intensity of 2.1×10^{18}-1.9×10^{19} *W/cm*^{2} and laser wavelength of 1 μm). The values of r_0, v_{th}/c and ω_p/ω have been kept same throughout this chapter. In Eq. (4.10), the relative value of the diffractive and the refractive term decides the focusing and defocusing of the laser beam. The q-value signifies the deviation of intensity distribution of laser beam from Gaussian profile. For q-Gaussian beam, the value of q is smaller. That means a larger deviation is there in pulse shape with respect to the Gaussian profile. The

Monika Yadav, *Department of Applied Physics, Delhi Technological University, Delhi, India*

smaller value of q represents a q-Gaussian profile. And q tends to infinity gives the usual Gaussian distribution. For Gaussian profile, Eq. (4.10) turns out to be $\varepsilon_0 \frac{d^2 f}{d\xi^2} = \frac{1}{\rho^4 f^3} - \frac{\phi}{\rho^2} f$, where ϕ and ε_0 are modified according to the q-Gaussian profile (if $q \to \infty$). And the matched laser spot size for this case would be $\rho^2 = 1/\phi$, which, in fact, can be obtained from Eq. (4.10). The compression of both equations shows the evolution of beam width parameter as the intensity distribution deviates from the usual Gaussian profile.

In Fig. 4.2 (a), the variation of beam width parameter (*f*) with the normalized propagation distance is displayed for different values of q-parameter ($q =$ 0.5, 1.5, 10.5), keeping the laser strength parameter $a_0 = 2$ and the normalised spot size of laser $\rho = 60$. It has been observed that the self-focusing effect weakens due to pulse intensity distribution as the distribution goes towards Gaussian. Sharp and faster focusing can be observed for lower *q*-parameter as shown in Fig.4.2 (a). Self-focusing length also decreases for lower *q*-values. This can be explained using the fact that the different q value represents different intensity distribution. For the lower q values, the non-Gaussian profile is characterized by a long and expanded tail of intensity distribution as compared to the usual Gaussian distribution. This shows the intensity shift towards off-axial region. And the diffraction of off-axial rays is weaker comparative to the axial rays, which strengthens the plasma nonlinearity. Hence, the laser beam with lower *q*-values shows stronger and faster self-focusing.

Monika Yadav, Department of Applied Physics, Delhi Technological University, Delhi, India

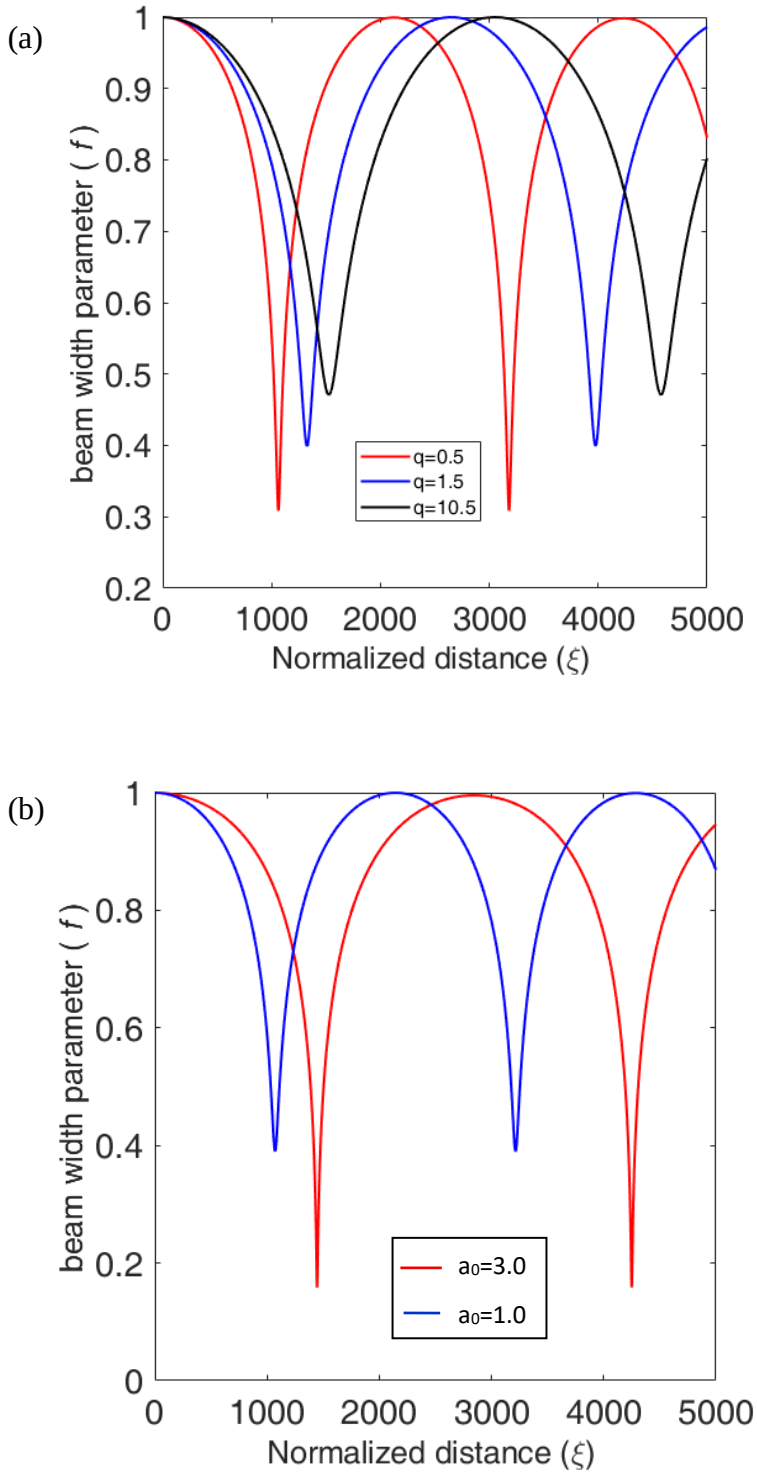

Fig. 4.2. The beam width parameter (f) with the normalized propagation distance (ξ) for (a) different values of q-parameter (q = 0.5, 1.5, 10.5) with $a_0 = 2$, $\omega_p/\omega_0 = 0.09$ and (b) different laser strength parameters ($a_0 = 1$ and 3), keeping $q = 0.5$.

Our results show that the laser intensity (a_0) also affects the self-focusing of q-Gaussian laser beam. Figure 4.2 (b) displays the variation of beam width parameter (f) for different values of a_0 (a_0 = 1, 3), keeping other laser parameters as $q = 0.5$ and $\rho = 60$. The rate of self-focusing is enhanced with the intensity of the laser beam for all q-values. The lower laser intensity reduces the non-linear refractive term, which causes the diffraction term to dominate. Thus the laser self-focusing weakens. However, the q-Gaussian laser beam converges earlier than the Gaussian beam, which makes it desirable for various application.

(b) Electron Plasma Wave Excitation

We now employ the self-focused q-Gaussian laser pulse to excite wakefields in plasmas. The ponderomotive force associated with the q-Gaussian laser pulse pushes away the plasma electrons to the low-intensity region. The ions remain immobile for such a short laser interaction, so that the electrons oscillate around the initial position due to restoring force. The density perturbation forms an electron plasma wave. In this study, the excitation EPW is due to non-linear interaction of a q-Gaussian laser beam with plasmas in the presence of relativistic and ponderomotive nonlinearities. As the amplitude of EPW depends on the background electron density, thus the plasma wave excitation also gets modified for q-Gaussian laser beam. Hence, there is a strong coupling between EPW and q-Gaussian laser beam on account of plasma nonlinearities. We use time averaged fluid equations and Poisson's equations to find out the electron velocity $\boldsymbol{v}$, electron density perturbation n, electric field **E**, magnetic field **B**, which are slowly varying over the laser period. The relevant equations can be written as

$$\frac{\partial n}{\partial t} + \nabla . n\boldsymbol{v} = 0, \tag{4.11}$$

$$\frac{\partial \boldsymbol{v}}{\partial t} + (v.\nabla)v = -\frac{e}{m}\boldsymbol{E} - \frac{e}{mc}(\boldsymbol{v} \times \boldsymbol{B}) - 2\Gamma_e \boldsymbol{v} - \frac{3K_B T_e}{\boldsymbol{m}}\frac{\nabla n}{n}, \tag{4.12}$$

$$\nabla . \boldsymbol{E} = -4\pi e n, \tag{4.13}$$

where $n = n_0 + n'$ is the total plasma electron density, $v = v_0 + v'$is the sum of the velocities of the electrons in the electromagnetic and self-consistent field (the physical quantities denoted by superscripts are at plasma electron frequency) , E is the sum of the electric field vector of the electromagnetic wave and the self-consistent field, Γ is the damping coefficient associated with particle collisions (which may be approximated by $\nu_e/2$, where ν_e is the electron collision frequency in plasmas), T_e is the electron temperature, and K_B is the Boltzmann constant. The damping term is included just for general mathematical formulation of equation of motion. We will neglect it to obtain the maximum plasma wave amplitude. Also, the phase velocity of plasma wave is very large as compared to the thermal velocity of electron. Hence, the damping would not be so important in this study. Using Eqs. (4.11)-(4.13), we obtain the equation for the EPW at frequency $\omega = \omega_p$.

$$\frac{\partial^2 n'}{\partial t^2} + 2\Gamma\frac{\partial n'}{\partial t} - v_{th}^2 \nabla^2 n' + \frac{\omega_p^2}{\gamma}\frac{n}{n_0}n' = 0, \tag{4.14}$$

where v_{th} is the electron thermal velocity. In this equation, the terms those are surviving at electron plasma frequency, are retained.

By neglecting the second and third terms in Eq. (4.14), one can obtain the density perturbation equation for wakefield excitation in bubble regime. Eq. (4.14) is valid for a relativistic warm plasma theory. For short-pulse laser interactions,

Monika Yadav, *Department of Applied Physics, Delhi Technological University, Delhi, India*

the relativistic warm plasma theory may be used such that the phase-space distribution has a small momentum spread about its means. This allows the hierarchy of moment equation to be treated asymptotically. No additional assumptions are necessary for closure of the fluid equations. We also apply the standard perturbation approximations to obtain the density perturbation associated with the EPW excited by a q-Gaussian laser beam. In order to get a solution of Eq. (4.14), we consider the quasi-static approximation, which states that in the co-moving frame the travelling wave appears static (i.e. changes gradually in time compared to the spatial scale). Under quasi-static approximation, the fluid quantities are assumed to be functions of the spatial variable. Moreover, by taking quasi-static approximation, one can obtain a finite maximum density perturbation (which does not become singular). Thus the absent of singularity confirms the validity of warm fluid equations for nonlinear wake evolution. However, the density perturbation associated with the wakefield evolution may have singularity beyond the wave breaking due to thermal effects, that we don't consider in this study. The validity of this model is for only below the wave-breaking amplitude. We now assume the plane wave solution of Eq. (4.14) (under WKB approximation) as

$$n' = n''(r,z)\exp\{i[\omega t - k(z + S(r,z))]\}, \tag{4.15}$$

where S is the eikonal of the plasma wave, ω and k are the EPW frequency and wave vector, respectively. After substituting n' in Eq. (4.14) and separating the real and imaginary parts, we obtain (neglecting the explicit dependence of the fluid variables on t)

$$2\frac{\partial S}{\partial z}+\left(\frac{\partial S}{\partial r}\right)^2=\frac{1}{k^2n''}\left(\frac{\partial^2 n''}{\partial r^2}+\frac{1}{r}\frac{\partial n''}{\partial r}\right)+\frac{\omega_p^2}{k^2v_{th}^2}\left(1-\frac{n}{\gamma n_0}\right), \quad (4.16)$$

$$\frac{\partial n''^2}{\partial z}+\frac{\partial S}{\partial z}\frac{\partial n''^2}{\partial r}+n''^2\left(\frac{\partial^2 S}{\partial r^2}+\frac{1}{r}\frac{\partial S}{\partial r}\right)+\frac{2\Gamma\omega}{kv_{th}^2}n''^2=0\,. \quad (4.17)$$

The variation of initial density is assumed as, $N''_{z=0}=N''(1+r^2/qh^2)^{-q/2}$, where *h* is the initial beam width of EPW. The solution of Eqs. (4.16) and (4.17) can be assumed as

$$n''=\frac{N''}{f_{pw}}\left[1+\frac{r^2}{qf_{pw}h^2}\right]^{-q/2}e^{-k_iz}, \quad (4.18)$$

where f_{pw} is the beam width parameter of EPW and $k_i=\Gamma\omega/kv_{th}^2$ is the damping factor. Substituting Eq. (4.18) in Eq. (4.16) and comparing the coefficients of r^2 on both sides, the expression for beam width parameter of EPW is obtained as

$$\frac{d^2f_{pw}}{f_{pw}d\xi^2}=\frac{(q+4)}{qh^4{f_{pw}}^4}+\frac{c^2}{v_t^2}\left[\frac{a_0^2}{4f^8r_0^4}\left(1+\frac{a_0^2}{2f^2}\right)^{-2}-\frac{2(q+1)a_0^2}{qf^6r_0^4}\left(1+\frac{a_0^2}{2f^2}\right)^{-2}\right] \quad (4.19)$$

Eq. (4.18) gives the amplitude of the electron density perturbation excited by the self-focused q-Gaussian laser beam. Eq. (4.19) shows the coupling of the EPW with a q-Gaussian laser beam under the relativistic and ponderomotive nonlinearities. Using Poisson's Equation, the electrostatic field of the excited EPW can easily be assumed as.

$$E=E_{pw}\exp[i(\omega t-kz)], \quad (4.20)$$

where E_{pw} is the amplitude of the EPW, which can be written as

$$E_{pw}=\frac{i\omega_p^2m}{kf_{pw}e}\left[1+\frac{r^2}{qf_{pw}h^2}\right]^{-q/2}e^{-k_iz} \quad (4.21)$$

Monika Yadav, *Department of Applied Physics, Delhi Technological University, Delhi, India*

Eq. (4.21) shows the electric field amplitude of EPW excited by a q-Gaussian laser beam. To obtain the maximum electric field, we neglect the damping term in this equation. Eq. (4.21) represents a nonlinear EPW of finite spot size (or beam width parameter). The beam width parameter of EPW is sensitive with the spot size evolution of the driver q-Gaussian laser beam.

The interactions of a q-Gaussian laser beam with plasmas under relativistic and ponderomotive nonlinearities lead to a change in the background plasma density, which excites the EPW. The excitation of EPW is governed by Eq. (4.14), where the last term signifies the coupling of modified background density required for EPW excitation (when both the relativistic and ponderomotive nonlinearities are operative). Eq. (4.19) represents the variation of beam width parameter (f_{pw}) of EPW with $df_{pw}/dz = 0$ and $f_{pw} = 1$ (corresponding to the initial density perturbation corresponding the initial EPW field amplitude) at $z = 0$. Eqs. (4.18) and (4.19) are numerically solved to estimate the effect of q-Gaussian laser beam on EPW excitation. We displayed the results in terms of EPW field intensity variation with the propagation distance. The EPW field intensity is approximated by taking the square of the electric field amplitude i.e. $\left|E_{pw}\right|^2$.

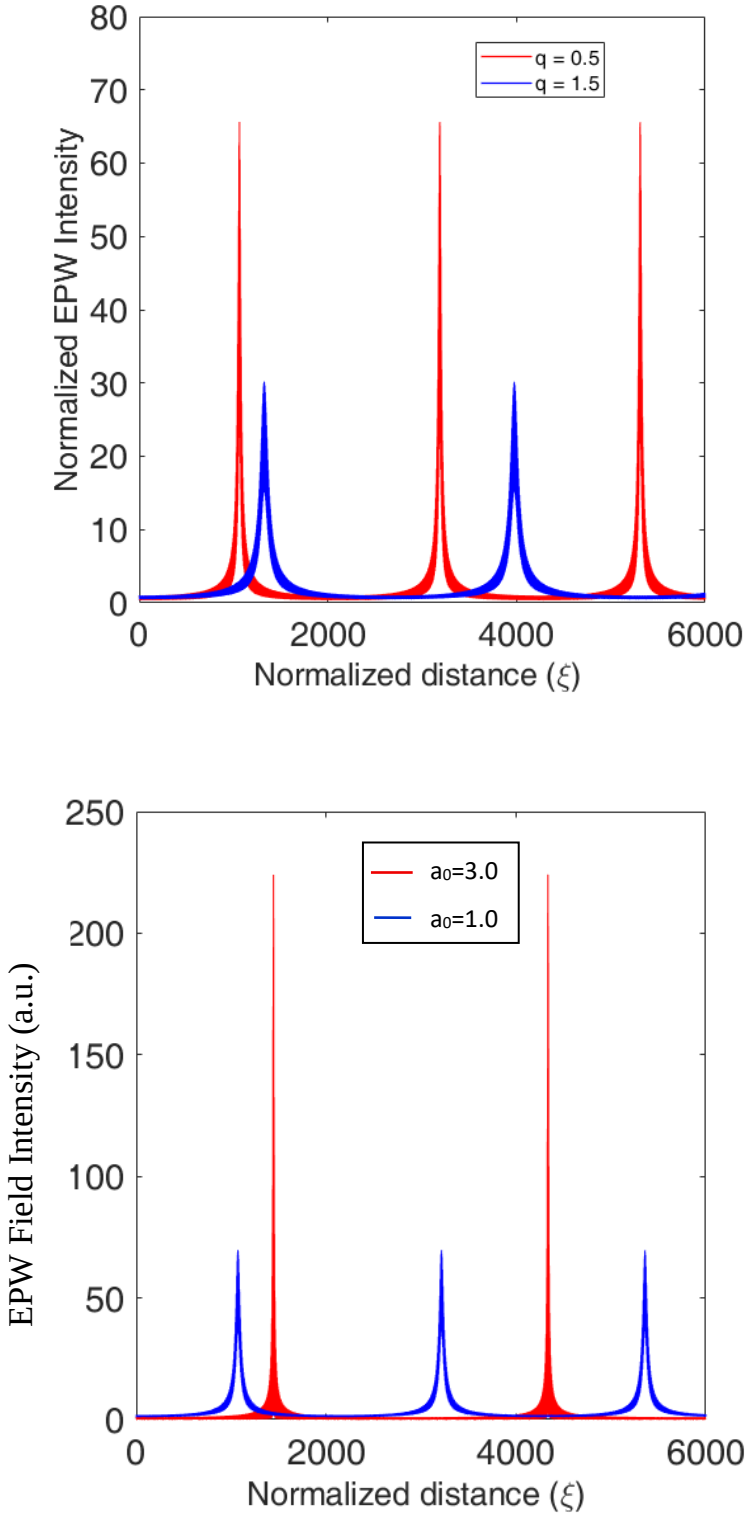

Fig. 4.3. EPW field intensity (in a.u.) with normalized propagation distance (ξ) (a) for q= 0.5 and 1.5, keeping other laser parameters same as in Fig. 4.1 (a) and Fig 4.2 (b) for a_0= 1 and 3, keeping other laser parameters same as in Fig. 4.1 (b).

Fig. 4.3 (a) displays the variation of EPW field intensity (in a.u.) with the normalized propagation distance for different values of q parameter, keeping a_0 =2. As predicted, the EPW field intensity is higher for q-Gaussian profile in comparison to the Gaussian profile. This is due to the stronger self-focusing of q-Gaussian laser beam. It can be seen that the distance, at which the intensity peak [Fig. 4.3 (a)] is observed, matches with the corresponding focusing points obtained in Fig. 4.2 (a). A focussed laser beam excites stronger large amplitude EPW. To see the effect of laser intensity on EPW excitation, we depicts the EPW field intensity for different, keeping q= 0.5. It has been observed that the amplitude of density perturbation strongly depends on the focusing and defocusing of the laser beam. Thus the lower laser intensity excites the EPW early in time. As seen from the focusing pattern of the laser beam shown in Fig. 4.2 (b), the laser beam with higher is focussed more. Thus it is revealed that the large amplitude EPW may be excited if an intense laser beam is employed for plasma interactions.

As we know that the laser beam will be Gaussian for larger q-parameter. To see the comparison of EPW field intensity for Gaussian and q-Gaussian laser beam, we show the EPW field intensity for different q-parameters. Fig. 4.4 shows the EPW field intensity for a q-Gaussian (q = 1.0) and an ordinary Gaussian laser beam (q = 1.5), respectively for different a_0=1, 3. We kept a_0 same for Gaussian and q-Gaussian laser beam for comparison.

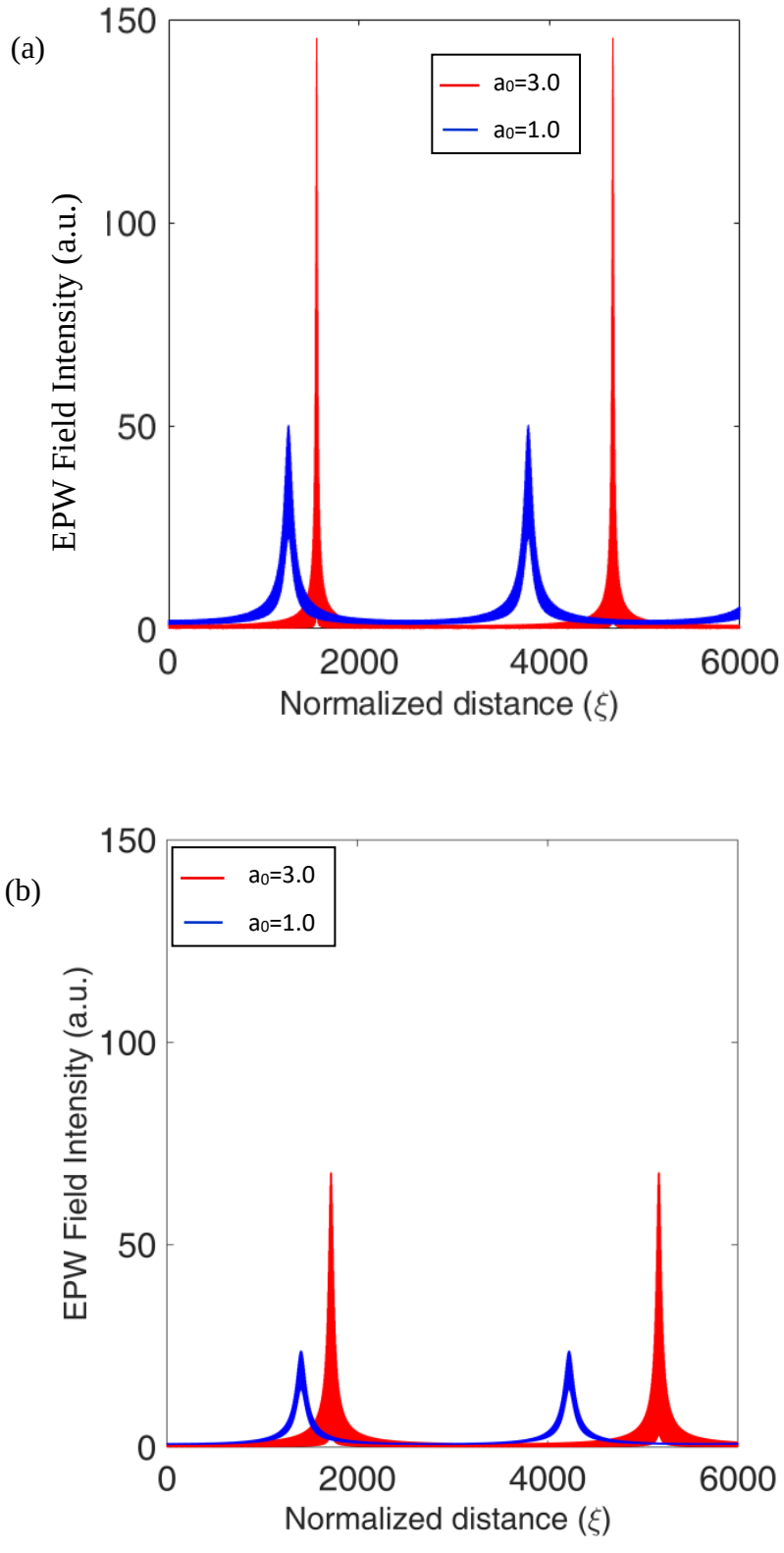

Fig. 4.4. EPW field intensity (in a.u.) with normalized distance (ξ) for (a) q= 1.0 and (b) q=1.5 for a_0=1, a_0=3.

We find that the q-Gaussian laser beam excites a more intense EPW. In both the cases, for a_0=3, the field intensity of EPW is enhanced significantly. For the case of q=1, the normalized EPW intensity is approximately 150 a.u. for a_0=3, that is, almost three times as compared to 50 a.u. for a_0=1. Also, for the case q=1.5, EPW intensity for the higher value of laser strength parameter (a_0=3) is approximately three times as compared to the lower value of laser strength parameter (a_0=1). This is quite obvious because q-Gaussian laser exhibits more self-focusing during propagation as mentioned in previous section. Hence, it exerts a stronger ponderomotive force on plasma electrons. Consequently, the excited EPW shows larger amplitude for q-Gaussian laser beam in comparison to the Gaussian laser beam.

(c) Electron Acceleration

In previous section, it was found that a large amplitude EPW can be excited by a q-Gaussian laser beam. This is resembled to the electrostatic wakefield excited by a short-pulse laser in plasmas. The longitudinal electric field associated with the EPW can accelerate the plasma electrons. We here employ the EPW field estimated from Eq. (4.21) to obtain the electron energy gain during acceleration. We use the equation of motion and energy equation to estimate the electron energy gain by the plasma wave excited by q-Gaussian laser beam. The equation of motion and energy equation for the electrons can be written as

$$\frac{d\boldsymbol{p}}{dt} = -e\boldsymbol{E_{pw}} \tag{4.22}$$

$$\frac{d\gamma}{dt} = -\frac{e}{m_0 c^2} E_{pw} v_z \,, \tag{4.23}$$

Monika Yadav, Department of Applied Physics, Delhi Technological University, Delhi, India

where $\boldsymbol{p} = m_0\gamma\boldsymbol{v}$is the electron momentum, γ is the relativistic factor.

Using Eqs. (4.22) and (4.23), the electron kinetic energy can be calculated as $E_{KE} = m_0c^2\gamma$. The electric field of EPW (E_{pw}) can be calculated using Poisson's Equation. We solve Eqs. (4.21)-(4.23) using appropriate numerical parameters to obtain the electron kinetic energy. It is also very clear that the electrons trapped in the accelerating phase of the large amplitude EPW are accelerated to higher energies. The similar findings have also been observed from the numerical results as shown in Fig. 4.5. In Fig.4.5, the maximum energy gained by the accelerated electrons trapped in the EPW excited by a q-Gaussian laser beam has been shown for different $a_0 = 1, 2$. The maximum electron energy reduces with increasing the q-parameter (i.e., approaching towards the Gaussian profile). That means the electrons gain larger energy for q-Gaussian laser beam. The maximum electron energy gain is obtained for $q = 0.5$. The deviation of q-parameter affects the laser self-focusing and consequently the electron energy gain. We claim that $q = 0.5$ is an optimized q-parameter to obtain the maximum electron energy gain during EPW acceleration. For smaller q-values, the focusing has not been observed for the given set of laser and plasma parameters. Thus the energy gain for smaller q-parameter is not reasonable. For smaller q-parameter, the radial variation of the laser amplitude would be large and hence the paraxial approximation is not valid for that propagation. The electron energy gain also depends on a_0. The maximum electron energy enhances for higher a_0. The reason behind this is the larger EPW amplitude excited by a stronger laser beam. We take parameter selection for an appropriate combination of parameters corresponding to the reasonable

Monika Yadav, Department of Applied Physics, Delhi Technological University, Delhi, India

electron energy gain. The electrons gain about 45 MeV maximum energy by employing a q-Gaussian laser beam (with $q = 0.5$) of intensity of the order of $\sim 10^{19} W cm^{-2}$. Malik *et al.* [37] have employed various shaped laser pulse for wakefield excitation and electron acceleration. They predicted about 33.5 MeV electron energy gain for a rectangular–triangular laser pulse of $3 \times 10^{18} W cm^{-2}$. The electron energy gain is reasonably higher for q-Gaussian laser beam. The maximum electron energy gain may be much larger, if a higher intensity q-Gaussian laser beam is employed for plasma interactions.

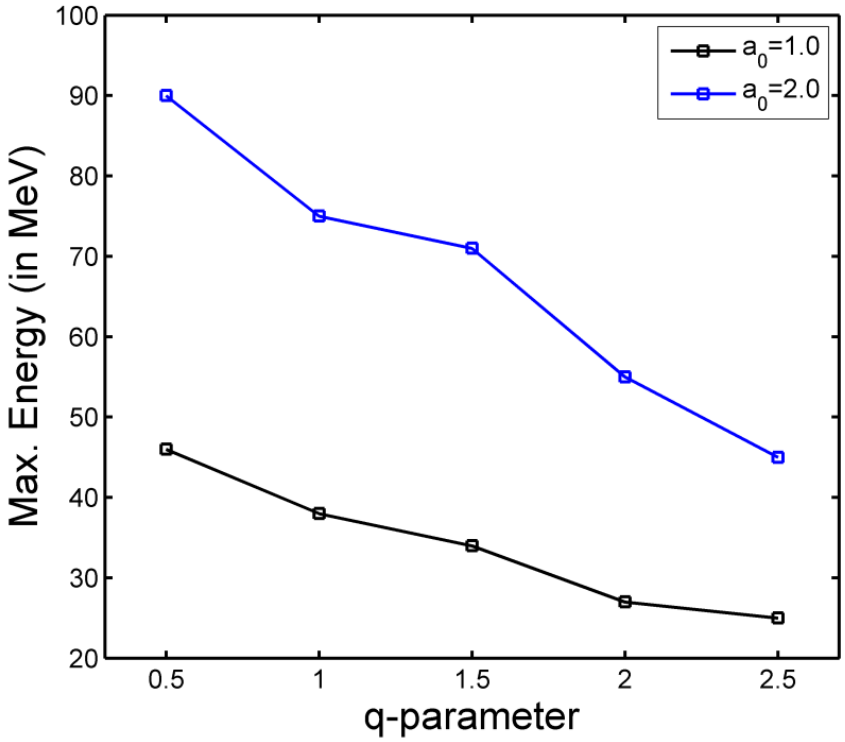

Fig. 4.5. Maximum electron kinetic energy (in MeV) with q-parameter of q-Gaussian laser beam for different laser intensity parameters of $a_0 = 1$ and $a_0 = 2$ with $\omega_p/\omega_0 = 0.09$.

As predicted, it is evident from the results that the energy gained by the accelerated electrons has a dependency on self-focusing of the laser beam and the

enhanced amplitude of the EPW. For higher values of q parameter, the energy gained by the electrons is also higher. It means as we approach to q-Gaussian laser beam from Gaussian laser beam, the maximum energy gained by the electrons increases. For the future prospect, the laser and plasma parameters can be further optimized and new techniques can be explored to increase the maximum energy of the accelerated electrons using a q-Gaussian laser beam. Hence, the q-Gaussian laser might be of great use in the field of laser wakefield electron acceleration and might replace Gaussian laser beam for this purpose.

4.4 Conclusion

This study examined the self-focusing phenomenon of an intense q-Gaussian laser beam and subsequently its significant effect on EPW excitation and electron acceleration. The self-focusing is found to be considerably enhanced for lower q-values of q-Gaussian laser beam. It has also been observed that the self-focusing is faster when the laser intensity is higher. Hence, the focusing length is less for higher intensity of the laser beam. We noticed that the self-focusing has a significant influence on EPW excitation. The EPW field intensity is seriously affected by the q-parameter of the q-Gaussian laser beam. This study shows that the field intensity of EPW is enhanced for lower q-values of laser beam (i.e. for q-Gaussian laser beam). The EPW amplitude is found to be maximum at the focal spots of the laser beam. In a result, the energy of the electrons accelerated by the EPW excited by a q-Gaussian laser beam is also increased. The numerical results show that he electron energy gain strongly depends on the q-value of the q-Gaussian laser

beam. We predict that q=0.5 is the optimized q-parameter corresponding to the maximum electron energy gain for all laser intensity parameters.

In conclusion, based on the proposed theoretical model, we suggest employing a q-Gaussian laser beam for better electron acceleration by the EPW. This study revealed the advantage of the propagation of q-Gaussian laser beam in plasmas under the relativistic and ponderomotive nonlinearities over Gaussian profile. This study also provides the optimized parameters of q-Gaussian laser beam to further study the possible nonlinear processes in plasmas, which may be crucial in demonstrating the plasma channel formation by a relativistic laser beam. It might be relevant to understand the various aspects of laser-plasma interactions such as plasma heating where an intense laser beam is required and particle acceleration schemes.

References

[1] D. Strickland and G. Mourou, *Opt. Commun.* **56**, 219 (1985).

[2] J. Krall, E. Esarey, P. Sprangle, and G. Joyce, *Phys. Plasmas* **1**, 1738 (1994).

[3] V. K. Tripathi and C. S. Liu, *Phys. Plasmas* **1**, 990 (1994).

[4] Modena, Z. Najmudin, A. E. Dangor, C. E. Clayton, K. H. Marsh, C. Joshi, V. Malka, C. B. Darrow, C. Danson, D. Neely, and F. N. Walsh, *Nature* **377**, 606 (1995).

[5] G. Geddes, C. S. Toth, J. V. Tilborg, E. Esarey, C. B. Schroeder, D. Bruhwiler, C. Nieter, J. Cary, and W. P. Leemans, *Nature* **431**, 538 (2004).

[6] S. M. Hooker, *Nat. Photonics* **7**, 775 (2013).

[7] M. Yadav, S.C. Sharma, and D. N. Gupta, *IEEE Trans. Plasma Science* **46**, 2521 (2018).

[8] D. N. Gupta, K. Gopal, V. V. Kulagin, and H. Suk, *Current App. Phys.* **15**, 174 (2015).

[9] W. L. Kruer, *The Physics of Laser Plasma Interaction*, Addison-Wesley, New York (1988).

[10] A. Y. Faenov, A. I. Magunov, T. A. Pikuz, I. Y. Skobelev, S. V. Gasilov, S. Stagira, F. Calegari, M. Nisoli, S. D. Silvestri, L. Poletto, P. Villoresi, and A. A. Andreev, *Laser Part. Beams* **25**, 267 (2007).

[11] W. Zhang and M. Y. Yu, *Appl. Phys. Lett.* **99**, 141501 (2011).

[12] P. Sprangle, E. Esarey, and A. Ting, *Phys. Rev. Lett.* **64**, 2011 (1990).

[13] H. Hora, J. *Opt. Soc. Am*. **65**,882 (1975).

[14] X. L. Chen and R. N. Sudan, *Phys. Rev. Lett.* **70**, 2082 (1993).

[15] C. S. Liu and V. K. Tripathi, *Interaction of Electromagnetic Waves and Electron Beams with Plasmas*, World Scientific (1994).

[16] E. Esary, P. Sprangle, J. Krall, and A. Ting, *IEEE J. Quant. Electron.* **33**, 1879 (1997).

[17] A. G. Litvak, *Zh. Eksp. Teor. Fiz.* **57**, 629 (1969).

[18] G. Z. Sun, E. Ott, Y. C. Lee, and P. Guzdar, *Phys. Fluids* **30**, 526 (1987).

[19] P. Sprangle, C. M. Tang, and E. Esarey, *IEEE Trans. Plasma Sci.* **15**, 145 (1987).

[20] P. Sprangle, E. Esarey, J. Krall, and G. Joyce, *Phys. Rev. Lett.* **69**, 2200 (1992).

[21] B. Hafizi, E. Esarey, and P. Sprangle, *Phys. Rev. E* **55**, 3539 (1997).

[22] S. A. Akhmanov, A. P. Sukhorukov, and R. V. Khokhlov, *Sov. Phys. JTEP* **10**, 609 (1968).

[23] M. S. Sodha, A. K. Ghatak, and V. K. Tripathi, *Prog. Opt.* **13**, 169 (1976).

[24] M. S. Sodha, A. K. Ghatak, and V. K. Tripathi, *Self-Focusing of Laser Beams in Dielectric, Plasmas and Semiconductors*, Tata McGraw-Hill (1974).

[25] P. Kaw, G. Schmidt, and T. Wilcox, *Phys. Fluids* **16**, 1522 (1973).

[26] D. N. Gupta, M. S. Hur, I. Hwang, H. Suk, and A. K. Sharma, *Opt. Soc. Am. B* **24**, 1155 (2007).

[27] M. S. Sodha, R. P. Sharma, and S. C. Kaushik, *Plasma Phys.* **18**, 879 (1976).

[28] D. N. Gupta and H. Suk, *Phys. Plasmas* **18**, 124501 (2011).

[29] H. S. Ghotra and N. Kant, *Phys. Plasmas* **23**, 013101 (2016).

[30] H. S. Ghotra and N. Kant, *Opt. Commun*. **383**, 169 (2017).

[31] P. Rawat, R. Gauniyal, and G. Purohit, *Phys. Plasmas* **21**, 062109 (2014).

[32] P. Johannisson, D. Anderson, M. Lisak, and M. Marklund, *Opt. Commun.* **222**, 107 (2003).

[33] B. Gaur, P. Rawat, and G. Purohit, *Laser Part. Beams* **34**, 621 (2016).

[34] T. S. Gill, N. S. Saini, and S. S. Kaul, *Optik* **115**, 493 (2004).

[35] A. Sharma and I. Kourakis, *Laser Part. Beams* **28**, 479 (2010).

[36] L. Wang, X. Hong, J. A. Sun , R. A. Tang, Y. Yang, W. J. Zhou, J. M. Tian, and W. S. Duan, *Phys. Lett. A* **381**, 2065 (2017).

[37] H. K. Malik, S. Kumar, and Y. Nishida, *Opt. Commun.* **280**, 417 (2007).

[38] S. Kumar, H. K. Malik, and Y. Nishida, *Phys. Scripta* **74**, 525 (2006)

[39] R.Kaur, T.S. Gill,and R. Mahajan, *Phys. Plasmas* **24**, 053105 (2017).

[40] N. Gupta and A. Singh, *Optik* **127**, 8542 (2016).

[41] H. K. Malik and L. Devi, *Results in Phys.* **17**, 103070 (2020).

[42] L. Devi and H. K. Malik, *Optik* **207**, 164439 (2020).

[43] P. K. Patel, M. H. Key, A. J. Mackinnon, R Berry, M Borghesi, D. M. Chambers, H. Chen, R. Clarke, C. Damian, R. Eagleton, R. Freeman, S. Glenzer, G. Gregori, R. Heathcote, D. Hey, N. Izumi, S. Kar, J. King, A. Nikroo, A. Niles, H-S. Park, J. Pasley, N. Patel, R. Shepherd, R. A. Snavely, D. Steinman, C. Stoeckl, M. Storm, W. Theobald, R. Town, R. Van Maren, S. C. Wilks and B. Zhang, *Plasma Phys. Control. Fusion* **47**, B833 (2005).

[44] M. Nakatsutsumi, J. R. Davies, R. Kodama, J. S. Green, K. L. Lancaster, K. U. Akli, F. N. Beg, S. N. Chen, D. Clark, R. R. Freeman, C. D. Gregory, H. Habara, R. Heathcote, D. S. Hey, K. Highbarger, P. Jaanimagi, M. H. Key, K. Krushelnick, T. Ma, A. MacPhee, A. J. MacKinnon, H. Nakamura, R. B. Stephens, M. Storm, M. Tampo, W. Theobald, L. Van Woerkom, R. L. Weber, M. S. Wei, N. C. Woolsey, and P. A. Norreys, *New J. Phys.* **10**, 043046 (2008).

[45] M. Dwivedi and H. K. Malik, *Opt. Laser Engineering* **129**, 106070 (2020).

[46] H. K. Malik, *J. Appl. Phys.* **104**, 053308 (2008).

[47] A. K. Aria and H. K. Malik, *Opt. Commun*. **282**, 423 (2009).

[48] M. Yadav, D. N. Gupta, and S. C. Sharma, *Phys. Plasmas*, 27 093106 (2020).

5

LASER WAKEFIELD ACCELERATION IN PRESENCE OF MAGNETIC WIGGLER

5.1 Brief outline of the chapter

In this chapter, it is revealed that a relativistic plasma wave associated with the laser wakefield, having an extremely large electric field, may be utilized for the acceleration of plasma particles. The large accelerating field gradient driven by a plasma wave is the basic motivation behind the acceleration mechanism. Such a plasma wave can be excited by a single laser in the form wakefield due to laser-plasma interactions. In this particular work, we study the enhancement of electron acceleration by plasma wave in presence of a wiggler magnetic field. Electrons trapped in the plasma wave are accelerated due to the additional resonance provided effectively by the wiggler field, which contributes to the large energy gain of electrons during acceleration. The resonant enhancement of electron acceleration by the wiggler magnetic field has been validated by single particle simulations. The dependence of energy gain on plasma wave amplitude, initial electron energy, wiggler magnetic field strength and electron trajectories have been investigated. Using the model, the involvement and importance of inverse free-electron laser (IFEL) mechanism in electron acceleration is analyzed. A scaling law for electron energy optimization is proposed for future electron accelerator development.

5.2 Introduction

The generation of high-intensity laser pulses (≥10TW) has led to the development of laser-driven electron acceleration, electromagnetic radiation generation and free-electron laser [1-5]. Large amplitude plasma wave has been considered a potential mode for accelerating charged particles. It was first proposed in 1979 by Tajima and Dawson that the plasma wakefield can be excited due to the ponderomotive force generated by high-intensity laser and plasma interactions. Electrons from plasma background (or injected from outside) can get trapped [8] in the wakefield and accelerated to very high energies (GeV) [9,10]. These large amplitude plasma waves can be generated through different accelerator schemes [11-14] such as plasma beat-wave accelerator (PBWA), laser wakefield accelerator (LWFA), self-modulated laser wakefield accelerator (SM-LWFA) and plasma wakefield accelerator (PWFA). LWFA scheme utilizes a single laser pulse to generate the plasma wakefield. In PBWA, two laser pulses with frequency difference comparable to the plasma frequency are used to excite a large amplitude plasma wave.

Everett *et al.* [15] observed an energy gain of 28 MeV when 2 MeV electrons are injected into the plasma wave, excited by beating of two laser beams in hydrogen plasma. Modena *et al.* [16] observed the electron energy gain of 44 MeV at wave-breaking and a sudden increase in number of accelerated plasma electrons also. In this scheme, the electron gain is limited by wave particle dephasing, which can be addressed using surfatron concept. Leemans *et al.* [17] have experimentally demonstrated upto 1 GeV high quality electron bunches using a plasma channel guided laser. It has also been observed theoretically that the electron gain can be increased by imposing a transverse and oblique magnetic field to the plasma wave [18,19]. This prevents the electrons to outrun the wave and thus the electrons remain in phase with it. A model has also been developed for azimuthal magnetic field to study the electron acceleration by the plasma wave[20,21]. Gahn *et al.* [22] experimentally measured multi millielectronvolt electrons in high-density gas

jet using 1.2-TW power, 200-fs laser pulses and verified it by 3-D PIC simulation. Kaur and Gupta [23] studied the increment in electron acceleration by plasma wave in an ion channel in presence of guiding azimuthal magnetic field. As we have implemented the Inverse-FEL mechanism in this study, it becomes inevitable to discuss FEL and Inverse-FEL schemes.

(a) Free electron laser (FEL)

FEL is a highly tunable synchrotron light source which produces extremely brilliant, short pulse radiations and is able to operate from Terahertz to x-ray region [24]. In FEL, the emission process does not take place in atomic or molecular system with population inversion, like conventional lasers. On the contrary, the optical amplification takes place when the relativistic electrons from an electron accelerator are traversed in an undulator or wiggler. A wiggler is a periodic arrangment of magnets with alternating poles (see Fig. 5.1). It generates a side to side periodically varying magnetic field.

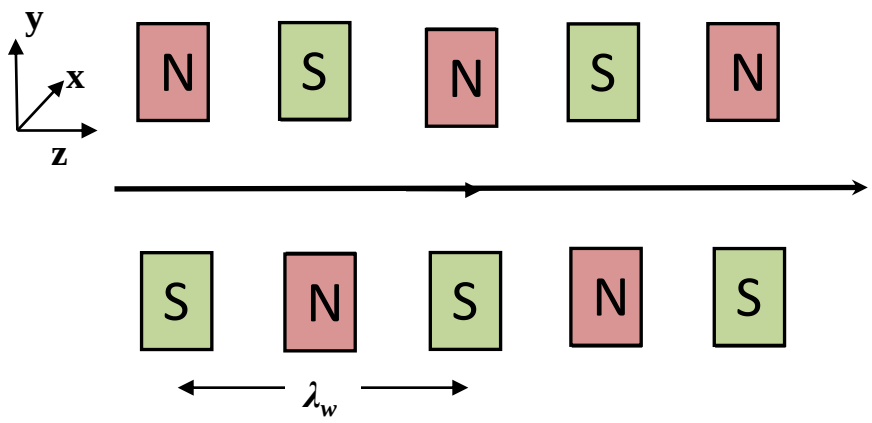

Fig. 5.1. Schematic of the wiggler illustrating periodic arrangements of magnets with alternating poles.

When an electron beam passes through the magnetic field produced by wiggler, it experiences a Lorentz force due to that field. The electrons start wiggling due to the transverse velocity component. The transverse acceleration of charge leads to the radiation generation, which is incoherent in nature till that

point. The transverse field of radiation interacts with the transverse electric current of wiggling electrons. Energy exchange occurs between the transverse electron current and transverse electric field of a co-propagating light beam. Depending on the phase of the light beam with the electrons wiggling motion, some electrons gain energy while others lose energy. The electrons that gain energy begin to move ahead of the average electron, while the electrons that lose energy begin to fall behind the average. Thus, modulation in energy results in a spatial modulation leading to bunching of electrons along the axial direction. These bunches have period equal to an optical wavelength. Hence, microbunched electrons radiate coherently, at higher power, amplifing co-propagating light beam. The wavelength of the radiation can be tuned by choosing the electron beam energy, wiggler period and wiggler magnetic field.

$$\lambda_l = \frac{\lambda_w}{2\gamma^2}\left(1 + \frac{K^2}{2}\right), \tag{5.1}$$

where λ_l is the wavelength of the emitted radiation, λ_w is the wiggler wavelength, γ is the relativistic gamma factor, and K is the dimensionless parameter called wiggler strength parameter. It is related to wiggler period (b_w in *T*) and wiggler magnetic field (λ_w in *cm*) as:

$$K = 0.934(b_w.\lambda_w)\,. \tag{5.2}$$

(b) Inverse-Free electron laser (IFEL)

Inverse-FEL (IFEL), as a vacuum acceleration process, was first proposed by Palmer [25] in 1972. IFEL acceleration experiments were performed at Brookhaven National Laboratory (BNL) using CO2 laser in 1990s [26]. In an IFEL, electron beam and laser co- propagate through a magnetic array called wiggler. Here, energy is transferred from laser beam to electrons, contrary to FEL. For the maximum transfer of energy from laser to electrons, the IFEL resonance condition [27] is given by $\lambda_l \approx (1 + b_w^2)\,\lambda_w/2\gamma^2$, where λ_l is the laser wavelength, λ_w is the wiggler wavelength, b_w is the wiggler field amplitude, and γ is the relativistic gamma factor. In this acceleration

mechanism, it is important to maintain synchronism between the radiation and the elecron beam. It can be done by tapering of the wiggler period or wiggler magnetic field. Keeping the wiggler period and field constant limits the energy gain due to synchrotron losses. Hence, it is necessary to vary these parameters to maintain the resonance condition. Mirzanejhad *et al.* [28] examined the electron bunch acceleration using circularly polarized laser pulse in helical wiggler. Hartemann *et al.* [29] have demonstrated the increment in the IFEL interaction bandwidth and energy gain by using ultrashort and super intense laser pulse. Good focusing and high quality electron beams in IFEL makes it suitable for advanced light sources, next linear collider (NLC), and biomedical applications [30]. One of the major drawbacks of this acceleration process is the electron wave dephasing. Diffraction of laser pulse over the IFEL length is also a limiting factor. With the increase in the electron energy gain, FEL resonance condition no longer holds. One of the way to prevent this discrepancy is to taper the wiggler period or using chirped laser pulse [29]. Kumar and Yoon [31] investigated the combined effect of chirped laser pulse and tapered wiggler on the electron acceleration and hence explained dependence of electron energy on these parameters. Electron capture and high accelerating gradient of monoenergetic electron beam using IFEL was first shown by Duris *et al.* [32] in 2014. Energy gain >20 MeV was demonstrated using laser pulse of intensity $\sim 10^{13}\ W/cm^2$ and a tapered undulator of length 0.5m.

In this work, we, first time, use the IFEL mechanism to study the electron acceleration using a plasma wave. Here, in order to overcome the above mentioned drawbacks of lasing in IFEL, the plasma wave is used to accelerate the electrons. A transverse velocity component is provided by the wiggler field, which further enhances the longitudinal momentum and accelerated the electrons considerably. The transverse motion of electrons is stabilized using the focusing property of wiggler field. The FEL arrangement prevents the accelerated electrons to escape and thus helps to extract electrons when required.

In this chapter, the electron dynamics is discussed analytically using energy and momentum equations. Single particle MATLAB code is utilized to

validate the theoretical model. The dependence of various plasma wave parameters and wiggler parameters on electron acceleration is examined. Scaling laws are also given for optimization of electron energy to obtain efficient electron acceleration. Plasma wave intensity, wiggler magnetic field, wiggler period and tapering parameter are optimized to overcome the dephasing limits and to attain substantial electron acceleration. We draw the conclusions in the last section of this chapter.

5.3 Governing Equations

In an underdense plasma, when an intense enough laser pulse is propagated, the electrons are expelled from the high intensity region creating a density depression on the axis of the laser. It leads to the non-uniform plasma frequency across the laser cross section. Thus, considering a nonlinear profile of plasma wave propagating in the z-direction as [14,33]

$$\boldsymbol{E}_p = \boldsymbol{A} e^{-x^2/r_p^2}\left[\hat{z}\cos\eta + \hat{x}\, e^{-x^2/r_p^2}\frac{2x}{kr_p^2}\sin\eta\right], \tag{5.3}$$

where r_p is the radius of the wakefield, $\eta = (\omega t - kz + \delta)$ is the phase of the plasma wave, δ is the initial phase, the potential Φ of the wave can be calculated using $\boldsymbol{E} = -\nabla\Phi$. Here, $\boldsymbol{E}_p$ can be written as $\boldsymbol{E}_p = \boldsymbol{E}_x\hat{x} + \boldsymbol{E}_z\hat{z}$ for our convenience.

We also assume a planar tapered wiggler magnetic field given by

$$\boldsymbol{B}_w = \hat{x}B_{ow}\sin[k_w z/(1+\alpha z)], \tag{5.4}$$

where B_{ow} represents the wiggler magnetic field, k_w is the wiggler wave number, α is the tapering parameter along z axis, and the wiggler magnetic field is polarized in the x-direction. The value of wiggler wave number k_w is optimized using the resonance condition. This condition shows a unique relation between wiggler wavelength (λ_w), laser wavelength (λ_l), wiggler magnetic field amplitude (B_{ow}) and electron energy gain (γmc^2). Hence, the deviation from the resonance condition limits the electron energy gain.

In the presence of plasma wave and the wiggler magnetic field, the governing energy and momentum equations are given by

$$\frac{d\boldsymbol{p}}{dt} = -e\left(\boldsymbol{E}_p + \boldsymbol{v} \times \boldsymbol{B}\right), \tag{5.5}$$

and $$(mc^2)\frac{d\gamma}{dt} = -e\left(\boldsymbol{E}_p . \boldsymbol{v}\right), \tag{4.6}$$

respectively. Here, $p = \gamma mv$ is the electron momentum, γmc^2 is the electron energy, and $\gamma^2 = 1 + \{\left(p_x^2 + p_y^2 + p_z^2\right)/m^2c^2\}$ stands for the relativistic gamma factor. Writing energy and momentum equations in components, we get

$$m\left[\gamma\frac{dv_x}{dt} + v_x\frac{d\gamma}{dt}\right] = -e(E_x) \tag{5.7}$$

$$m\left[\gamma\frac{dv_y}{dt} + v_y\frac{d\gamma}{dt}\right] = -e(v_z B_w) \tag{5.8}$$

$$m\left[\gamma\frac{dv_z}{dt} + v_z\frac{d\gamma}{dt}\right] = -e(E_z) + e\left(v_y B_w\right) \tag{5.9}$$

$$\frac{d\gamma}{dt} = -\frac{e}{mc^2}(v_x E_x + v_z E_z) \tag{5.10}$$

Substituting $d\gamma/dt$ from Eq. (5.10) in Eqs. (5.7)-(5.9) and also putting the plasma wave electric field and wiggler magnetic field from Eqs. (5.3) and (5.4) in energy and momentum equations. Normalizing the resulting equations, we get,

$$\gamma\frac{dv_x}{dt} = (v_x^2 - 1)a_x + v_x v_z a_z, \tag{5.11}$$

$$\gamma\frac{dv_y}{dt} = -v_z b_w + v_x v_y a_x + v_y v_z a_z, \tag{5.12}$$

$$\gamma\frac{dv_z}{dt} = (v_z^2 - 1)a_z + v_x v_z a_x + v_y b_{w,} \tag{5.13}$$

Monika Yadav, *Department of Applied Physics, Delhi Technological University, Delhi, India*

$$\frac{d\gamma}{dt} = -v_x a_x - v_z a_z. \quad (5.14)$$

Eqs. (5.11)-(5.14) are normalized using dimensionless physical quantities as : $t \to \omega t, x \to kx, z \to kz, v_x \to v_x/c\,, v_z \to v_z/c\,, k_w \to ck_w/\omega_p,\ \alpha \to \alpha/k,\ \ a_x = eE_x/m\omega c\,, a_z = eE_z/m\omega c\,,\ a_p = eE_p/m\omega c\,, b_w = eB_w/m\omega c,$, where -*e* and *m* are electron charge and mass, respectively. Eqs. (5.11)-(5.14) are ordinary coupled differential equations describing relativistic electron dynamics. These equations are solved numerically using a relativistic single-particle code.

5.4 Numerical Results

We numerically solve the relativistic equations of motion and the energy equations using the fourth order Runge-Kutta method in MATLAB with adaptive step size. The dimensionless parameters are used for the calculations. Electron acceleration and energy gain are estimated for distinct plasma and wiggler parameters. These parameters are optimized to get the maximum acceleration. We consider a plasma wave with the normalized amplitude of $a_p = 0.3$ and the wavelength of 3.3μm. The optimized value of normalized plasma wave spot size is 40. The wiggler parameters have been optimized as: the normalized wiggler magnetic field strength is b_w= 0.06 (corresponds to the tapered wiggler field of 2 KG), the wiggler period is $\lambda_w = 3.07$ cm, and the tapering parameter α = 9×10^{-3}. The electron is assumed to be originated at (x_0, y_0, z_0) = (0, 0, 0.2) with the initial velocity components (v_{x0}, v_{y0}, v_{z0}) = (0, 0, 0.92c). The electron trajectories and the variation of electron energy gain with different numerical parameters have been investigated and discussed in this section. In our study, we observed that the plasma wave gives an initial kick to the electrons by transferring the energy. The tapered wiggler magnetic field sustains the energy gain resonantly due to its longer wavelength.

IFEL concept has already been proposed and investigated as an efficient source of electron beam. Laser pulse has been utilized to accelerate electrons in IFEL mechanism till now. To maintain the IFEL resonance condition over the

interaction region, effect of tapering of magnetic wiggler and chirping of laser pulse has also been studied. And it has been observed that these parameters are quite effective in enhancing the electron energy gain. The maximum electron energy gain (without taking chirping parameter into account) recorded is approximately 200 MeV [29]. Because, confining the high-intensity laser beam over the acceleration region is a major challenge. Diffraction also limits the acceleration length. To overcome these issues, we here propose to study the electron acceleration by the plasma wave instead of the laser pulse in the presence of magnetic wiggler. The electron Larmor frequency for the used wiggler magnetic field is very less compare to the pump frequency. Thus the dispersion relation of the plasma wave may not be affected for this strength of the magnetic field. The smaller magnetic field justifies avoiding the modification in plasma wave dispersion relation. Enhancement in electron energy has been confirmed from the results (~400 MeV) to validate our proposed idea for feasible numerical parameters.

(a) Dependence of electron energy on plasma wave amplitude

The plasma wave is one of the major source for electron energy gain. Thus the plasma wave amplitude plays a crucial role in this mechanism. Fig. 5.2 shows the electron energy during acceleration for different plasma wave amplitudes (a_p = 0.25, 0.3, 0.4). For these estimations, the initial electron energy $\gamma_0 mc^2$=2.5 MeV is considered for the corresponding initial electron velocity v_{z0} = 0.92c. It could easily be understood by momentum equations that the electrons trapped in high-intensity plasma waves experience a stronger longitudinal force (in the direction of propagation of the plasma wave). Thus, in a result, the electrons are accelerated to higher energies due to the dominant ponderomotive effects. Higher electron energy gain is predicted for large amplitude plasma wave in this mechanism. However, the electron acceleration would be limited due to the wave-breaking related nonlinearity.

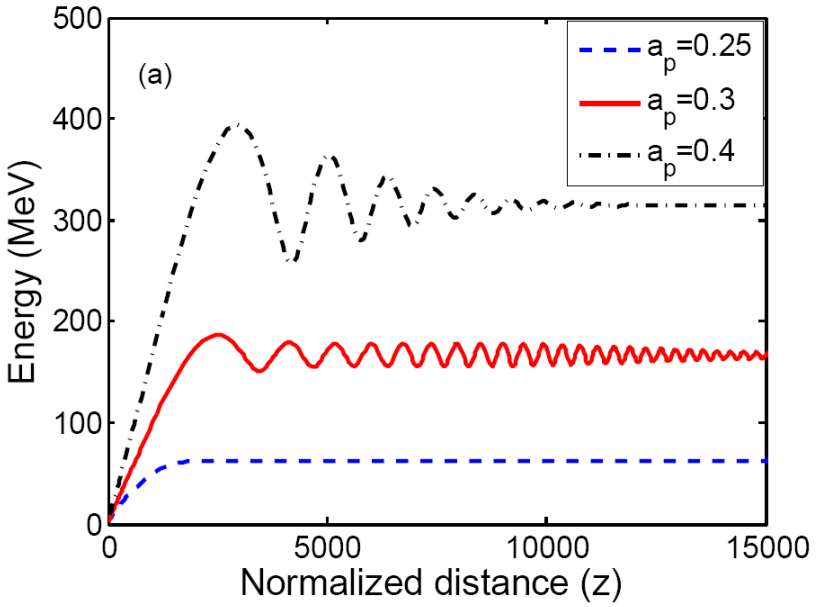

Fig. 5.2. Electron energy (γmc^2in MeV) as a function of normalized distance (z) for different plasma wave amplitudes, $a_p = 0.25$ (blue curve), $a_p = 0.3$ (red curve), $a_p = 0.4$ (green curve). Other parameters: b_w= 0.06, α = 9×10^{-3}, $a_p = 0.3$, $v_{z0} = 0.9c$, and $\gamma_0 mc^2 = 2.5$.

(b) Dependence of electron energy on plasma to wiggler wavelength

The optimum ratio of plasma to wiggler wavelength (λ_p/λ_w) also plays a significant role in electron energy gain. In Fig. 5.3, the electron energy gains for different ratios of plasma to wiggler wavelength (λ_p/λ_w=1/9320, 1/7320, 1/5320) have been estimated. Other optimized wiggler parameters are kept same as in Fig.5.2. It can be noted that the electron energy increases with the wiggler wavelength. This is due to the fact of interaction length enhancement for larger wiggler wavelength to sustain the resonant oscillations for longer time. That means the electrons can stay in the interaction region longer for the larger wiggler wavelength. Eventually, the electrons energy may be increased.

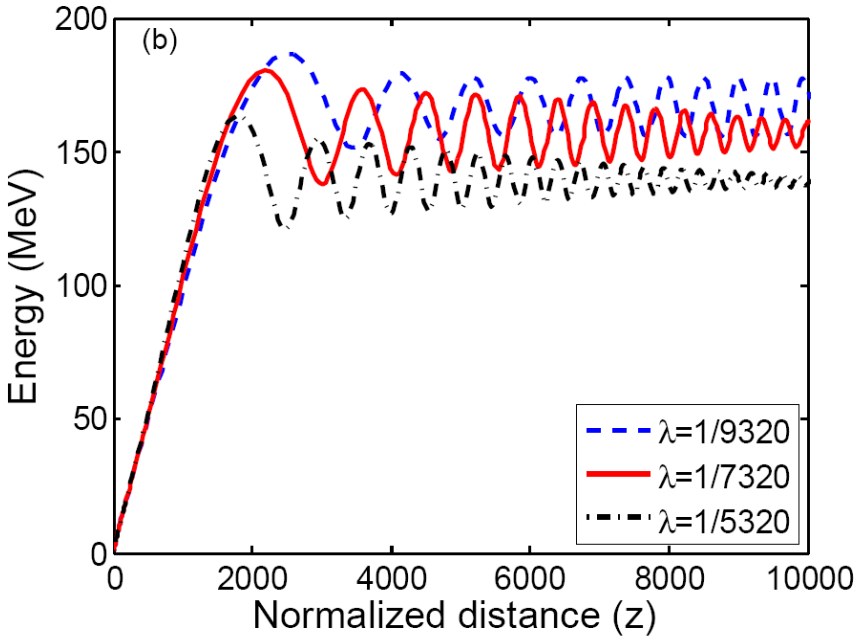

Fig. 5.3. The electron energy (γmc^2in MeV) for electrons originated at position of $z_0 = 0.2$ for different values of $\lambda = \lambda_p/\lambda_w$ = 1/9320 (blue curve), 1/7320 (red curve), 1/5320 (green curve) for $a_p = 0.3$. Other parameters are same as used in Fig. 5.2.

(c) Dependence of electron energy on wiggler magnetic field

Electrons trapped in the accelerating phase of the plasma wave can be accelerated to high energies. Here, the tapered planar wiggler magnetic field plays a crucial role in enhancement of electron energy gain during acceleration via IFEL mechanism. Fig. 5.4 represents the variation of electron energy gain with the propagation distance (z) for different wiggler field strength (b_w= 0, 0.02, 0.06), keeping, $a_p = 0.3$, λ_w/λ_p= 1/9320, and v_{z0}=0.92c. The electron energy gain increases with the wiggler magnetic field strength. However, the electron energy gain can be maximized for a particular value of the normalized wiggler magnetic field of b_w=0.06. Thus, this strength is the optimized wiggler magnetic field for which the electron energy gain is maximum and will be used in these estimations. The physics behind this can be understood as follows: the wiggler magnetic field provides an additional transverse component of velocity

to the electrons in the direction perpendicular to the propagation of plasma wave. The Lorentz force contributes to the net increase in longitudinal momentum. Hence, the net energy gain of the electrons trapped by the plasma wave is enhanced. It can also be seen from the results shown in Fig. 5.4 that the large wiggler magnetic field leads to energy oscillations to retain the electron energy. Our findings show that the electron energy gain is about two fold for an optimized strength of the magnetic field. For example, the electron energy gain is about 100 MeV in the absence of the magnetic field (where, the plasma wave is only the factor contributing in electron energy gain). The magnetic field bends the electrons to stay in the acceleration region, hence, the electron gains higher energy for an optimum magnetic field (i.e., 200 MeV for b_w=0.06) due the cyclotron resonance. However, the electron energy gain may be reduced for higher magnetic field due to mismatch in resonance during the acceleration. Thus a set of optimized parameters is necessary to achieve the energetic electrons in this mechanism.

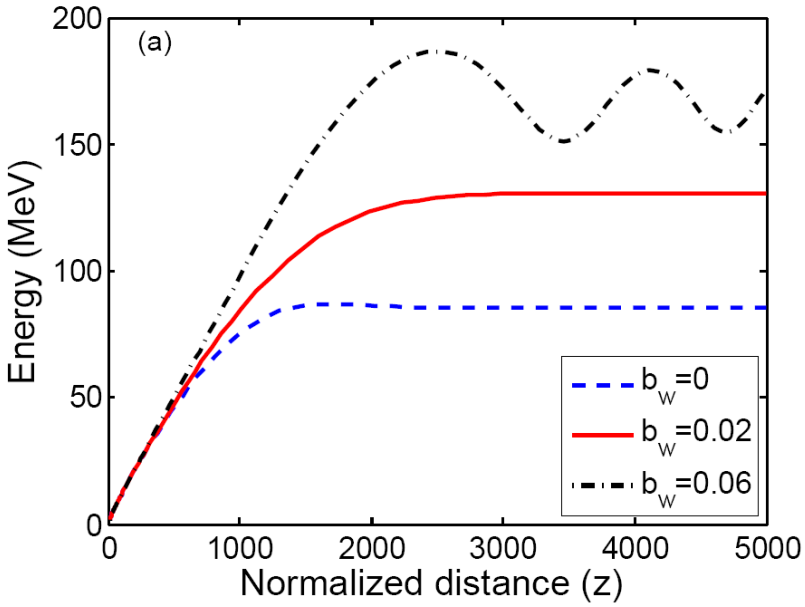

Fig. 5.4. Electron energy (γmc^2in MeV) as a function of normalized distance (z) for different values of wiggler magnetic field b_w= 0 (blue curve), b_w= 0.02 (red curve) and b_w= 0.06 (green curve).

(d) Dependence of electron energy on electron initial phase

The electron energy gain is sensitive with the initial phase by which it enters in the acceleration region. We estimate the contribution of initial phase (δ) of the electrons (with respect to the plasma wave) to the energy gain. It has already been known that an electron can only be accelerated if it is trapped in the accelerating phase of plasma wave. Hence, it is a necessity to inject the test electrons in the accelerating phase of the plasma. In Fig. 5.5, the electron energy gain for different initial phases ($\delta = 0, \pi/2, \pi$) have been plotted. It shows that the energy gain is maximum for the electrons those have the initial phase of $\delta = \pi$. This indicates that the electron in any other initial phase enters in deccelerating phase of the plasma wave. Hence, such electrons do not gain much energy and are deaccelerated. This means an optimum value of initial phase of electron is required for maximum energy gain.

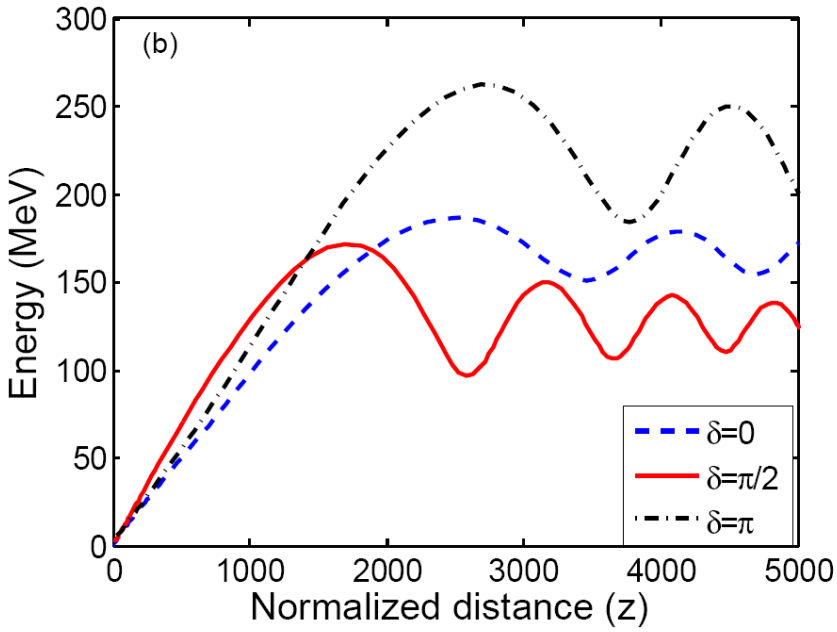

Fig. 5.5. Electron energy (γmc^2in MeV) as a function of normalized distance (z) for electrons originated at for different initial phases of the plasma wave $\delta = 0$ (blue curve), $\delta = \pi$ (red curve), and $\delta = \pi/2$ (green curve). Other

parameters are kept as $a_p = 0.3$, $\lambda = \lambda_p/\lambda_w$ = 1/9320, $v_{z0} = 0.9c$,and $b_w = 0.06$.

(e) Dependence of electron energy and trajectories on pre-acceleration

Electron energy can be enhanced if the pre-accelerated electrons are injected in the acceleration region. We have also confirmed this from our calculations. The effect of initial electron energy on plasma wave acceleration has been depicted in Fig. 5.6. It shows the variation of electron energy with the propagation distance for different initial electron energies (corresponding to the

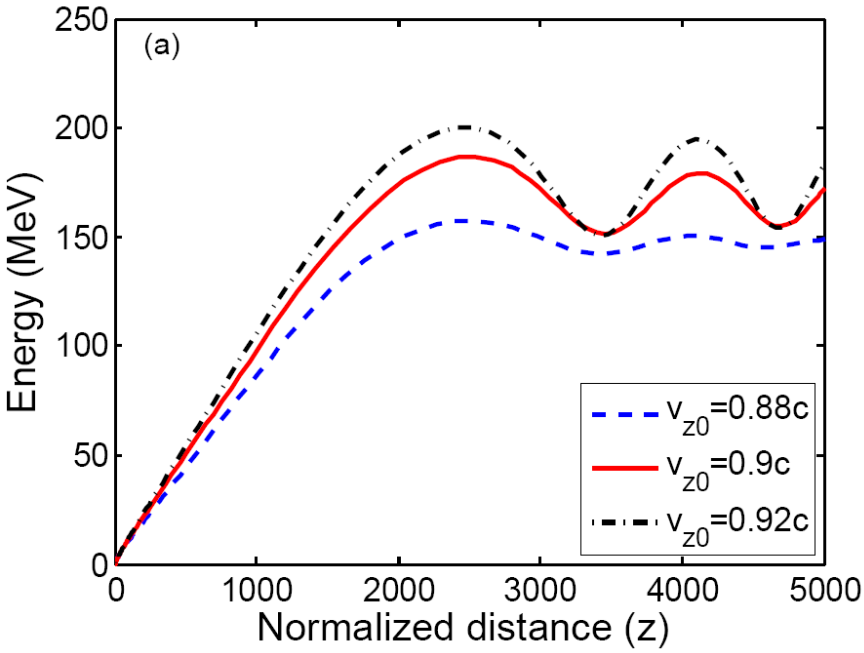

Fig. 5.6. Electron energy (γmc^2in MeV) as a function of normalized distance (z) for electrons originated at $z_0 = 0.2$ with normalized magnetic wiggler field b_w= 0.06 for different initial velocities $v_{z0} = 0.88c$ (blue curve) , $v_{z0} = 0.9c$ (red curve) and $v_{z0} = 0.92c$ (green curve).

different initial electron velocities $v_{z0} = 0.88c, 0.9c, o.92c$). It is concluded that the electron energy increases with the initial electron kinetic energy due to the strengthening of the relativistic effect. The electrons with higher initial kinetic energy are more collimated, thus they interact with the plasma wave

more efficiently to gain the energy via cyclotron resonance in IFEL mechanism. The electrons with velocity close to the speed of light in vacuum c remain in phase with the accelerating phase of the plasma wave. Thus the efficient acceleration may be occured for the electrons injected with higher kinetic energies.

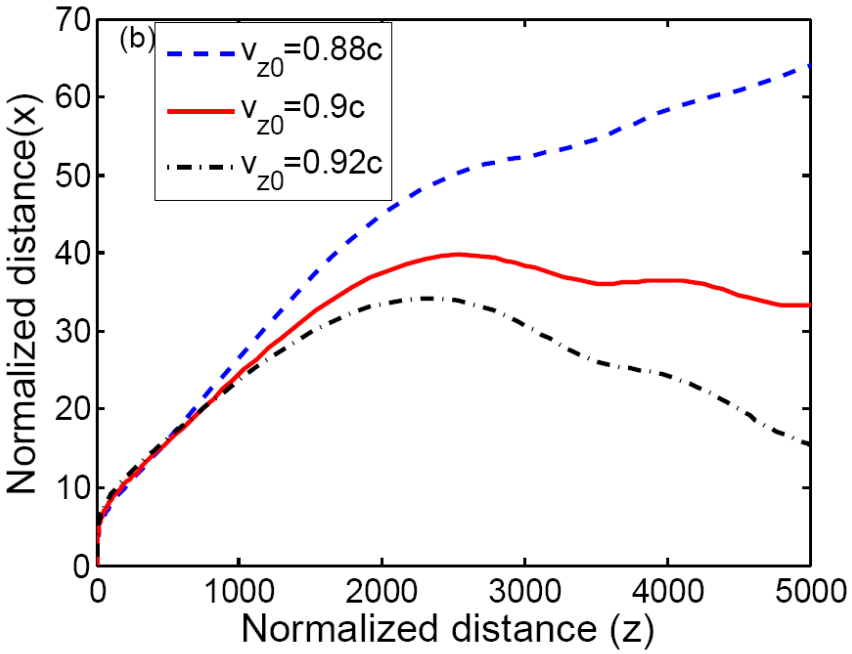

Fig. 5.7. The corresponding electron trajectories in x-z plane for the same parameters used in Fig. 5.6.

The emission angle (θ) of electrons can be calculated using

$$\tan\theta(\gamma) = \frac{\sqrt{2(\gamma/\gamma_0 - 1)/1 + \beta_0}}{\gamma - \gamma_0(1 - \beta_0)} \qquad (4.15)$$

where $\beta_0 = v_0/c$, and $\gamma_0 = (1 - \beta_0)^{1/2}$. The scattering angle for electron initial velocities (v_{z0}= 0.92c , 0.9c and 0.88c) are approximately 0.04 radian, 0.05 radian and 0.06 radian, respectively. This indicates that the electron preaccelerated with greater initial velocity is scattered less and trajects towards the interaction region to gain energy during acceleration (Fig. 5.7). Our results

shows that the electrons having large initial kinetic energy may be accelerated to higher energy.

(f) Dependence of electron energy on tapering parameter

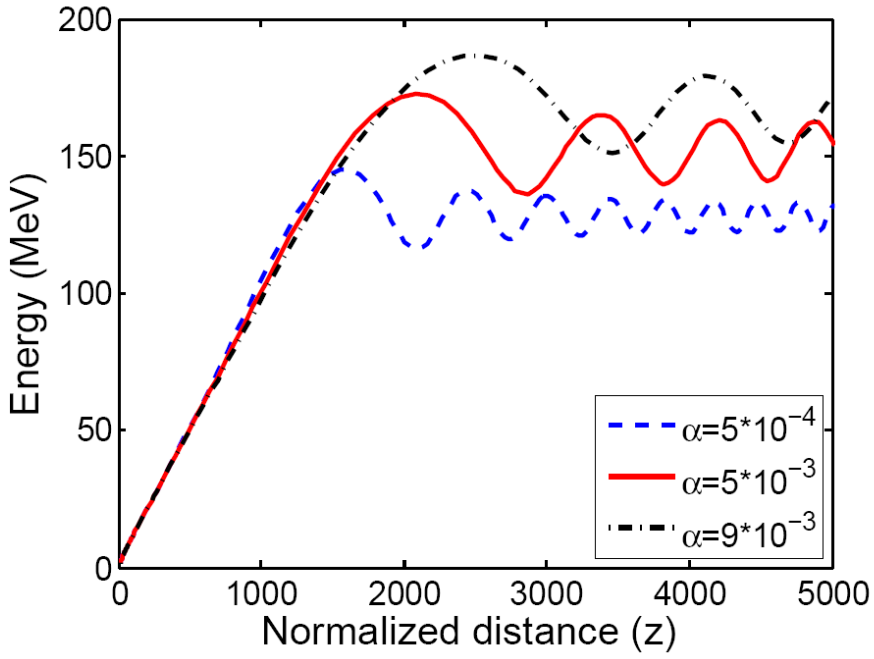

Fig. 5.8. Electron energy (γmc^2) as a function of normalized distance (z) for different values of tapering parameter (α) in the presence of a wiggler magnetic field of 2 KG. Other parameters are same as Fig.5.2.

The tapering parameter of wiggler is one of the key parameters to sustain the electron acceleration to enhance the electron energy gain. It is an arbitrary constant which indicates the tapering in the magnetic field. Fig. 5.8 shows the variation of electron energy for distinct values of normalized tapering parameter $\alpha = 5\times10^{-4}$ (blue curve), 5×10^{-3} (red curve), 9×10^{-3} (green curve). It can be noted from the figure that the electron energy is enhanced with tapering of the wiggler (i.e. for larger tapering parameter, the electron energy is improved). The larger tapering parameter enhances the acceleration gradient. Thus the electron can be trapped in the accelerating phase to gain higher energy. In other words,

the larger tapering parameter can compensate the electron dephasing by increasing the interaction bandwidth. The magnetic wiggler sustains the energy gain by maintaining the resonance due to longer wiggler wavelength. In this paper, scaling laws have been developed for electron energy gain (γmc^2) with the tapered normalized wiggler magnetic field (b_w) by keeping the ratio of wiggler to plasma wavelength λ_p/λ_w= 1/9320. In the absence of wiggler magnetic field ($b_w = 0$), the observed energy gain of electron is 80 MeV. Our results shows that the electron energy can be enhanced more than twofold using suitable plasma parameters in the presence of wiggler magnetic field. Moreover, this energy gain can be fivefold if a large amplitude plasma wave is introduced for acceleration (i.e. $a_p = 0.4$). The results shown here suggest the use of the plasma wave in IFEL mechanism for significant electron energy gain.

(g) Scaling laws for electron energy gain

The strength of wiggler magnetic field is also crucial in this mechanism. The scaling law for electron energy gain with the wiggler magnetic field can also be understood from this study. The electron energy gain increases with the magnetic field and starts to decrease after attaining the peak energy. The results of Fig. 5.9 show that the electron energy gain increases with the wiggler magnetic field strength (b_w = 0.0 to 0.06). Beyond a certain strength of wiggler magnetic field, the energy gain of electron starts to decrease due to resonance mismatch. The maximum energy attained by the electron is about 200 MeV for the wiggler magnetic field of b_w= 0.06. The peak arises at the specific value of magnetic field strength because the most of energy of the plasma wave transfers to the electrons via cyclotron resonance for that magnetic field. Moreover, after achieving a particular accelerating gradient, IFEL interaction region detunes and gets saturated. Hence, this optimized wiggler magnetic field has been considered to study the dependence of electron energy gain on other parameters.

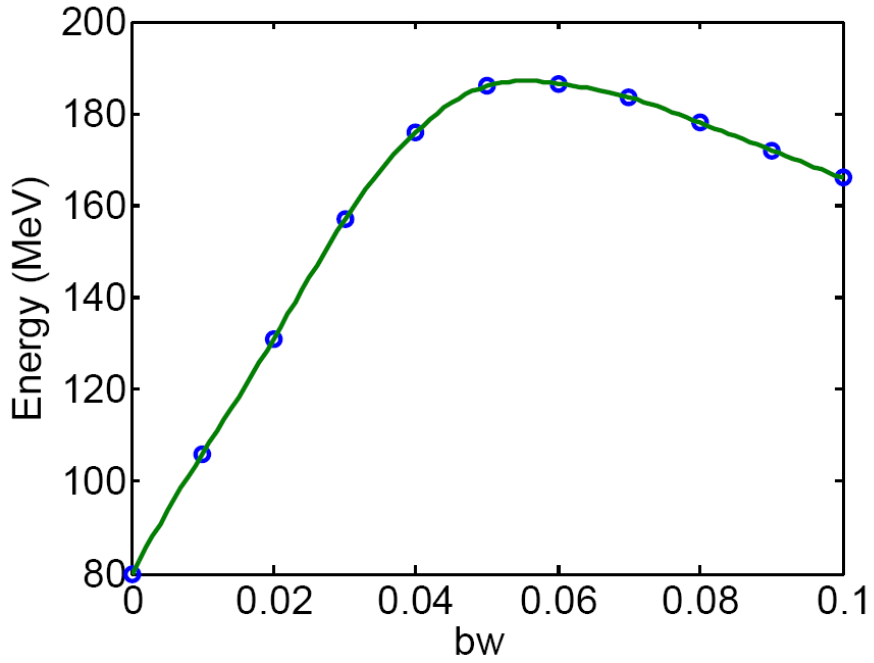

Fig. 5.9. Electron energy (γmc^2) with the wiggler magnetic field strength (b_w) for plasma wave amplitude $a_p = 0.3$. Other parameters are same as in Fig. 5.2.

5.5 Conclusion

Electrons injected at 2.5 MeV have been accelerated to 200 MeV by the plasma wave over an interaction length of approximately 2.5 mm for an optimized wiggler magnetic field of 2 KG. This corresponds to the optimized wiggler magnetic field and electrons and plasma wave parameters. Higher electron energy can be predicted for large amplitude plasma wave in this mechanism.

The maximum electron energy is obtained due to the cyclotron resonance for an optimum wiggler magnetic field. The energy gain of electrons is measured for an optimum magnetic field strength and plasma wave amplitude. We have estimated the electron energy gain by optimizing the plasma wave amplitude, the wiggler magnetic field, and the initial momentum of electrons while keeping the initial position fixed. There is a considerable increase in electron energy gain for higher plasma wave amplitude. The magnetic field focuses and stabilizes the motion of the electrons to keep them in the accelerating zone. Thus the electron gains improved energy level during

acceleration by the plasma wave. The electrons having initial velocity close to the velocity of light in vacuum can interact resonantly with the plasma wave and the wiggler magnetic field leading to significantly enhanced energy gain during acceleration. The dependency of electron energy gain with the initial phase of plasma wave was also estimated. The electron gains a maximum energy for an optimum initial phase of the plasma wave. The electron energy gain can also be increased if they are pre-accelerated. Optimization of the magnetic field along with the electron and plasma parameters is necessary for appropriate electron energy gain in this mechanism. This idea may replace the laser pulse in IFEL mechanism to accelerate the electrons to high-energy level. One may overcome the laser related critical issues by using the plasma wave in IFEL. This study may be crucial to produce an energetic electron beam in IFEL mechanism, which may further be used in X-FEL for compact electromagnetic radiation source generation.

References

[1] V. Malka, J. Faure, Y. A. Gauduel, E. Lefebvre, A. Rousse, and K. Ta Phuoc, *Nature Phys.* **4**, 447-453 (2008).

[2] T. Tajima and J. M. Dawson, *Phys. Rev. Lett*. **43**, 267 (1979).

[3] K. Nakajima, D. Fisher, T. Kawakubo, H. Nakanishi, A. Ogata, Y. Kato, Y. Kitagawa, R. Kodama, K. Mima, H. Shiraga, K. Suzuki, K. Yamakawa, T. Zhang, Y. Sakawa, T. Shoji, Y. Nishida, N. Yugami, M. Downer, and T. Tajima, *Phy. Rev. Lett*. **75**, 4428 (1995).

[4] J. Panwar, and S. C. Sharma, *Phys. Plasmas* **24**, 083101 (2017).

[5] S. C. Sharma, J. Panwar, and R. Sharma, *Contr. to Plasma Phys*. **57**, 167 (2017).

[6] P. Gibbon, *Short Pulse Laser Interactions with Matter: An Introduction*, London, U.K.: Imperial college Press (2005).

[7] D. Umstadter, "Relativistic laser plasma interactions," *J. Appl. Phys*. **36**, R151 (2003).

[8] A. Pukhov and J. Meyer-ter-Vehn, *Appl. Phys. B, Lasers Opt*. **74**, 355 (2002).

[9] C. Joshi, W. B. Mori, T. Katsouleas, J. M. Dawson, J. M. Kindel, and D. W. Forslund, *Nature* **311** , 525 (1984).

[10] M. Yadav, S. C. Sharma, and D. N. Gupta, *IEEE Trans. Plasma Sci*. **46** 2521 (2018).

[11] C. E. Clayton, K. A. Marsh, A. Dyson, M. Everett, A. Lal, W. Leemans, R Williams, and C. Joshi, *Phys. Rev. Lett*. **70** , 37 (1993).

[12] C. S. Liu and V. K. Tripathi, *Interaction of Electromagnetic waves with Electron Beams and Plasmas*, Singapore:World Scientific (2005).

[13] W.Leemans and E. Esarey, *Phys. Today* **62**, 44 (2009).

[14] P. Sprangle, E. Esarey, and J. Krall, *Phys. Plasmas* **3**, 2183 (1996).

[15] M. Everett, A. Lal, D. Gordon, C. E. Clayton, K. A. Marsh, and C. Joshi, *Nature* **368**, 527 (1994).

[16] A. Modena, Z. Najmudin, A. E. Dangor, C. E. Clayton, K. A. Marsh, C. Joshi, V. Malka, C. B. Darrow, C. Danson, D. Neely, and F. N. Walsh, *Nature* **377**, 606 (2002).

[17] W. P. Leemans W. P. Leemans, B. Nagler, A. J. Gonsalves, Cs. Toth, K. Nakamura, C. G. R. Geddes, E. Esarey, C. B. Schroder, and S. M. Hooker, *Nature* **2**, 696 (2006).

[18] T. Katsouleas and J. M. Dawson, *Phys. Rev. Lett*. **51,** 392 (1983).

[19] H. Mehdian, A. Kargarian, and A. Hasanbeigi, *Optik* **126**, 3299 (2015).

[20] K. P. Singh, V. L. Gupta, Lalita Bhasin, and V. K. Tripathi, *Phys. Plasmas* **10**, 1493 (2003).

[21] D. N. Gupta, M. Kaur, K. Gopal, and H. Suk, *IEEE Trans. Plasma Sci*. **44**, 2867 (2016).

[22] C. Gahn, G. D. Tsakiris, A. Pukhov, J. Meyer-ter-Vehn, G. Pretzler, P. Thirolf, D. Habs, and K. J. Witte, *Phys. Rev. Lett*. **83**, 4772 (1999).

[23] M. Kaur and D. N. Gupta, *IEEE Trans. Plasma Sci*. **45**, 2841 (2017).

[24] Levy and D. H. C. C, *Free electron lasers and other advanced sources of light: scientific research opportunities*, National Academy Press, Washington, DC (1994).

[25] R. B. Palmer, *J. App. Phys*. **43**, 3014 (1972).

[26] A. V. Steenbergen and J. C. Gallardo, in *Proc. PAC*, Vancouver, Canada (1997).

[27] E. D. Courant, C. Pellegrini, and W. Zakowicz, *Phys. Rev. A* **32**, 2813 (1985).

[28] S. Mirzanejhad, F. Sohbatzadeh, M. Asri, and E. S. Toosi, *Phys. Plasmas* **13**, 123105 (2006).

[29] F. V. Hartemann, E. C. Landahl, A. L. Troha, Jr., J. R. Van Meter, H. A. Baldis, R. R. Freeman, N. C. Luhmann, L. Song, A. K. Kerman, and D. U. L. Yu, *Phys. Plasmas* **6**, 4104 (1999).

[30] K. P. Singh and V. K. Tripathi, *Phys. Plasmas* **11**, 743 (2004).

[31] S. Kumar and M. Yoon, *Phys. Scr*. **77**, 025404 (2008).

[32] J. Duris *et al.*, *Nature Communications* **5**, 4928 (2014).

[33] N.E. Andreev, L. M. Gorbunov, and S. V. Kuznetsov, *IEEE Trans. Plasma Sci*. **24**, 448 (1996).

6

CONCLUSION AND FUTURE SCOPE

6.1 Conclusion

In the framework of this thesis, the electron acceleration process utilizing high-intensity laser and plasma interactions has been elucidated. The work carried out in the present thesis aims to develop the understanding of the phenomena of propagation of ultra-intense laser pulse in underdense plasma and subsequent generation of energetic electrons. The main objective of this thesis is to obtain improved highly energetic and coherent electron beam. For this motive, various aspects of high-intensity short laser pulse interaction with underdense plasmas have been explored such as evolution of laser pulse, wakefield excitation, electron beam generation, optimizing laser and plasma parameters for refining electron energy and electron beam quality such as bunch charge, energy spread, emittance, divergence, etc. This study has been carried out using analytic study and particle-in-cell (PIC) simulations. The theoretical study enabled the verification of the results estimated using simulation study. Numerical simulations have been able to provide an insight into the laser-plasma interaction physics, thus making the path towards improving the laser plasma accelerators quality much easier. Our results targeted two main issues. One is the understanding of the evolution of the bubble wake structure in order to control and manipulate the electron injection in the bubble. Thus, we are able to improve the electron beam quality by controlling the continuous electron injection. Secondly, the effect of pulse shape on the electron beam parameters has been put forth. The pulse shape decides the amount of pulse distortion

during propagation. It means that the pulse evolution varies for different pulse shapes, and thus excites different wakefields. Henceforth, it modifies the electron beam properties. Our findings set forth in this thesis may be expected to have a strong impact on the applications of laser-plasma interactions. The inferences drawn through this work might be quite relevant in enhancing the efficiency of laser-plasma accelerators, which have potential applications in almost all the major disciplines.

- Firstly, the bubble evolution in laser wakefield acceleration has been elucidated via 2D-PIC simulations in order to predict the electron injection process. The bubble longitudinal and transverse radii are estimated using density plots obtained from the PIC simulations. The evolution of bubble radii is shown to be dependent on driver evolution. The linear dependence of bubble radius on laser intensity parameter (a_0) is manifested. As laser propagates in plasma, pulse compression and self-steepening of the laser pulse become the responsible factors for laser pulse intensity enhancement. Thus, the bubble radii evolves with the laser pulse intensity evolution. The self-injection dynamics and its relation with the bubble evolution have been elaborated. It has been revealed that injection is facilitated by bubble expansion and contraction suppresses it. As beam energy and the beam quality is determined by the electron injection, hence, it became necessary to understand the bubble evolution. The evolution of bubble with time and the correlation of bubble length (longitudinal and transverse radius) with the intensity of laser pulse are presented. The change of bubble dimensions can be estimated by various determining factors such as the laser pulse focusing, the beam loading, the residual electrons, and the bubble velocity. It is revealed that the residual electrons lead to an increase in the longitudinal radius as compared to the transverse one. Also, the phase velocity of the wake is modified because the front of the laser pulse etches back due to pump depletion. Hence, it also has an impact on the bubble shape. Therefore, considering the variable shape of the bubble in further blow-out region studies is highly desirable to obtain more realistic results. It is found that details of bubble evolution describe the mechanism of self-injection, which in turn describes key properties of electron beam such as

energy spread, angular divergence, emittance etc. It has also been demonstrated that continuous injection sometimes degrades the beam quality, therefore controlling injection is fundamental. Plasma density optimization has also been done to obtain the improved electron beam quality. It has been presented that low-plasma density leads to increase the bunch charge but at the cost of beam energy. It may be quite significant for various applications demanding high charge and low energy beam such as non-destructive-testing, condensed matter physics, radiolysis, radiotherapy etc.

- Then, we have explored the effect of laser pulse profile on electron bunch quality in LWFA scheme. The comparison of bunch energy and quality using Gaussian and flattened-Gaussian pulse profile is presented and discussed. Both, numerical study as well as PIC simulations are carried out to validate the concept. The evolution of laser strength parameter for both the laser profiles is investigated to understand the wakefield evolution. It was found that the wakefield excited by the flattened-Gaussian laser pulse was stronger as compared to the Gaussian pulse till the effect of beam loading dominates. As the total injected charge in flattened-Gaussian case is almost twice the Gaussian case, thus the beam loading perturbs the wakefield substantially. The peak energy of the electron bunch is also affected to a large extent due to large beam load. However, it is noteworthy that the bunch charge obtained using flattened-Gaussian laser is significantly higher than the Gaussian case. The peak current of the injected electron beam in flattened-Gaussian case is also better by a factor of two. The energy spread in flattened-Gaussian case also displayed a modest improvement. Such a high charge, low energy spread electron beam makes the replacement of Gaussian laser profile by flattened-Gaussian laser profile desirable, depending on the requirement of the applications.

- Further in this thesis, it is demonstrated that a relativistic plasma wave, having an extremely large electric field may be utilized for the acceleration of plasma particles. The large accelerating field gradient driven by a plasma wave is the basic motivation behind the acceleration

mechanism. Such a plasma wave can be excited by a single laser in the form wakefield due to laser-plasma interactions. In this particular work, it has been revealed that electron energy can be significantly enhanced by traversing a LWFA driven accelerated electron in a magnetic wiggler. Electrons injected at 2.5 MeV have been accelerated to 200 MeV by the plasma wave over an interaction length of approximately 2.5 mm for an optimized wiggler magnetic field of 2 kG. This corresponds to the optimized wiggler magnetic field and electrons and plasma wave parameters. Higher electron energy has been achieved for large amplitude plasma wave in this mechanism. The maximum electron energy is obtained due to the cyclotron resonance for an optimum wiggler magnetic field. The energy gain of electrons is measured for an optimum magnetic field strength and plasma wave amplitude. We have estimated the electron energy gain by optimizing the plasma wave amplitude, the wiggler magnetic field, and the initial momentum of electrons while keeping the initial position fixed. There is a considerable increment in electron energy gain for higher plasma wave amplitude. The magnetic field focuses and stabilizes the motion of the electrons to keep them in the accelerating zone. Thus the electron gains improved energy level during acceleration by the plasma wave. The influence of tapering parameter on the electron energy gain is also estimated. It is found that larger tapering parameter can compensate the electron dephasing by increasing the interaction bandwidth. The electrons having initial velocity close to the velocity of light in vacuum can interact resonantly with the plasma wave and the wiggler magnetic field leading to significantly enhanced energy gain during acceleration. The dependency of electron energy gain with the initial phase of plasma wave was also estimated. The electron gains a maximum energy for an optimum initial phase of the plasma wave. The electron energy gain can also be increased if they are pre-accelerated. It is also indicated that the electron preaccelerated with greater initial velocity is scattered less and trajects towards the interaction region to gain energy during acceleration. Optimization of the magnetic field along with the electron and plasma parameters is necessary for appropriate electron

energy gain in this mechanism. Hence, a scaling law for electron energy gain with the wiggler magnetic field is deduced from this study. The electron energy gain is increased with the magnetic field and started to decrease after attaining the peak energy. At a certain strength of wiggler magnetic field, the energy gain of electron is found to decrease due to resonance mismatch. An optimized value of magnetic field has been suggested to carry out further study and might be employed as an experimental parameter. This idea may replace the laser pulse in IFEL mechanism to accelerate the electrons to high-energy level. One may overcome the laser related critical issues by using the plasma wave in IFEL. This study may be crucial to produce an energetic electron beam in IFEL mechanism, which may further be used in X-FEL for compact electromagnetic radiation source generation.

- Finally, a q-Gaussian pulse shape is utilized to investigate its effect on electron acceleration in LWFA scheme. The results are compared with the usual Gaussian laser pulse case. Firstly, the self-focusing phenomenon of an intense q-Gaussian laser beam and subsequently its effect on EPW excitation and electron acceleration have been examined. The self-focusing is found to be considerably enhanced for lower q-values of q-Gaussian laser beam. It has also been observed that the self-focusing is faster when the laser intensity is higher. Hence, the focusing length is less for higher intensity of the laser beam. We noticed that the self-focusing has a significant influence on EPW excitation. The EPW field intensity is seriously affected by the q-parameter of the q-Gaussian laser beam. This study shows that the field intensity of EPW is enhanced for lower q-values of laser beam (i.e. for q-Gaussian laser beam). The EPW amplitude is found to be maximum at the focal spots of the laser beam. In a result, the energy of the electrons accelerated by the EPW excited by a q-Gaussian laser beam is also increased. The numerical results suggest that the electron energy gain strongly depends on the q-value of the q-Gaussian laser beam. We found that q=0.5 is the optimized q-parameter corresponding to the maximum electron energy gain for all laser intensities.

Based on the proposed theoretical model, we suggest employing a q-Gaussian laser beam for better electron acceleration by the EPW. This study revealed the advantage of the propagation of q-Gaussian laser beam in plasmas under the relativistic and ponderomotive nonlinearities over Gaussian profile. This study also provides the optimized parameters of q-Gaussian laser beam to further study the possible nonlinear processes in plasmas, which may be crucial in demonstrating the plasma channel formation by a relativistic laser beam. It might be relevant to understand the various aspects of laser-plasma interactions such as plasma heating where an intense laser beam is required and particle acceleration schemes.

6.2 Future scope of the present work

The field of laser-plasma dynamics is very fascinating and progressive branch of physics. This thesis proposition can lead to numerous potential applications such as laser-driven plasma accelerators, x-ray and gamma sources, laser-driven fusion, plasma heating, radioactive waste incineration, synchrotron light sources, medical diagnostics etc. As the accelerating field in conventional rf accelerators is limited to 100 MeV/m due to material breakdown constraints, laser plasma accelerators were proposed as a next generation compact accelerator. Laser plasma accelerators have the capability to generate hundreds of GeV/m accelerating fields. The unique features of laser-driven particle beams are anticipated to have a remarkable usage in many practical applications, including proton therapy for the treatment of cancers, materials characterization, radiation-driven chemistry, and high energy particle physics, condensed matter physics, cosmology and astrophysics and so on. The fundamental and experimental research should be pursued to optimize the design and parameters of plasma based accelerators to explore new regime and to validate theories and numerical codes. These laser plasma accelerators have potential to produce beams of energetic electrons, protons and γ-rays. Exploring a new physics during laser-plasma interaction may help to generate the monoenergetic particle beam from plasmas. Generation of collimated beams of relativistic electrons and

ions with ultra-high currents in hundreds of kA and huge magnetic fields (up to gigagauss) is a new regime worth further exploration. The possibility to produce ultra-short, ultra-bright secondary beams of x-rays, neutrons and positrons may lead to a variety of applications, specially in materials research (diagnostics) and in medicine (radiation therapy, isotope production).

The potential for new types of accelerators for TeV electrons and ions as well as new types of particle sources for existing accelerators is also anticipated. New developments tend to strive for higher efficiency which means maximum transfer of energy to the particles from the driver. High quality is also a much desirable features of a beam, like the energy spread of the accelerated particles—we want all of the accelerated particles to have about the same energy. New pulse compression techniques coming nowadays are anticipated to achieve exawatt and zeptosecond laser. As, the zeptosecond X-ray laser matches very well with nuclear physics, we can anticipate their implications in future. Also, it is expected that instead of larger machines and higher energies, the progress made in this area will tend to achieve highly intense, efficient and more compact accelerators for bringing many of suggested applications into reality.